

Rejection of disturbances in multivariable motion systems

Citation for published version (APA):

Boerlage, M. L. G. (2008). *Rejection of disturbances in multivariable motion systems*. [Phd Thesis 1 (Research TU/e / Graduation TU/e), Mechanical Engineering]. Technische Universiteit Eindhoven.
<https://doi.org/10.6100/IR637314>

DOI:

[10.6100/IR637314](https://doi.org/10.6100/IR637314)

Document status and date:

Published: 01/01/2008

Document Version:

Publisher's PDF, also known as Version of Record (includes final page, issue and volume numbers)

Please check the document version of this publication:

- A submitted manuscript is the version of the article upon submission and before peer-review. There can be important differences between the submitted version and the official published version of record. People interested in the research are advised to contact the author for the final version of the publication, or visit the DOI to the publisher's website.
- The final author version and the galley proof are versions of the publication after peer review.
- The final published version features the final layout of the paper including the volume, issue and page numbers.

[Link to publication](#)

General rights

Copyright and moral rights for the publications made accessible in the public portal are retained by the authors and/or other copyright owners and it is a condition of accessing publications that users recognise and abide by the legal requirements associated with these rights.

- Users may download and print one copy of any publication from the public portal for the purpose of private study or research.
- You may not further distribute the material or use it for any profit-making activity or commercial gain
- You may freely distribute the URL identifying the publication in the public portal.

If the publication is distributed under the terms of Article 25fa of the Dutch Copyright Act, indicated by the "Taverne" license above, please follow below link for the End User Agreement:

www.tue.nl/taverne

Take down policy

If you believe that this document breaches copyright please contact us at:

openaccess@tue.nl

providing details and we will investigate your claim.

Rejection of disturbances in multivariable motion systems

PROEFSCHRIFT

ter verkrijging van de graad van doctor
aan de Technische Universiteit Eindhoven,
op gezag van de Rector Magnificus, prof.dr.ir. C.J. van Duijn,
voor een commissie aangewezen door het College voor Promoties
in het openbaar te verdedigen
op woensdag 3 september 2008 om 16.00 uur

door

Matthijs Leonardus Gerardus Boerlage

geboren te Nijmegen

Dit proefschrift is goedgekeurd door de promotor:

prof.dr.ir. M. Steinbuch

Copromotor:
dr.ir. A.G. de Jager

The logo for the Dutch Institute of Systems and Control (DISC) features the word "disc" in a lowercase, sans-serif font. The letters "d", "i", and "c" are black, while the letter "s" is a vibrant green.

The research reported in this thesis is part of the research program of the Dutch Institute of Systems and Control (DISC). The author has successfully completed the educational program of the Graduate School DISC.

A catalogue record is available from the Eindhoven University of Technology Library.

Rejection of disturbances in multivariable motion systems by
Matthijs Leonardus Gerardus Boerlage – Eindhoven : Technische Universiteit
Eindhoven, 2008
Proefschrift. – ISBN: 978-90-386-1375-8

Copyright © 2008 by M.L.G.Boerlage. All rights reserved

This thesis was prepared with the pdfL^AT_EX documentation system.
Cover Design: Oranje Vormgevers, Eindhoven, The Netherlands
Reproduction: Universiteitsdrukkerij TU Eindhoven, Eindhoven, The Netherlands

List of symbols and acronyms

Symbol	Meaning
\bar{d}	direction of d normalized to unity
d_o, d_i	disturbance at the output, input of the plant respectively
\mathbf{D}	space D
$\text{diag}\{(\cdot)\}$	square matrix with diagonal terms taken from (\cdot)
$\text{diag}\{(\cdot)_i\}$	square matrix with $(\cdot)_i$ on each i^{th} diagonal term
f	frequency in Hz.
$\mathcal{F}_l, \mathcal{F}_u$	lower, upper fractional transformation
G	plant
G_p	plant from physical inputs to physical outputs
G_d	disturbance model, diagonal terms of G
G_n	sensor noise model
G_s	mixing matrix
$G_{\hat{s}}$	estimate of mixing matrix G_s within indeterminacies
G_{nd}	non-diagonal terms of G
I_n	identity matrix with size $n \times n$
ICA	Independent Component Analysis
K	feedback controller
$\kappa(\cdot)$	condition number of (\cdot)
L	open loop function evaluated at the output of the plant
L_i	open loop function evaluated at the input of the plant
$\lambda_i(\cdot)$	eigenvalue of (\cdot)
Λ_{RGA}	relative gain array
M	weighted closed loop
$MIMO$	multiple input multiple output
\mathcal{N}	number of clock-wise encirclements
ω	frequency in radians
P	generalized plant
PCA	Principle Component Analysis
\bar{P}	generalized plant without weighting filters
s	disturbances source $s(t)$, Laplace variable when used as, e.g., $H(s)$.

Continued on next page

Symbol	Description
<i>SISO</i>	single input single output
<i>SOBI</i>	Second Order Blind Identification
S_o, S_i	output, input sensitivity function respectively
$\rho(\cdot)$	spectral radius of (\cdot)
$\bar{\sigma}(\cdot), \underline{\sigma}(\cdot)$	the maximum, minimum singular value of (\cdot)
$\sigma_i(\cdot)$	i^{th} singular value of (\cdot)
$\mu_T(\cdot)$	structured singular value of (\cdot) with respect to the structure of T
T_o, T_i	output, input complementary sensitivity function respectively
τ	shift operator
u	plant input
y	plant output
z	performance variable

Contents

List of symbols and acronyms	iii
1 Introduction	1
1.1 Motion systems	1
1.2 Disturbance rejection	2
1.2.1 Manual loopshaping	4
1.2.2 Norm based loopshaping	5
1.3 Problem formulation	7
1.4 Applications used in this thesis	7
1.5 Outline of the thesis	8
2 Multivariable control	9
2.1 Control design	9
2.1.1 Stability	10
2.1.2 Performance	11
2.1.3 Loopshaping	13
2.1.4 Discussion	14
2.2 Limitations in performance	14
2.2.1 Algebraic limitations	15
2.2.2 Analytical limitations	15
2.3 Decentralized control	19
2.3.1 Independent design	20
Stability by independent design	20
Performance by independent design	24
2.3.2 Sequential design	27
Stability by sequential design	28
Performance by sequential design	29
2.4 Open loop decoupling	30
2.4.1 Dyadic systems	31
2.4.2 Pseudo SVD systems	33
2.4.3 Mechanical systems	35
2.5 Decentralized control design for the AVIS	40
2.5.1 The AVIS	40
2.5.2 Feedback control design	42

2.5.3	Discussion	45
2.5.4	Conclusion	47
2.6	Disturbance rejection	47
3	Characterization of disturbances in multivariable systems	51
3.1	Multivariate disturbance identification	53
3.2	Blind identification	55
3.2.1	Whitening	57
3.2.2	Unitary diagonalization	58
3.2.3	Influence of noise signals	59
3.3	Identification results	61
3.3.1	Case 1, $W \in \mathbb{R}^{2 \times 6}$	63
3.3.2	Case 2, $W \in \mathbb{R}^{6 \times 6}$	65
3.3.3	Validation and interpretation of results	66
3.4	Localization of sources	68
3.5	Disturbance driven multivariable feedback control	70
3.6	Conclusion	73
4	Directionality in multivariable control design	75
4.1	Norm based design	76
4.1.1	Disturbance rejection with \mathcal{H}_∞ control design	77
	Disturbance direction fixed, sources unknown	79
	Disturbance direction not fixed, hence worst case	80
	Disturbance direction fixed, blindly identified	80
4.1.2	Simulation Example	81
	Blind identification	82
	Weighting filter design	83
	Discussion	85
4.1.3	Conclusion	92
4.2	Disturbance decoupling design	92
4.2.1	Control design in disturbance directions	93
4.2.2	Application example	94
	Multiloop SISO design in control coordinates	95
	Design in disturbance coordinates	99
	\mathcal{H}_∞ design in control coordinates	100
4.2.3	Discussion	100
4.2.4	Conclusions	101
4.3	Non uniform noise and disturbance rejection	101
4.3.1	Analysis of non-uniform gain controllers	102
4.3.2	Disturbance rejection	105
	Manual loopshaping design	106
	\mathcal{H}_∞ design	107
4.3.3	Example	108
4.3.4	Discussion	111
4.3.5	Conclusions	113
4.4	MIMO control design of a metrological AFM	114

4.4.1	The metrological AFM	114
4.4.2	Uniform controller design	118
4.4.3	Disturbance decoupling design	120
4.4.4	High bandwidth decentralized independent control	121
4.4.5	Discussion	124
4.4.6	Conclusions	127
4.5	Concluding remarks	128
5	Conclusions and Recommendations	129
5.1	Conclusions	129
5.2	Recommendations	130
A	Figures AVIS control design	133
B	Principal angles	143
	Bibliography	145
	Summary	157
	Samenvatting	159
	Dankwoord	161
	Curriculum Vitae	163

Chapter 1

Introduction

1.1 Motion systems

Advanced motion systems are widely used in the high tech systems industry. Examples are active vibration platforms, wafersteppers, robotic manipulators, and atomic force microscopes, Fig. 1.1a, Fig. 1.1b. The behavior of high performance motion systems is typically dominated by mechanical dynamics. Therefore, mechanical systems are constructed to be light and stiff, with the objective to move bandwidth limiting phenomena to high frequencies. A common trend is to equip systems with more actuators and sensors in order to improve dynamical behavior, [62, 115]. In other applications, it is required to actuate motion systems in multiple degrees of freedom, [143]. The mechanics of such systems are typically constructed with the objective to allow each degree of freedom to be controlled independently. These systems naturally have multiple inputs and multiple outputs (MIMO). In order to meet high performance requirements, multivariable control is a necessity.

Motion systems are often controlled by a combination of feedback and feedforward control. If disturbances (such as the reference trajectory) can be directly measured, feedforward control can be applied, [13]. Disturbances that are not known beforehand are often dealt with by means of feedback control. This thesis focusses on the design of feedback controllers to reject such disturbances in multivariable motion systems.



Figure 1.1: Two motion systems. Left: Multi-degree of freedom positioning stage developed by Philips Applied Technologies, [15]. Right: Active vibration isolation system developed by Integrated Dynamics Engineering.

1.2 Disturbance rejection

The rejection of disturbances in multivariable motion systems can be studied considering the unity feedback control problem, with performance variable $z = y - r$, depicted in Fig. 1.2. The MIMO plant G is subjected to exogenous signals

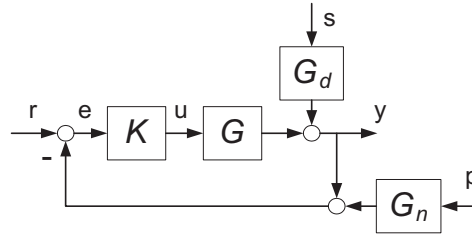


Figure 1.2: Unity feedback control architecture.

$w = [s, p, r]^T$ containing the source of disturbances, s , source of noise, p , and reference signals, r . We focus on linear time invariant (LTI) plants, so that we may perform analysis in the Laplace domain, [125]. This model, expressed in the generalized plant framework, becomes,

$$\begin{bmatrix} z \\ e \end{bmatrix} = \left[\begin{array}{ccc|c} G_d & 0 & -I & G \\ -G_d & -G_n & I & -G \end{array} \right] \begin{bmatrix} s \\ p \\ r \\ u \end{bmatrix}. \quad (1.1)$$

With, $u = Ke$, we find,

$$z = S_o G_d s - T_o G_n p - S_o r, \quad (1.2)$$

where, $S_o = (I + GK)^{-1}$, $T_o = GK(I + GK)^{-1}$, are the output sensitivity and output complementary sensitivity respectively. If the reference signals can be measured or are known beforehand, either model based, [13], or iterative learning, [21, 144], feedforward can be applied. If the reference signal can not be measured or is not known beforehand, it can be treated as a disturbance on the outputs of the plant without loss of generality. We study the disturbance rejection problem without reference trajectory, $r = 0$. Then, the objective is to minimize the influence of disturbances and noise on the performance variable. Therefore, by suitable design of controller K , both S_o and T_o are to be minimized with respect to the characteristics of the disturbances and sensor noise. As known from the internal model principle, [41], disturbances can be asymptotically rejected when a model of the disturbance is contained in the controller. Approaches that build on this concept are disturbance observers, [116, 121], disturbance accommodating controllers, [69, 70], and \mathcal{H}_2 - or \mathcal{H}_∞ controllers, [39, 125]. Although each design approach has its own favorable delicacies, results are similar when considered in the frequency domain, [72]. Models of both plant and disturbances are essential for high performance motion control.

In most motion systems, the dynamics of the plant can be considered to be linear time invariant. Then, a common technique is to measure the frequency response under closed loop conditions, [108]. The frequency response is a *non-parametric* model of the plant. This frequency response function can be used to acquire *parametric* (e.g., state space, transfer functions) models using (polynomial) fitting procedures, [96, 108]. A disturbance model can be obtained as a by-product of plant identification, [127], or by filtering closed loop measurements with a model of the relevant closed loop functions, [3, 133]. If the plant is linear, disturbances can be considered as additive signals at either the input or the output of the plant. Accurate models of plant and disturbances are usually difficult to develop. Therefore, in order to compensate for the lack of total knowledge of the system, intuition and insight play a significant role in designing feedback controllers.

In SISO control, the power spectra of disturbances assist the control engineer to determine the ideal closed loop functions. With the known power spectrum of the disturbances, the shape of the ideal open loop function can be determined straightforwardly from the closed loop functions. The open loop frequency response function can be shaped intuitively as the open loop function is linear in the controller. Control design methods for motion systems therefore are mostly developed in the frequency domain. In control of high performance SISO motion systems, inherent limitations imply tradeoffs between disturbance rejection and other design objectives, [89]. In the frequency domain, these tradeoffs can be addressed directly during the design process, [3].

Things are not quite that simple for MIMO systems. First, for general cases, it is not straightforward to relate closed loop functions with specific elements of the controller transfer function matrix. Manual (re)tuning of the controller, as is common in industrial SISO control, is therefore complicated. Second, aside from

the power spectrum, the directions of disturbances determine the amplification of disturbances by a closed loop function. Third, interaction between inputs and outputs complicates control design significantly. For MIMO systems, these inherent performance limitations are rather incomprehensible, and therefore it is not intuitive to make either tradeoffs in control design or to predict achievable performance, [26]. Therefore, interpretation and development of multivariable control strategies, for a given design problem, poses challenges for academia and practising engineers, even though considerable effort has been made over recent decades, [82, 103]. It is well known that developing a general intuitive design approach for multivariable control problems is inherently problematic, [103].

In order to cope with the inherent complexity of multivariable control design issues, pragmatic simplifications are a necessity. In many practical applications, physical structure of the plant dynamics is exploited to simplify the multivariable control design problem. This leads to successful applications of multivariable control to, for instance, nuclear plants, [98], paper machines, [59, 146], and automotive test rigs, [140, 141]. In, [48, 49], it is discussed how MIMO control problems can be reduced to SIMO or MISO control problems in certain frequency regions due to the presence of certain performance limitations. In, [43], it is demonstrated how an optimal LQG controller can be reconstructed on the basis of this physical insight.

The design methods discussed above, show that satisfactory approaches for SISO problems can not always be extended to MIMO systems, while preserving physical insights. In this thesis, we investigate how these issues can be handled for disturbance rejection control design for motion systems. Two frequency domain design methods, that are commonly used in motion control, are discussed next.

1.2.1 Manual loopshaping

For SISO systems, the powerful concepts such as Bode gain-phase relation and the Nyquist stability criterion, [10], allow quantitative and intuitive design of feedback controllers. This gave rise to development of manual loopshaping techniques in the frequency domain, [129], and Quantitative Feedback Theory, [150]. Due to straightforward relations between open loop and closed loop transfer functions in SISO systems, closed loop specifications can be translated to an “ideal shape” of the open loop function. As there exists a linear relation between the open loop function and the controller, controller parameters can be designed rather intuitively. With this, physical insight can be preserved throughout the control design process. Therefore, SISO control has found application in a wide area in industry.

Motivated by the success of SISO control theory, there has been a strong desire to extend these concepts for control design of MIMO systems. At least since the 1960’s, the so-called “British School” techniques were developed, [113], [63],

[82], [103]. These techniques extended SISO frequency domain concepts to find stabilizing controllers for MIMO plants, [82], [84], [22]. Alternative approaches exploit the structure of plant dynamics to decouple controlled variables, [102], [56], [59], [140]. Most of these decoupling techniques are ad-hoc or at least very application specific. These methods aim to factorize criteria for closed loop stability by decomposing a MIMO plant into (simpler) SISO subsystems. If each subsystem is stabilized, the total MIMO system is closed loop stable. These “divide and conquer” strategies, may work for stability, but do not necessary imply that the performance of a MIMO system can be considered independently. Practical solutions to reject disturbances are therefore high gain feedback control to enforce minimization of the sensitivity function. With this decoupling approach, it is not straightforward to exploit the directional information in a multivariable control problem.

1.2.2 Norm based loopshaping

The generalized plant framework, Fig. 1.3, provides a way to formulate practical control design issues, [154]. The input signals of the transfer function matrix P

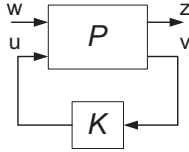


Figure 1.3: Generalized plant configuration

are partitioned in two groups, the exogenous signals, w , and the control inputs, u . Likewise, the output signals are divided in measurable signals, v , and performance variables, z . The transfer function matrix P is arranged according to the signals,

$$P = \left[\begin{array}{c|c} P_{zw} & P_{zu} \\ \hline P_{vw} & P_{vu} \end{array} \right] \quad (1.3)$$

Herein, P_{vu} is the plant to be controlled. We find, using the lower fractional transformation,

$$\mathcal{F}_l(P, K) = P_{zw} + P_{zu}K(I - GK)^{-1}P_{vw}, \quad (1.4)$$

the transfer function from w to z ,

$$z = Mw, \quad M = \mathcal{F}_l(P, K). \quad (1.5)$$

So that by careful modeling of P , the interplay of plant, disturbances and performance variables can be analyzed. Furthermore, model uncertainty can easily be

taken into account using this formalism, [125]. Modeling is non-trivial, especially because many elements of P can often not be measured directly. The generalized plant can be augmented with weighting functions in order to characterize exogenous signals and performance variables, so that,

$$z = W\tilde{M}Vw, \quad M = W\tilde{M}V. \quad (1.6)$$

thereby specifying closed loop specifications. The control synthesis problem is to find a controller K that internally stabilizes M and minimizes the transfer function from w to z in some operator norm. Typical operator norms on M are the \mathcal{H}_∞ norm and the \mathcal{H}_2 norm. For these cases, powerful control synthesis methods exist, [37].

The norm based control methods rely on the sensible choice of weighting filters and accurate models of the generalized plant. For SISO plants, models are often straightforward to acquire from least square fits on frequency response data, [108]. Weighting filters, that express closed loop performance objectives, are often designed in the frequency domain. Herein, the same insights as in manual loopshaping can be used, [143]. Typically, design leads to iterative choices of the weighting filters while evaluating the resulting closed loop functions. As the controller from norm based techniques has the same order as the order of the generalized plant, plant model and controller reduction techniques are essential for practical application, [148, 149]. The ad-hoc adjustments and design iterations in plant modeling, weighting filter design and model reduction requires engineering interventions and therefore relies on physical insight. For SISO systems, this is relatively straightforward so that results of norm based control synthesis can be related to results of manual loopshaping design techniques. Therefore, norm based controllers have been successfully applied in industrial applications, [39, 79, 129].

For MIMO systems, norm based control is much more delicate. First, identification of MIMO plants is laborious, especially if low order models are to be acquired, [96]. Second, since there is no linear relation between closed loop functions and the controller transfer function, the effects of weighting filter choices are not easily related to changes of the controller. Third, one has little insight into the loss of performance associated with model and controller order reduction. Therefore, the iterative tuning of weighting filters, that is natural in norm based design, is much more involved and physical interpretation is difficult to maintain throughout the design process.

If the plant is almost decoupled and all design objectives are stated as independent objectives at each decoupled part of the plant, it is natural to choose weighting filters diagonal. As an example of this, we mention the successful MIMO design with \mathcal{H}_∞ reported in [143]. Many applications require more general design objectives or more general disturbance models. However, even in those cases, weighting filters are often chosen diagonal in an attempt to reduce control design complexity, [125]. With this, multivariable aspects of the control problem are neglected in the design, compromising achievable performance and failing in preserving physical

insight and intuition. These are serious obstacles for norm based control design to be adopted in industry.

1.3 Problem formulation

Conventional frequency domain design methods lack the ability to take into account multivariable aspects of disturbances. It is not expected that a general solution to this design problem can be obtained. Therefore, we investigate how properties of motion systems may be exploited to develop insightful multivariable control design methods for disturbance rejection. This leads to the following problem statement:

Investigate how directions of disturbances can be identified and accommodated in multivariable frequency domain loopshaping control design techniques for motion systems, given the inherent limitations of feedback control design.

This gives rise to the following research issues. First, it must be investigated how properties of motion systems can be exploited in MIMO control design. Herein, concepts of frequency domain MIMO control design and physical insights into the dynamics of motion systems are merged. Second, a physically motivated model of disturbances is to be acquired to further simplify MIMO control design. Therefore, a technique is to be developed to characterize multivariable aspects of disturbances in MIMO motion systems. Third, the inherent limitations in MIMO control design are to be investigated to understand tradeoffs of performance in MIMO control design. This may also motivate the choice of specific control design strategies. Fourth, combining all insights of disturbance characteristics, plant dynamics and the inherent limitations of feedback control, a design method is to be developed for MIMO motion control. With this, we aim to develop intuitive frequency domain manual and \mathcal{H}_∞ loopshaping design techniques for the rejection of disturbances in MIMO motion systems.

1.4 Applications used in this thesis

The proposed design control methods are demonstrated on different application examples. We apply conventional MIMO control design techniques to a six input, six output active vibration isolation system (AVIS). This system has significant plant interaction and demonstrates the complexity issues of industrial MIMO motion control problems. This system is also used to demonstrate how synthetically applied disturbances can be characterized using the techniques proposed in this thesis. In Chapter 4, different MIMO feedback controllers are designed

for a metrological atomic force microscope (AFM). This system has three inputs and three outputs and little plant interaction. With this, it is illustrated how disturbance directionality accommodating centralized control design techniques, developed in this thesis, can be applied. Further examples are several simulation models, a laboratory MIMO system and a simulation model of an industrial waferstage.

1.5 Outline of the thesis

The outline of this thesis is as follows. In chapter 2, a general introduction of the concepts of multivariable control for motion systems is presented. Specific attention is paid to inherent design limitations induced by extensions of Bode's integral relations for MIMO systems. Decentralized design methods are discussed and open loop decoupling strategies are shown. The theory is applied on an active vibration isolation system. Chapter 3 proposes a method to identify the root causes (sources) of disturbances with a fixed direction. It is shown how these sources can be allocated in the active vibration isolation setup. Also, it is discussed how one may formulate a multivariable disturbance model that can assist decentralized control (re)design. In chapter 4 control design methods are proposed that specifically exploit the directions of disturbances and sensor noise in shaping closed loop functions in the frequency domain. Manual and \mathcal{H}_∞ techniques are adapted to take into account the properties of fixed direction disturbances and noise for a specific class of motion systems. Chapter 5 closes with conclusions and suggestions for future research.

Chapter 2

Multivariable control

This chapter introduces definitions and concepts in feedback control of linear time invariant (LTI) multiple input multiple output (MIMO) systems that are used in this thesis. A general introduction to multivariable control can be found in [55, 84, 92]. Classical frequency domain loopshaping techniques for multivariable systems can be found in [22, 83, 84, 102, 113]. In [114, 125, 154], an overview of robust and optimal control methods for multivariable systems is presented. Modal control techniques are discussed in [52, 66, 91]. This chapter merges some of these concepts that are relevant for multivariable motion control.

After the introduction of some general concepts, we investigate the inherent limitations of MIMO feedback control. Next, design techniques for decentralized control are developed. Different design approaches are applied to an active vibration isolation system in Section 2.5. The chapter closes with a discussion on disturbance rejection in MIMO systems.

2.1 Control design

We limit ourselves to feedback control design for LTI plants with n inputs and n outputs, denoted by the transfer function matrix $G(s)$. This transfer function matrix relates the $n \times 1$ vector valued input $u(s)$ to the $n \times 1$ vector valued output $y(s)$ as $y(s) = G(s)u(s)$. A common phenomenon in a multivariable system is the presence of *interaction*.

Definition 2.1.1. *A system $H(s)$, with $z(s) = H(s)d(s)$, has interaction when input $d_i(s)$ changes output $z_j(s)$ for $i \neq j$. If input $d_i(s)$ only changes output $z_i(s)$, the system is said to be non-interacting or decoupled.*

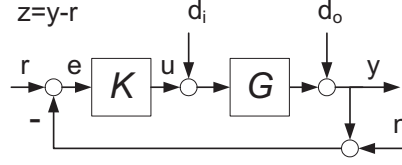


Figure 2.1: Single degree of freedom unit feedback configuration.

Note that by this definition, a system described by a skew-diagonal transfer function matrix has interaction. In that particular case, one may choose alternative input output pairings in order to reduce interaction, [142]. A system that is described by a transfer function matrix where all off-diagonal terms of that matrix are zero, is decoupled. If a controller, K , is described by a transfer function matrix where all off-diagonal terms are zero, we call this controller a *decentralized* controller. A controller where the structure is not constrained, is called a *centralized* controller. As both the plant and the controller are matrices, the commutative property does not hold in general, hence $GK \neq KG$. This makes it difficult to extend SISO concepts to MIMO control design.

A single degree of freedom feedback system is depicted in Fig. 2.1. Typical control objectives are to 1) stabilize the closed loop system, and 2) achieve a satisfactory level of performance. Performance typically implies that the transfer from vector valued signals d_i, d_o, n to the vector valued variable z has to be minimized, with minimal control effort u . The challenge is to satisfy these control objectives in presence of uncertain dynamics in the plant model. If stability and performance are achieved for a set of described uncertain plants, we say that we have achieved robust stability and robust performance.

2.1.1 Stability

The first requirement of feedback control, is to achieve closed loop stability. Most design approaches in this work are formulated in the frequency domain. Therefore, a condition for closed loop stability in the frequency domain will be presented. Let p_L be the number of open loop unstable poles in the open loop transfer function matrix $L(s) = G(s)K(s)$. Then, the negative feedback closed loop system, with open loop $L(s)$, is stable when,

$$\det(I + L(s)), \quad (2.1)$$

makes p_L anti-clockwise encirclements of the origin and does not pass through the origin as s traverses the usual Nyquist contour, [84, p.59]. We use the property,

$$\det(I + L(s)) = \prod_i (1 + \lambda_i(L(s))). \quad (2.2)$$

Herein, $\lambda_i(L(s))$, as s goes once round the Nyquist contour, is the i^{th} characteristic locus of $L(s)$. This gives rise to the frequency domain criterion for closed loop stability, known as the Generalized Nyquist criterion, [110].

Definition 2.1.2. A feedback system, depicted in Fig. 2.1, is closed loop stable when there are no pole zero cancelations between $G(s)$ and $K(s)$, the open loop $L(s) = G(s)K(s)$ has p_L unstable poles and the characteristic loci, $\lambda_i(L(s))$, $i = \{1, \dots, n\}$, taken together, encircle the point $(-1, 0)$ in the Nyquist plane, p_L times.

For SISO systems, the characteristic locus, $\lambda(L(s))$, evaluated at frequency $s = j\omega$ is equal to the frequency response of the open loop. As the open loop is linear in K , the shape of the controller frequency response function directly determines the shape of the open loop frequency response function, and thereby the characteristic locus. In MIMO systems, the characteristic loci are the eigenvalues of the frequency response function of the open loop transfer function matrix. In general, it is not straightforward to relate a single element of the controller transfer function matrix to the shape of a particular characteristic locus. Methods that aim at directly shaping the characteristic loci are developed in [84, 113]. Herein, a certain degree of open loop decoupling is required. With this, the structure of the controller is constrained. If the plant is decoupled, $G(s) = \text{diag}\{g_i(s)\}$, and the controller is chosen diagonal $K(s) = \text{diag}\{k_i(s)\}$, it follows that $\det(I + L(s)) = \prod_{i=1}^n \det(1 + g_i(s)k_i(s))$. If each single input, single output loop is stable, the MIMO system is stable. Alternative approaches to factorize (2.1) are discussed in Section 2.3.

As in classical SISO control design, one may define gain and phase margins on the characteristic loci in the Nyquist plane. However, these margins can only be used to express robustness for simultaneous parameter change in all the loops, [47]. More general methods to describe robust stability construct uncertainty templates about the characteristic locus of a nominal system, [74]. Although construction of these templates is not straightforward, it can be shown that these conditions for robust stability are both necessary and sufficient, [77]. A common approach to derive necessary and sufficient, conditions for robust stability, is by using the structured singular value, [35].

2.1.2 Performance

The performance objectives in the example shown in Fig. 2.1, imply that the transfer function from exogenous signals, d_i, d_o and n , to the vector valued variable z is minimized with minimal control effort. In classical control, this is accomplished by minimizing the gain of the corresponding transfer functions. In multivariable systems, the gain of a transfer function is not unique and depends on the *direction* of the input signal. For a vector valued signal $d \in \mathbf{D}$, where $\mathbf{D} = \text{Span}\{e_1, \dots, e_n\}$, $e_i e_i^T = 1$, $e_i e_j^T = 0$, $i \neq j$, the direction is defined as follows.

Definition 2.1.3. The direction \bar{d} of a vector valued signal $d \in \mathbf{D}$ is defined as,

$$\bar{d} = \frac{1}{\|d\|_2} d. \quad (2.3)$$

The direction \bar{d} of disturbance d can be interpreted as the normalized ratio in which d enters at a point in a feedback system. A signal that has a *canonical* direction, namely if $\bar{d} = e_i$, acts only at a single channel of the feedback system.

In the special case that the open loop transfer function $L = GK$ is decoupled, all closed loop transfer functions in Fig. 2.1 are decoupled. If then all disturbances and sensor noise have canonical directions and the performance variables are defined in each decoupled loop independently, performance analysis is similar to that of SISO systems. For more general cases, performance analysis is not that straightforward. This is due to the fact that MIMO systems do not have a unique gain as this depends on the direction of the input. Therefore, the gain of a transfer function matrix $H(s)$, with $z(s) = H(s)d(s)$, is often studied using the ratio,

$$\frac{\|H(s)d(s)\|_2}{\|d(s)\|_2}, \quad (2.4)$$

where $\|\cdot\|_2$ is the Euclidian vector norm. We can take $s = j\omega$ to study this ratio at a single frequency ω . It then follows that, as $z(j\omega) = H(j\omega)d(j\omega)$,

$$\underline{\sigma}(H(j\omega)) \leq \frac{\|H(j\omega)d(j\omega)\|_2}{\|d(j\omega)\|_2} \leq \bar{\sigma}(H(j\omega)). \quad (2.5)$$

The largest and smallest gain of the system H , at frequency ω , are defined as the maximum and minimum singular value of $H(j\omega)$, namely $\bar{\sigma}(H(j\omega))$, $\underline{\sigma}(H(j\omega))$ respectively. If $\underline{\sigma}(H(j\omega)) \approx \bar{\sigma}(H(j\omega))$, the gain of H , at frequency ω , does not change with different directions of d . The condition number of a system H , evaluated at frequency ω , is defined as,

$$\kappa(H(j\omega)) = \frac{\bar{\sigma}(H(j\omega))}{\underline{\sigma}(H(j\omega))}. \quad (2.6)$$

A transfer function, evaluated at frequency ω , is called *ill-conditioned*, *skew*, or *not-normal* if $\kappa(H(j\omega)) \gg 1$, [63]. The gain of an ill-conditioned system depends strongly on the direction of the input signals. For the control objectives of the feedback system shown in Fig. 2.1, one must minimize $\bar{\sigma}(S_o)$, $\bar{\sigma}(T_o)$, $\bar{\sigma}(S_o G)$ and $\bar{\sigma}(K S_o)$. As will be shown in Section 2.2, these objectives are conflicting so that tradeoffs in achievable performance are to be made. In classical control design methods, closed loop objectives are translated to specifications on the shape of the open loop transfer function. The next section shows how a similar approach can be followed using the singular values of transfer functions.

2.1.3 Loopshaping

Classical control design methods aim at shaping the frequency response function of the open loop transfer function to achieve closed loop performance objectives. For SISO systems, the relation between open loop and closed loop functions is straightforward. Hence, closed loop specification can be used to construct a preferred shape of the open loop function. This may lead to insights in the achievable performance and facilitates transparent control (re)design, [58, 129]. For MIMO systems, a similar approach can be followed using the concepts of the singular value decomposition of a transfer function matrix per frequency, [63].

Definition 2.1.4. *The i^{th} principal gain of a system H is the i^{th} singular value of $H(j\omega)$ at each frequency ω .*

The input or output *principal vector*, is the input (right) or output (left) singular vector that belongs to each principal gain. The direction of a principal vector is called the *principal direction*. We have that, [125, p.522],

$$\underline{\sigma}(L(j\omega)) \leq |\lambda_i(L(j\omega))| \leq \bar{\sigma}(L(j\omega)), \quad (2.7)$$

where $\lambda_i(\cdot)$ is the i^{th} characteristic locus. This provides a relation between stability and the principal gains of a multivariable system. When, $\kappa(L(j\omega)) \rightarrow 1$, it follows that $\underline{\sigma}(L(j\omega)) \approx |\lambda_i(L(j\omega))| \approx \bar{\sigma}(L(j\omega))$, [63].

The principal gains can be studied to relate closed loop transfer functions to the open loop transfer function at single frequency ω , [38]. For the sake of notational brevity, the system H evaluated at $s = j\omega$ is written as H instead of $H(j\omega)$. Considering the output sensitivity function, $S_o = (I + GK)^{-1}$, for example, basic linear algebra results in,

$$\underline{\sigma}(L) - 1 \leq \frac{1}{\bar{\sigma}(S_o)} \leq \underline{\sigma}(L) + 1 \quad (2.8)$$

$$|\bar{\sigma}(L) - 1| \leq \frac{1}{\underline{\sigma}(S_o)} \leq \bar{\sigma}(L) + 1. \quad (2.9)$$

At frequencies where $\underline{\sigma}(L) \gg 1$, $\bar{\sigma}(S_o) \approx \frac{1}{\underline{\sigma}(L)}$. At frequencies where $\bar{\sigma}(L) \ll 1$, $\bar{\sigma}(S_o) \approx 1$. So that only in these extreme cases, relations between closed loop and open loop are straightforward. The consistency condition, [125, p.532], implies that,

$$\bar{\sigma}(S_o)\underline{\sigma}(L) \leq \bar{\sigma}(T_o) \leq \bar{\sigma}(S_o)\bar{\sigma}(L). \quad (2.10)$$

If $\underline{\sigma}(L) \approx \bar{\sigma}(L)$, relations between different transfer functions can be made. Using the property that $S_i = G^{-1}S_oG$, $S_i = KS_oK^{-1}$ and the minimax property of the singular values, [53], we find,

$$\begin{aligned} \kappa(G)^{-1}\sigma_i(S_o) &\leq \sigma_i(S_i) \leq \kappa(G)\sigma_i(S_o) \\ \kappa(K)^{-1}\sigma_i(S_o) &\leq \sigma_i(S_i) \leq \kappa(K)\sigma_i(S_o), \end{aligned} \quad (2.11)$$

which shows that the sensitivity at the plant input and the sensitivity at the plant output can only be related straightforwardly if either $\kappa(K) = 1$ or $\kappa(G) = 1$. Restricting a controller so that $\kappa(K) = 1$ is unrealistic, especially if $\kappa(G) \gg 1$ or the specifications, e.g. induced by uncertainty, are strongly direction dependent.

These relations show that stability and worst case performance at different loop breaking points can only be simplified when transfer function matrices are not skew. Also, these relations only consider worst case directions and provide little information about the performance of inputs with other directions. Furthermore, the relation between the principal gains and the elements of the controller transfer function matrix is not straightforward.

2.1.4 Discussion

In multivariable systems, redesign of a single element of a controller transfer function matrix may change performance and closed loop stability of the whole multivariable system. There exist no simplified relations between open loop and closed loop transfer functions for the general case. Also, it is difficult to relate transfer functions at different loop breaking points. Therefore, one can not make use of simplifications that are typically exploited in single input single output control design. Worst case measures, that can be derived using properties of the singular value decomposition, provide less insight if the plant is skew or when the plant has many inputs and outputs.

A common approach is to modify the multivariable system so that the performance objectives and stability conditions can be factorized in simpler sub problems. These approaches typically require a deep physical understanding of the multivariable control problem. Also, the structure of the controller can be restricted to reduce the degrees of freedom of the control design problem. This is discussed in Section 2.3. As many performance objectives may be conflicting, feedback control design involves tradeoffs. These tradeoffs are discussed in the next section.

2.2 Limitations in performance

Disturbance rejection by feedback design involves minimizing relevant closed loop transfer functions. As is widely recognized in practise, minimization of sensitivity functions is limited due to inherent constraints. Due to these constraints, feedback control design has to face tradeoffs in achievable performance, [89]. Understanding these tradeoffs facilitates formulating realistic specifications in control design. We follow the convention from [45] where limitations are divided in limitations that are either *algebraic* or *analytical* in nature. The implication of these for MIMO control design will be discussed in this section.

2.2.1 Algebraic limitations

Algebraic limitations relate properties of closed loop transfer functions at different loop breaking points. The following holds at a single frequency ω ,

$$S_o + T_o = I, \quad S_i + T_i = I. \quad (2.12)$$

This results straightforwardly from the definition of the sensitivity and complementary sensitivity function. Hence, at a single frequency, perfect disturbance rejection implies amplification of sensor noise. In multivariable systems, directions of disturbances and noise play an important role in (2.12). From (2.12) it follows that if an output disturbance with direction \bar{d} , at one frequency, is perfectly rejected,

$$S_o \bar{d} = 0, \quad (2.13)$$

then, at that same frequency, sensor noise with direction $\bar{n} = \bar{d}$, is amplified with a factor 1, as $T_o \bar{d} = \bar{d}$. Likewise, when in the output space spanned by \bar{z} , disturbances are not visible,

$$\bar{z} S_o = 0, \quad (2.14)$$

sensor noise is passed through with a factor 1 in the output space of T_o spanned by \bar{z} , as $\bar{z} T_o = \bar{z}$. In cases where the direction of sensor noise and the direction of disturbances are orthogonal, these algebraic relations do not necessary imply that performance is compromised.

2.2.2 Analytical limitations

Analytical limitations are induced by integral relations, such as the Bode sensitivity integral, [10]. These limitations lead to delicate tradeoffs when the (complementary) sensitivity function is to be minimized across frequencies. In SISO motion control, analytical limitations are eminent, leading to considerable performance degradation in practical applications, [3], [89]. In this section, we express the analytical limitations in terms of the sensitivity functions. In [90] these limitations are also expressed for the complementary sensitivity function. Performance limitations within a single input and single output generalized plant framework are discussed in [44]. For our analysis, the following lemma is required.

Lemma 2.2.1. *A single input single output, stable, closed loop sensitivity function $S = (I + L)^{-1}$, with L the open loop function, and where L has N_p RHP zeros and has N_z RHP poles can be factorized as,*

$$S(s) = \tilde{S}(s) B_p(s) B_z(s) \quad (2.15)$$

where $\tilde{S}(s)$ is minimum phase and has no RHP poles and $B_p(s)$, $B_z(s)$ are (all-pass) Blaschke products defined as,

$$B_p(s) = \prod_{i=1}^{N_p} \frac{p_i - s}{\bar{p}_i + s}, \quad B_z(s) = \prod_{i=1}^{N_z} \frac{z_i - s}{\bar{z}_i + s} \quad (2.16)$$

for the set of poles $\{p_i : i = 1, \dots, N_p\}$ and zeros $\{z_i : i = 1, \dots, N_z\}$ of $S(s)$ that lie in the open right half plane. Then,

$$\int_0^\infty \log(|S(j\omega)|) - \log(|S(j\infty)|) d\omega = \frac{\pi}{2} k_{HF} + \pi \sum_{i=1}^{N_p} \operatorname{Re} p_i + \pi \sum_{i=1}^{N_z} \operatorname{Re} z_i, \quad (2.17)$$

where,

$$k_{HF} = \lim_{s \rightarrow \infty} \frac{s(S(s) - S(\infty))}{S(\infty)}. \quad (2.18)$$

Proof. see [119, p. 54]. □

This leads to the Bode sensitivity integral for SISO systems, [10, 45].

Theorem 2.2.1. *A stable single input single output closed loop sensitivity function $S(s)$, with open loop $L(s)$ with relative degree two or more, must satisfy the following integral relation,*

$$\int_0^\infty \log |S(j\omega)| d\omega = \pi \sum_{i=1}^{N_p} \operatorname{Re} p_i + \pi \sum_{i=1}^{N_z} \operatorname{Re} z_i. \quad (2.19)$$

Proof. If the relative degree of the open loop is more than one, it follows that $\log(|S(\infty)|) = 0$ and $k_{HF} = 0$, in (2.17), [119, p. 318]. The N_p RHP zeros of the open loop are RHP poles of the sensitivity function. the N_z RHP poles of the open loop are the RHP zeros of the sensitivity function. So that (2.17) reduces to Thm. 2.2.1. □

This shows that reducing the sensitivity function in one frequency range, implies that the sensitivity function must increase at other frequencies. Most literature discusses the influence of unstable poles and zeros onto the performance tradeoffs, [45, 119]. In motion control systems, a common issue are bandwidth constraints imposed by plant uncertainty or sensor noise. At frequencies where plant uncertainty or sensor noise are large, the complementary sensitivity function must be small. By means of the algebraic relation, this implies that the sensitivity function is close to unity at those frequencies. Hence, the range where the sensitivity can be increased is limited. This leads to a frequency range where $|S| > 1$ if disturbances are to be rejected at other frequency ranges. Hence, the desirable property of the sensitivity function in one frequency range, must be traded off against an undesirable property of that sensitivity function at another frequency range.

In MIMO systems, poles, zeros, uncertainty and noise have directions associated with them. The influence of directions associated with unstable poles and

zeros on the performance limitations is discussed extensively in [26, 54]. Here, we are particularly interested in the influence of directions of noise and disturbances. An integral relation for MIMO systems was presented in [19, 47] and is repeated below.

Theorem 2.2.2. *Assume that the open loop function $L(s)$ is stable and all entries are rational functions with at least two more poles than zeros. Then, if the closed loop system is stable, the determinant of the output sensitivity function, $S_o = (I + L)^{-1}$, must satisfy,*

$$\int_0^\infty \log |\det(S_o(j\omega))| d\omega = 0 \quad (2.20)$$

Proof. See [19, 47]. □

Corollary 2.2.1. *With $\sigma_i(S_o)$ the i^{th} principal gain (singular value per frequency) of the output sensitivity matrix and the fact that $|\det(A)| = \prod_{i=1}^n \sigma_i(A)$, Thm. 2.2.2 implies that,*

$$\int_0^\infty \log \sigma_i(S_o(j\omega)) d\omega = F_i, \quad \text{and} \quad \sum_{i=1}^n F_i = 0. \quad (2.21)$$

So that,

$$\int_0^\infty \log \bar{\sigma}(S_o(j\omega)) d\omega \geq 0, \quad \int_0^\infty \log \underline{\sigma}(S_o(j\omega)) d\omega \leq 0. \quad (2.22)$$

From Cor.2.2.1 it follows that there exists a tradeoff for the *sum* of the log magnitudes of the principal gains. The terms F_i can be non-zero, hence, it is possible to exchange frequency wise tradeoffs between principal gains. Each principal gain is related to a principal input and output direction. In [26, 47] it is shown that the terms F_i become non-zero when the principal directions of the sensitivity function change rapidly in a small frequency region. If the principal directions change per frequency, it is difficult to relate a specific input and output of the sensitivity function to a particular principal gain of the sensitivity function. Therefore, it is difficult to exchange frequency wise tradeoffs between principal gains in practical control design.

Using Lem. 2.2.1, an alternative integral relation, originally proposed in [45] and studied elaborately in [132], can be useful to study performance tradeoffs in MIMO systems.

Theorem 2.2.3. *Consider a stable, minimum phase¹, $n \times n$ multivariable output sensitivity function, $S_o(s)$, with a stable open loop function with relative degree two*

¹For MIMO systems holds that ζ is a zero of system $H(s)$ if the rank of $H(\zeta)$ is less than the normal rank of $H(s)$. A system $H(s)$ is minimum phase if its transfer function matrix has only zeros in the open left half plane. A system $H(s)$ is non-minimum phase if its transfer function matrix contains zeros in the closed right half plane.

or more. Then, by pre and post multiplication with vectors $v, u \in \mathbb{C}^n, v^H u \neq 0$ the scalar transfer function $S_{vu}(s) = v^H S_o(s) u$, which has $z_i, i = \{1, \dots, N_z\}$ closed right half plane zeros, must satisfy,

$$\int_0^\infty \log |S_{vu}(j\omega)| d\omega = \log |v^H u| + \pi \sum_{i=1}^{N_z} \text{Re } z_i \quad (2.23)$$

Proof. As S_o is stable, the scalar transfer function S_{vu} is stable, and has at most the relative degree of $S_o(s)$. With Lem. 2.2.1, we have that $k_{HF} = 0$ and $\log |S_{vu}(\infty)| = \log |v^H u|$. Even if S_o is minimum phase, S_{vu} can become non-minimum phase. These zeros are contained in the set $\{z_i : i = 1, \dots, N_z\}$. \square

This implies that at an area where $|S_{vu}(j\omega)|$ is small, must be balanced by an equal area where $|S_{vu}(j\omega)|$ is large. As, due to uncertainty, the frequency interval where $|S_{vu}(j\omega)|$ is small is constrained, there must exist a frequency range where $|S_{vu}(j\omega)|$ is significantly larger than $|v^H u|$. If S_{vu} has non-minimum phase zeros, this tradeoff is even harder. The determination of those non-minimum phase zeros is not straightforward as there exist no simple relations between the MIMO open loop function $L(s) = G(s)K(s)$ and the non-minimum phase zeros of $S_{vu}(s)$. Typical choices of v, u illustrate how these frequency wise tradeoffs dictate multivariable control design.

Corollary 2.2.2. *When v, u are chosen to be elementary vectors e_i , $S_{vu}(s) = S_{o,ii}(s)$ equals the i^{th} diagonal element of the sensitivity transfer function matrix. As $e_i^T e_i = 1$, Theorem 2.2.3 reduces to the Bode integral relation for scalar systems, Theorem 2.2.1.*

Corollary 2.2.3. *To study non-diagonal terms of the sensitivity transfer function matrix, v, u can be chosen to approach orthogonal elementary vectors, $e_i^H e_j = \epsilon$, $0 < \epsilon \ll 1$, $S_{vu}(s) = e_i^T S_o(s) e_j$. Then,*

$$\lim_{\epsilon \rightarrow 0} \log(|e_i^H e_j|) = -\infty. \quad (2.24)$$

Then, considering (2.23), there is no limitation in minimizing $|S_{vu}|$.

Corollary 2.2.4. *By choosing $M = \text{Span}\{v_1, v_2, \dots, v_n\}$ with $u_i = v_j \in \mathbb{R}^n$ and $v_i^T v_j = 0$, an orthogonal transformation $S_{o,M}(s) = M^T S_o(s) M$ can be made. As this is a non-singular input output transformation, $S_{o,M}$ is minimum phase if S_o is minimum phase. Then on each new base Thm. 2.2.3 applies with $N_z = 0$.*

From Cor. 2.2.2 it follows that performance in each feedback loop from the i^{th} input of the plant to the i^{th} output of the plant, is bounded by the classical SISO integral relation. Hence, even if a system is multivariable and a multivariable centralized controller may be designed, the same performance limitations as in SISO systems apply for each loop. Considering, Cor. 2.2.3, it follows that there is no limitation to minimize a single non-diagonal term of the sensitivity function. Corollary 2.2.4, shows that if a system is decoupled with orthogonal transformations, the classical SISO integral relation apply in each decoupled direction.

Corollary 2.2.5. *The response to a disturbance entering the $n \times n$ closed loop stable system in a direction spanned by \bar{d} is given by $S_o(s)\bar{d}$. Then, $S_{\bar{z}\bar{d}}(s) = \bar{z}^H S_o(s)\bar{d}$ is the component of that disturbance that appears in the output direction spanned by \bar{z} . The transfer function from a single disturbance in direction \bar{d} to a single constant linear combination of outputs with direction \bar{z} must satisfy,*

$$\int_0^\infty \log |S_{\bar{z}\bar{d}}(j\omega)| d\omega = \log |\bar{z}^H \bar{d}| + \pi \sum_{i=1}^{N_z} \text{Re } z_i \quad (2.25)$$

where $z_i, i = \{1, \dots, N_z\}$ are the closed right half plane zeros of $S_{\bar{z}\bar{d}}(s)$.

Hence, it follows that if the direction of a disturbance is constant for all frequencies, and the performance is defined as a constant linear combination z , rejection of that disturbance at one frequency implies that the sensitivity function has to be increased at other frequencies *in that same direction*. Therefore, if specifications become tighter, it is crucial to reject disturbances only at frequencies and in directions that are relevant. If the structure of the controller is constrained, e.g. in the case of decentralized control, it may be impossible to reduce the sensitivity functions in only those directions that are relevant for disturbance rejection. In those cases, centralized control may be beneficial. This is illustrated with several examples in Chapter 4.

2.3 Decentralized control

Decentralized control involves the design of a diagonal controller, K , for a MIMO plant. Restricting the controller to a diagonal structure limits the class of controllers and thereby reduces the class of achievable closed loop functions. Requiring the controller to have a decentralized structure, may therefore lead to unnecessary limitations in achievable performance. Advantages of decentralized control are of practical nature. First, the number of elements of the transfer function matrix of the controller that are to be designed is reduced with $n^2 - n$ for square controllers. Second, in some applications, interaction of the plant is small, then, design of each element of the transfer function matrix of the controller can be carried out using SISO techniques. Hence, online re-tuning can be straightforward, as redesign has only localized effect.

The elements of the transfer function matrix of the decentralized controller can be designed either sequentially or independently. Both approaches will be discussed next. For notational clarity, the discussion is limited to diagonal decentralized controllers. With little work, the present framework can be extended to study block diagonal controllers (partially diagonal, partially centralized). Most of the theory of this chapter is a natural extension of concepts from robust control and was developed in [56, 109] and discussed in great detail in [92, 125].

2.3.1 Independent design

With independent decentralized control design, each element of the transfer function matrix of a decentralized controller is designed independently. This implies that in each design, the effects of other elements of the transfer function matrix of the decentralized controller are not taken into account. With the design of each element of the controller, a single output of the plant is fed back to a single input of the plant. Clearly, if plant interaction increases, the coupling between each control design increases. Therefore, one can expect that it is more difficult to design a decentralized controller independently if plant interaction is large. In this section, sufficient conditions for the independent designs are derived to account for stability and performance objectives of the total MIMO system. With this, it is illustrated how much plant interaction can be tolerated using an independent decentralized control design approach.

Stability by independent design

The goal is to derive sufficient conditions for each independent design that, if satisfied, guarantee closed loop stability of the total MIMO closed loop system. Plant interaction can be described as additive perturbations on the diagonal terms, $G_d = \text{diag}\{G\}$, of the plant,

$$G = G_d + G_{nd} \quad (2.26)$$

see also, Fig. 2.2a. In the following, it is assumed that G_d is invertible, a more general approach is discussed in [22]. The following closed loop functions are defined,

$$S_d = (I + G_d K)^{-1}, \quad T_d = I - S_d. \quad (2.27)$$

Herein, K , is the decentralized controller and has a diagonal transfer function matrix. Therefore, both S_d and T_d have diagonal transfer function matrices. Each diagonal element of S_d and T_d is determined by the design of a single element of the decentralized controller. It is investigated how interaction constraints the shape of S_d, T_d if each element of the decentralized controller is to be designed independently. An alternative way to study interaction due to non-diagonal terms of the plant, is to describe interaction as either a multiplicative output perturbation, E_T , Fig. 2.2b, or inverse multiplicative output perturbation, E_S , Fig. 2.2c, [109]. So that,

$$E_T = (G - G_d)G_d^{-1}, \quad E_S = (G - G_d)G^{-1}. \quad (2.28)$$

First, the influence of E_T is discussed, we will return to E_S later. The return difference matrix of the MIMO system can be factorized as,

$$(I + GK) = (I + E_T T_d)(I + G_d K). \quad (2.29)$$

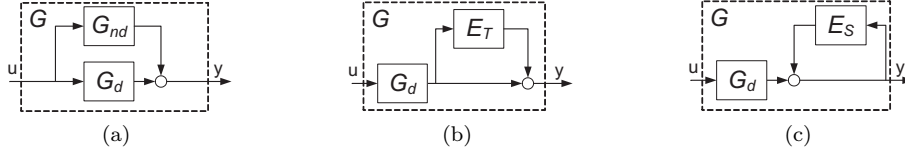


Figure 2.2: Different ways to describe interaction. *a)* Interaction as additive perturbation. *b)* Interaction as multiplicative output perturbation. *c)* Interaction as inverse multiplicative output perturbation.

To study nominal stability, the generalized Nyquist criterion can be factorized in a similar fashion, [56]. It is assumed that T_d is stable and the number of open loop unstable poles of $G_d K$ and GK equals p_d , p respectively. Then, using the Generalized Nyquist criterion, a necessary and sufficient condition for the closed loop stability of a system with open loop $L(s) = G(s)K(s)$ is that,

$$\mathcal{N}(\det(I + E_T(s)T_d(s))) = p_d - p \quad (2.30)$$

where $\mathcal{N}(\cdot)$ is the number or clockwise encirclement of the origin as s travels the Nyquist D-contour in a clockwise direction, see also [125, Lemma A.5, p.543], [56]. If $T_d(s)$ is stable and $G(s)$ is stable, a sufficient condition for stability of the overall MIMO system is, for $s = j\omega$,

$$\rho(E_T(j\omega)T_d(j\omega)) < 1, \forall \omega. \quad (2.31)$$

Herein, $\rho(\cdot)$, is the spectral radius, $\rho(\cdot) = \max_i |\lambda_i(\cdot)|$, [125]. The objective is to determine an interaction induced bound on T_d . Therefore, we will have to split up (2.31). The least conservative way to split up $\rho(E_T T_d)$ is by using the structured singular value² $\rho(E_T T_d) \leq \mu(E_T T_d)$ and the property that $\mu(E_T T_d) \leq \mu_{T_d}(E_T) \bar{\sigma}(T_d)$. Herein, $\mu_{T_d}(\cdot)$ means, that μ is calculated with respect to the block diagonal structure of T_d . Then, the following sufficient condition for closed loop stability becomes evident.

Theorem 2.3.1. *The MIMO system $(I + G(s)K(s))$ is stable if $G(s)$ is stable, $(I + G_d(s)K(s))$ is stable, and if, for $s = j\omega$*

$$\bar{\sigma}(T_d(j\omega)) < \mu_{T_d}^{-1}(E_T(j\omega)) \quad (2.32)$$

is satisfied for all frequencies ω .

Proof. See [92, p.371]. □

As $T_d(s)$ is a diagonal transfer function matrix, we find,

$$\bar{\sigma}(T_d(s)) = \max_i |T_{d,i}(s)|, \quad i = \{1, \dots, n\} \quad (2.33)$$

²The structured singular value with respect to the structure of Δ , namely $\mu_\Delta(M(s))$, is defined as $\mu_\Delta(M(s)) = \min_{\Delta} \{\bar{\sigma}(\Delta) \mid \det(I - M(s)\Delta) = 0, \text{ for structured } \Delta\}$, see [154, p.277].

where $T_{d,i}$ is the complementary sensitivity function of the i^{th} individual loop. Hence, it is clear that Thm. 2.3.1 provides a single bound for all n loops of a control system. Herein, only a non-parametric model, e.g., frequency response data, of the plant is required. Considering the inverse multiplicative output perturbation, E_s , (2.28), the same line of reasoning as in Thm. 2.3.1 can then be followed to derive the following theorem.

Theorem 2.3.2. *The MIMO system $(I + G(s)K(s))$ is stable if $G(s)$ is stable, $(I + G_d(s)K(s))$ is stable, and if, for $s = j\omega$*

$$\bar{\sigma}(S_d(j\omega)) < \mu_{S_d}^{-1}(E_S(j\omega)) \quad (2.34)$$

is satisfied for all frequencies ω .

Proof. See [92, p. 372]. □

Either the criterion of Thm. 2.3.1 or Thm. 2.3.2 must be achieved at all frequencies. Depending on the specific characteristics of T_d and S_d and the nature of E_T , E_S , one may prefer to use either Thm. 2.3.1 or Thm. 2.3.2. The theorems can not be combined over different frequency ranges, [124].

From Thm. 2.3.1, it follows that $\mu_{T_d}(E_T)$ must be small at frequencies where $\bar{\sigma}(T_d) \approx 1$, so at frequencies within the closed loop bandwidth. In case of integral control, or rigid body plant dynamics, $T_d \approx I$ at low frequencies. Hence, Thm. 2.3.1 shows that $\mu_{T_d}^{-1}(E_T) < 1$ at those frequencies. These observations give rise to controller independent measures of plant interaction that will be discussed later in this chapter.

Using, either Thm. 2.3.1 or Thm. 2.3.2, a single criterion is derived for all loops of the decentralized control design, see (2.33). As interaction can be highly structured, this single criterion may not provide enough information for the individual designs. Inspired by Gershgorin's theorem, [113], one can find an alternative way to split up Equation 2.31 which leads to the following sufficient condition for stability.

Theorem 2.3.3. *The MIMO system $(I + G(s)K(s))$ is stable if $G(s)$ is stable, $(I + G_d(s)K(s))$ is stable, and if for each i^{th} individual loop with scalar complementary sensitivity function $T_{d,i}(s)$ holds that, for $s = j\omega$,*

$$|T_{d,i}(j\omega)| < \frac{|G_{ii}(j\omega)|}{\sum_{i,i \neq j}^n |G_{ij}(j\omega)|} \quad \text{or} \quad |T_{d,i}(j\omega)| < \frac{|G_{ii}(j\omega)|}{\sum_{i,i \neq j}^n |G_{ji}(j\omega)|} \quad i = \{1, \dots, n\} \quad (2.35)$$

for all frequencies ω .

Proof. See [125, p.439] □

With this, we have obtained a bound for every loop of a decentralized control design. A bound for a single design may be smaller than the bound obtained from Thm. 2.3.1. The smallest bound in Thm. 2.3.3 is always smaller or equal than the bound obtained from Thm. 2.3.1, hence Thm. 2.3.3 is more restrictive.

The terms at the right hand side of (2.35), are the inverse of the Gershgorin bands and are related to the concepts of row and column dominance³ as used in classical Inverse Nyquist Array (INA) design method and Perron-Frobenius theory, see [113], [84, p.182]. Row and column dominance are dependent on the scaling of the inputs and outputs of the plant. A scaling independent measure is defined in the following.

Definition 2.3.1. *A system G , factorized using (2.28), is generalized diagonal dominant at frequencies ω_d when holds that either*

$$\mu_{T_d}(E_T(j\omega_d)) < 1 \quad \text{or} \quad \mu_{S_d}(E_S(j\omega_d)) < 1. \quad (2.36)$$

If a system is generalized diagonal dominant at frequency ω_d , there exists a similarity transformation, e.g., regular scaling matrix, D , so that $DG(j\omega_d)D^{-1}$, is diagonally dominant at frequency ω_d . This scaling matrix can be determined by calculating the upper bound of $\mu_{T_d}(E_T(j\omega_d))$,

$$\mu_{T_d}(E_T(j\omega_d)) \leq \min_{D \in \mathcal{D}} \bar{\sigma}(D(j\omega_d)E_T(j\omega_d)D(j\omega_d)^{-1}), \quad DT_d = T_dD. \quad (2.37)$$

A system $G(s)$ that is not diagonal dominant, but is generalized diagonal dominant, may be scaled with matrix D ,

$$G_s(j\omega_d) = D^{-1}G(j\omega_d)D \quad (2.38)$$

so that G_s is diagonal dominant at frequency ω_d , if,

$$\min_{D \in \mathcal{D}} \bar{\sigma}(D(j\omega_d)E_T(j\omega_d)D(j\omega_d)^{-1}) < 1, \quad (2.39)$$

[84, p.119]. The generalized dominance measure defined here, is less strict than the classical generalized dominance measure used in Perron-Frobenius theory, [84, p.182].

The generalized dominance concept is strongly related to so called *interaction measures*, [56]. The Rijnsdorp interaction measure, [112], per frequency ω , is defined for 2×2 systems as,

$$\kappa_R(G(j\omega)) = \frac{G_{12}(j\omega)G_{21}(j\omega)}{G_{11}(j\omega)G_{22}(j\omega)}. \quad (2.40)$$

³Let us define a square system G with $E_T = (G - \text{diag}\{G\})\text{diag}\{G\}^{-1}$ as in (2.28). Then, G is called row dominant if $\max_i \sum_j |e_{ij}| < 1$. The system G is column dominant if $\max_j \sum_i |e_{ij}| < 1$. A system is diagonal dominant if it is either row or column dominant, [84, p.65].

If $\kappa_R(G) \approx 0$, there is no interaction. As $\mu_{T_d}(E_T) = \sqrt{\kappa_R(|G|)}$, it is clear that Rijnsdorp interaction measure is related to generalized dominance. The relative gain array, [20], per frequency ω is defined as,

$$\Lambda_{RGA}(\omega) = G(j\omega) \times (G(j\omega)^{-1})^T \quad (2.41)$$

where \times denotes element-wise multiplication. At frequencies where the relative gain array approaches the identity matrix, two sided interaction is small. For 2×2 systems holds that,

$$\Lambda_{RGA}(\omega) = \begin{bmatrix} \lambda_{RGA} & 1 - \lambda_{RGA} \\ 1 - \lambda_{RGA} & \lambda_{RGA} \end{bmatrix}, \quad \lambda_{RGA} = \frac{1}{1 - \kappa_R(G)}. \quad (2.42)$$

Which again shows the relation between the relative gain array and the generalized dominance measure. In some applications, interaction measures may provide more insight than the generalized dominance measure. Some control relevant interpretations are presented in [125, p.89]. While most of these interpretations have proven to be useful in proces industry, control relevant interpretation of the relative gain array is still challenging for motion system applications, [145]. The relative gain array is commonly used as a scaling independent measure to visualize plant interaction.

Performance by independent design

The objective is to relate performance specifications of the overall MIMO system, to the specifications of the independent individual loop designs. Sufficient conditions can be derived for each independent design, that, if satisfied, guarantee performance of the total MIMO system. Considering (2.29), it follows that,

$$S_o = S_d(I + E_T T_d)^{-1}, \quad (2.43)$$

so that when E_T is large, disturbance rejection properties of S_o are not explicitly related to the properties of S_d . In [92], [124], theory is developed to translate overall robust performance objectives into bounds on individual designs. Herein, theory from [123] and [56] is combined for analysis within the generalized plant framework.

A standard condition for robust performance of the MIMO system is achieved when the system is nominally stable and

$$\mu_{\Delta_p}(M) < 1, \quad \forall \omega, \|\Delta_p\|_\infty \leq 1, \quad (2.44)$$

where Δ_p is full, $M = \mathcal{F}_l(P, K)$ with the generalized plant P , [125]. Considering $\Delta = \text{diag}\{\Delta_p, \Delta_s\}$, where Δ_s can be used to take into account uncertainty, Fig. 2.3a, a sufficient condition for robust performance is stated with the following theorem, [124].

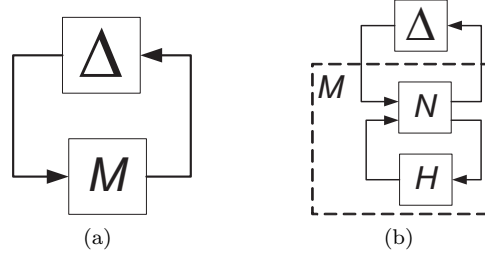


Figure 2.3: Using the LFT to derive sufficient conditions for robust performance. a) General $M\Delta$ robust performance problem. b) Robust performance expressed as a bound on H .

Theorem 2.3.4. *The lower fractional transformation of N and H , is defined as $M = N_{11} + N_{12}H(I - N_{22}H)^{-1}N_{21}$, Fig. 2.3b. Assume that $\mu_{\Delta}(N_{11}) < k$ and $\det(I - N_{22}H) \neq 0$. Then, for a given constant k , holds that,*

$$\mu_{\Delta}(M) \leq k, \quad (2.45)$$

if

$$\bar{\sigma}(H) \leq c_H, \quad (2.46)$$

where c_H solves,

$$\mu_{\tilde{\Delta}} \left[\begin{array}{cc} N_{11} & N_{12} \\ kc_H N_{21} & kc_H N_{22} \end{array} \right] = k, \quad \tilde{\Delta} = \text{diag}\{\Delta, H\}. \quad (2.47)$$

Proof. See [124]. □

This shows that (robust) performance specifications of the overall, $M\Delta$, MIMO system can be translated into sufficient conditions on a specific closed loop function H . The frequency dependent variable c_H , that appears in this sufficient condition, can be determined at each frequency, by solving (2.47) implicitly. For this, one may use a bisection method or skewed- μ , [125, p. 312].

The transfer function H can be any closed loop function of interest, for example, M can be written as the LFT of S_d or T_d . This can be done in two steps. The first step is to write M as an LFT of S_o , T_o ,

$$\begin{aligned} M &= \mathcal{F}_l(N^{T_o}, T_o) \\ &= N_{11}^{T_o} + N_{12}^{T_o} T_o N_{21}^{T_o}, \end{aligned} \quad (2.48)$$

and

$$\begin{aligned} M &= \mathcal{F}_l(N^{S_o}, S_o) \\ &= N_{11}^{S_o} + N_{12}^{S_o} S_o N_{21}^{S_o}. \end{aligned} \quad (2.49)$$

Then, the second step is to use the observation that, [92],

$$\begin{aligned} T_o &= GG_d^{-1}T_d(I + E_T T_d)^{-1} \\ S_o &= S_d(I - E_S S_d)^{-1}G_d G^{-1}, \end{aligned} \quad (2.50)$$

which are LFT's in T_d and S_d respectively. Hence, M can be written as the LFT of S_d, T_d ,

$$\begin{aligned} M &= \mathcal{F}_l(N^{T_d}, T_d) \\ &= \mathcal{F}_l(N^{S_d}, S_d), \end{aligned} \quad (2.51)$$

with,

$$N^{T_d} = \begin{bmatrix} N_{11}^{T_o} & N_{12}^{T_o} G G_d^{-1} \\ N_{21}^{T_o} & -E_T \end{bmatrix}, \quad N^{S_d} = \begin{bmatrix} N_{11}^{S_o} & N_{12}^{S_o} \\ G_d G^{-1} N_{21}^{S_o} & E_S \end{bmatrix}. \quad (2.52)$$

Now, Theorem 2.3.4 implies that, at the frequency ω_p , the performance of the overall closed loop system is guaranteed if either,

$$\bar{\sigma}(T_d) \leq c_{T_d}, \quad \text{or} \quad \bar{\sigma}(S_d) \leq c_{S_d}, \quad (2.53)$$

is satisfied at that particular frequency, where c_{T_d}, c_{S_d} solve,

$$\mu_{\tilde{\Delta}} \begin{bmatrix} N_{11}^{T_o} & N_{12}^{T_o} G G_d^{-1} \\ c_{T_d} N_{21}^{T_o} & -c_{T_d} E_T \end{bmatrix} = 1, \quad \text{and} \quad \mu_{\tilde{\Delta}} \begin{bmatrix} N_{11}^{S_o} & N_{12}^{S_o} \\ c_{S_d} G_d G^{-1} N_{21}^{S_o} & c_{S_d} E_S \end{bmatrix} = 1, \quad (2.54)$$

with $\tilde{\Delta} = \text{diag}\{\Delta_p, K\}$ where Δ_p has full and K a diagonal structure. In contrast to the nominal stability conditions from Thm. 2.3.1, Thm. 2.3.2, the conditions (2.53) may be combined over different frequencies. The robust performance conditions are only sufficient, but tight, [123]. This implies that there can exist controllers that do not satisfy the bounds, but still achieve robust performance. In that case, there also exist controllers that result in the same values of $\bar{\sigma}(S_d)$ and $\bar{\sigma}(T_d)$ that do not achieve robust performance.

Only in the case that these conditions are satisfied over *all* frequencies, robust stability is achieved as a by-product of robust performance. Alternatively, one can use the test for robust performance to derive relations for nominal performance. This will be illustrated in Example 2.3.1. From (2.54), it follows that robust performance of the overall system may be quite different from robust performance of the sub-parts of the system as E_T and E_S increase. Interaction can be beneficial, high E_S, E_T do not necessarily imply degradation of robust performance. Illustrative examples of this can be found in [92]. An example for the disturbance and noise rejection control problem is shown next.

Example 2.3.1. *For the disturbance and noise rejection control problem studied later in Chapter 4.3, we have,*

$$M = \begin{bmatrix} W_{z_1} S_o V_d & -W_{z_1} T_o V_n \\ -W_{z_2} K S_o V_d & -W_{z_2} K S_o V_n \end{bmatrix}. \quad (2.55)$$

The objective is to derive sufficient conditions for decentralized control design to achieve nominal performance of the overall MIMO system. It follows straightforwardly that,

$$N^{T_o} = \left[\begin{array}{cc|c} W_{z1}V_d & 0 & -W_{z1} \\ 0 & 0 & -W_{z2}G^{-1} \\ \hline V_d & V_n & 0 \end{array} \right] \quad (2.56)$$

and

$$N^{S_o} = \left[\begin{array}{cc|c} 0 & -W_{z1}V_n & W_{z1} \\ -W_{z2}G^{-1}V_d & -W_{z2}G^{-1}V_n & W_{z2}G^{-1} \\ \hline V_d & V_n & 0 \end{array} \right]. \quad (2.57)$$

Using (2.52) and Thm. 2.3.4, it follows that at a given frequency ω_p , performance of the overall MIMO system is guaranteed if either

$$\bar{\sigma}(T_d(j\omega_p)) \leq c_{T_d}(\omega_p), \quad \text{or} \quad \bar{\sigma}(S_d(j\omega_p)) \leq c_{S_d}(\omega_p) \quad (2.58)$$

is satisfied. Where c_{T_d} , c_{S_d} solve, e.g., by means of skewed- μ or a bisection method,

$$\mu_{\tilde{\Delta}} \left[\begin{array}{cc|c} W_{z1}V_d & 0 & -W_{z1}GG_d^{-1} \\ 0 & 0 & -W_{z2}G_d^{-1} \\ \hline c_{T_d}V_d & c_{T_d}V_n & -c_{T_d}E_T \end{array} \right] = 1 \quad (2.59)$$

and

$$\mu_{\tilde{\Delta}} \left[\begin{array}{cc|c} 0 & -W_{z1}V_n & W_{z1} \\ -W_{z2}G^{-1}V_d & -W_{z2}G^{-1}V_n & W_{z2}G^{-1} \\ \hline c_{S_d}G_dG^{-1}V_d & c_{S_d}G_dG^{-1}V_n & c_{S_d}E_S \end{array} \right] = 1 \quad (2.60)$$

respectively, with $\tilde{\Delta} = \text{diag}\{\Delta_p, K\}$.

In this section, stability and performance requirements are translated to criteria on independent designed loops of a decentralized control system. These criteria are controller independent. Hence, one can take no advantage from knowledge of earlier designed loops. A consequence of this, is that closed loop stability can only be proven if plant interaction is sufficiently small. This requirement may be rather demanding for some applications. In the next section, it is briefly discussed how decentralized controllers can be designed while specifically taking into account the effect of earlier designed control loops.

2.3.2 Sequential design

As was shown in the previous section, the independent design requires interaction to be small. If plant interaction is large, closed loop stability can not be proven,

rendering the independent design method infeasible. Also, from a practical perspective, the requirement to design a decentralized controller independently may be unnecessary restrictive. In many design procedures, controllers are designed one loop at a time. Between each design step, calculations may be performed where one utilizes information about the controllers specified in earlier design steps.

This sequential design procedure is central in this section. There are some drawbacks that are not straightforward to resolve. First, the ordering of the design steps may have great impact on the achievable performance. There is no general approach to determine the best sequence for design. This may lead to many design iterations, especially for large MIMO systems. Second, there are no guarantees that robustness margins in earlier designed loops are preserved. The robustness margins at each design step do not indicate robustness of the final closed loop system. Third, as each design step usually considers only a single output, the responses in earlier designed loops may degrade, making iterative design necessary.

In spite of these issues, sequential design is a technique that has found application in many practical control problems. Various sequential design methods are developed in the framework of Quantitative Feedback Analysis, [50, 58, 150]. In, [22, 85], relations between sequential design and Gauss elimination of the return difference are investigated. Also, cascade control design, is often quite similar to sequential design, [125, p. 422].

Stability by sequential design

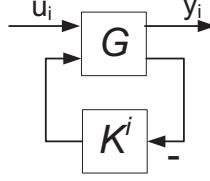
The underlying idea of achieving closed loop stability by means of sequential control design is yet another way to factorize the return difference, (2.1). In sequential design, each single input single output controller k_i , from $K = \text{diag}\{k_i\}$, $i = \{1, \dots, n\}$, is designed using the fact that, [86],

$$\det(I + GK) = \prod_{i=1}^n \det(1 + g^i k_i), \quad (2.61)$$

where for each i^{th} design step, the equivalent plant g^i is defined as,

$$g^i = \mathcal{F}_l(G, -K^i) \quad (2.62)$$

where $K^i = \text{diag}\{k_j\}$, $j = \{1, \dots, n\}$, $j \neq i$, see Figure 2.4. The multivariable system is nominally closed loop stable if in each design step the system is closed loop stable. The system remains closed loop stable if the loops are opened in the reverse order as in they were designed. If an arbitrary loop is opened there is no guarantee for closed loop stability. The robustness margins in each design step do not guarantee robust stability of the final multivariable system, [47]. However, sufficient conditions for robust stability can be derived as a by-product of robust performance using the framework presented below.

Figure 2.4: Equivalent plant for the i^{th} design step in sequential design

Performance by sequential design

Using Thm. 2.3.4, sufficient conditions for robust performance can be derived for sequential design, [28]. In each i^{th} design step, bounds on closed loop functions must be calculated. Herein, the effect of all earlier designed controllers is taken into account. The relations in Section 2.3.1 can be used to derive new sufficient conditions for sequential design.

For example, considering the diagonal sensitivity function S_d , we find,

$$S_d = \mathcal{F}_l(\bar{N}^{s_{d,i}}, s_{d,i}), \quad s_{d,i} = (1 + g_{ii}k_i)^{-1} \quad (2.63)$$

with

$$\bar{N}^{s_{d,i}} = \begin{bmatrix} S_d^i & e_i \\ e_i^T & 0 \end{bmatrix} \quad (2.64)$$

where e_i are elementary vectors and S_d^i is $n \times n$ and holds all the diagonal elements of S_d except the i^{th} one, $S_d^i = \text{diag}\{(1 - \delta_{ij})s_{d,j}\}$, $j = \{1, \dots, n\}$ where δ_{ij} is the Kronecker delta. So that using (2.51),

$$\begin{aligned} M &= \mathcal{F}_l(N^{S_d}, \mathcal{F}_l(\bar{N}^{s_{d,i}}, s_{d,i})) \\ &= \mathcal{F}_l(N^{s_{d,i}}, s_{d,i}) \end{aligned} \quad (2.65)$$

From Thm. 2.3.4, it follows that a sufficient condition for robust performance of the final design is obtained when in each i^{th} design step, the following is achieved,

$$|s_{d,i}| \leq c_{s_{d,i}} \quad (2.66)$$

where $c_{s_{d,i}}$ solves,

$$\mu_{\tilde{\Delta}} \begin{bmatrix} N_{11}^{S_o} - N_{12}^{S_o} S_d^i (I + E_S S_d^i)^{-1} G_d G^{-1} N_{21}^{S_o} & N_{12}^{S_o} (I - S_d^i E_S)^{-1} e_i \\ c_{s_{d,i}} e_i^T (I - E_S S_d^i)^{-1} G_d G^{-1} N_{21}^{S_o} & c_{s_{d,i}} e_i^T E_S (I - S_d^i E_S)^{-1} e_i \end{bmatrix} = 1,$$

with $\tilde{\Delta} = \text{diag}\{\Delta_p, k_i\}$. Sufficient conditions on different closed loop transfer functions may be combined. Compared to the sufficient conditions for the independent designs, (2.53), the sequential design conditions may be less restrictive

as the effect of all earlier designed controllers is taken into account. This is beneficial in particular when bandwidths are different in each loop. One must take care however, that the ordering of the sequential design steps may have significant effect on the sufficient conditions. Furthermore, as $N^{s_{d,i}}$ is a function of k_i , it is not straightforward to achieve (2.66). This is particularly difficult at frequencies where the plant interaction is large.

If the sufficient condition for robust performance are satisfied for each, s_{d_i} at all frequencies, one achieves robust stability of the MIMO system. For robust stability, multiple sufficient conditions can not be combined over different frequency regions. Alternatively, one may derive bounds on the sensitivity function of the equivalent plant,

$$s^i = (1 + g^i k_i)^{-1}, \quad g^i = \mathcal{F}_l(G, -K^i) \quad (2.67)$$

in the spirit of the factorization used in (2.61). Again, Thm. 2.3.4 can be used in combination with a lower fractional transformation, $M = \mathcal{F}_l(N^{s^i}, s^i)$. These relations are rather elaborate and are beyond the scope of this work. The reader is referred to [28, 60] for more information.

2.4 Open loop decoupling

Most complexity issues in multivariable control design arise from interaction between inputs and outputs of the plant. A method to reduce this complexity is to redefine the inputs and outputs of the plant so that the open loop has less interaction at a certain loop breaking point. Ideally, a MIMO plant can then be decoupled in SISO subsystems, and each SISO subsystem can be controlled independently. Decoupling the plant in physical variables, namely $G_p(s)$, boils down to finding input, $T_u(s)$, and output, $T_y(s)$, transformation transfer function matrices such that

$$G(s) = T_y(s)G_p(s)T_u(s), \quad (2.68)$$

has no interaction, so the transfer function matrix $G(s)$ is diagonal, Fig. 2.5. In that case, when choosing a diagonal controller K , the open loop, evaluated at loop breaking point X is decoupled. At other loop breaking points however, interaction may still be present and may even increase because of the decoupling transformations. Furthermore, a disturbance that acts on a single physical output of the plant, d_o , may now be observed in multiple newly defined outputs of the plant. Hence, to reject this disturbance, it can be required that more elements of the controller are to be used. In spite of these issues, the ability to decouple,

$$L = GK \quad (2.69)$$

implies that closed loop functions $S_o = (I + L)^{-1}$, $T_o = LS_o$ are decoupled as well and $S_i = S_o$, $T_i = T_o$. Then, stability of the MIMO system is achieved by

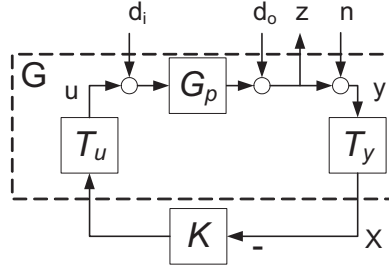


Figure 2.5: Decoupling control architecture, unity feedback.

stabilizing each decoupled loop. As each decoupled loop can be designed independently, the complexity of $n \times n$ MIMO control design is reduced to that of n independent SISO designs.

Finding dynamic decoupling transformations $T_u(s)$ and $T_y(s)$ normally boils down to a non-convex problem, [29, 140]. Therefore, in most methods, either $T_y(s)$ or $T_u(s)$ is fixed at the expense of design freedom, [29, 84]. Design of dynamic decoupling methods is often ad-hoc and therefore requires specific physical insights, [84]. Dynamic decoupling of mechanical systems often suffers from robustness issues, [73, 140]. A common strategy is to try to decouple $G_p(s)$ with frequency-independent input-output transformations, $T_u, T_y \in \mathbb{R}$ and study if the residual interaction is small enough to allow decentralized control design. If residual interaction is not sufficiently small, centralized control must be applied. Fortunately, there exists a large class of systems that can be decoupled using frequency-independent input and output transformations. Several classes of these systems are discussed next.

2.4.1 Dyadic systems

A general class of systems that can be decoupled with frequency independent input and output transformations are the so called *dyadic* systems. This system property was first introduced in [98, 99] and has been used in motion control in [4, 141].

Definition 2.4.1. An $n \times n$ multivariable system $G_p(s)$ is called *dyadic* when there exist $T_u, T_y \in \mathbb{R}^{n \times n}$, so that the transfer function matrix,

$$G(s) = T_y G_p(s) T_u \quad (2.70)$$

is *diagonal*.

A dyadic system can be considered as a system that has n natural modes, where each mode shape is aligned with a single column and row of T_y, T_u respectively,



Figure 2.6: The laboratory MIMO system.

[100]. Practical systems often have an infinite number of modes, but can be considered as approximately dyadic when n dominant modes can be decoupled using constant input and output transformations. Then, these systems can be decoupled up to a certain degree, or in a limited frequency range, [101]. We therefore may use the following definition.

Definition 2.4.2. An $n \times n$ multivariable system $G_p(s)$ is ϵ -approximately dyadic in a frequency interval $[\omega_1, \omega_2]$ if it holds that $\exists T_u, T_y \in \mathbb{R}^{n \times n}$ so that,

$$\bar{\sigma}(E_T(j\omega_p)) < \epsilon, \quad G(j\omega) = T_y G_p(j\omega) T_u, \quad \forall \omega \in [\omega_1, \omega_2] \quad (2.71)$$

for a sufficiently small value of $\epsilon \in \mathbb{R}$. Herein, $E_T(j\omega) = G_{nd}(j\omega)G_d(j\omega)^{-1}$, where $G_d(j\omega)$ holds the diagonal elements of $G(j\omega)$ and $G_{nd}(j\omega) = G(j\omega) - G_d(j\omega)$.

The term E_T can be considered as multiplicative output perturbation due to residual interaction of non-dyadic dynamics of the plant. A framework to take this into account in control design is presented in Section 2.3.1.

Input and output transformations T_y, T_u can be determined from a frequency response measurement, [15, 102]. For implementation, T_y, T_u must be realizable. Hence, T_y, T_u are to be approximated with real valued matrices. The ALIGN algorithm, [84], can be used to find real approximate inverses of complex matrices. Furthermore, decoupling transformation can be derived from a kinematic model of the system, [12]. Also, measures on the size of E_T can be used in a cost function to find decoupling transformations T_y, T_u by means of numerical optimization, [140] and [84, p.148]. The following example illustrates how the property of a dyadic system can be used to find decoupling transformations.

Example 2.4.1. This example shows how the concept of dyadic systems can be used to decouple a multivariable system. A laboratory MIMO motion system, consists of two DC motors with position measurements (encoders) connected with an elastic belt, Fig. 2.6, [32]. As the system is reflective symmetric, [102],

$$G_p(s) = \begin{bmatrix} G_1(s) & G_2(s) \\ G_2(s) & G_1(s) \end{bmatrix} \quad (2.72)$$

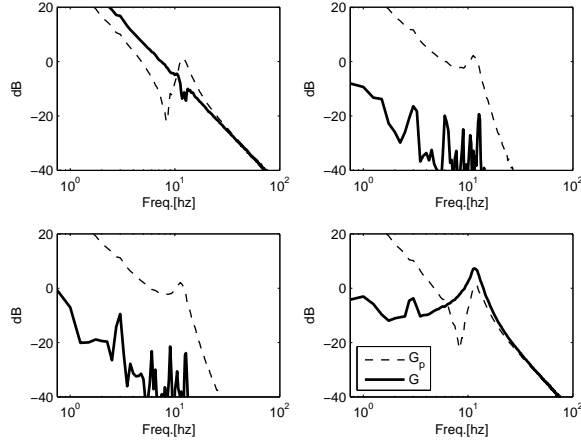


Figure 2.7: Bode magnitude of laboratory MIMO system before, $G_p(s)$, and after decoupling, $G(s)$

there exist eigen vectors,

$$u_1 = \begin{bmatrix} 1 \\ 1 \end{bmatrix}, u_2 = \begin{bmatrix} -1 \\ 1 \end{bmatrix}, \quad U = [u_1 \mid u_2], \quad (2.73)$$

with $G_p(s) = UG(s)U^{-1}$, where U is constant for all frequencies. Hence, the system is dyadic. The eigenvector u_1 is the rigid body mode shape, u_2 is the mode shape due to the elastic band. The decoupling transformations are $T_u = U$, $T_y = T_u^{-1}$. A Bode magnitude plot of the system before, $G_p(s)$, and after decoupling, $G(s)$, is depicted in Fig. 2.7. At frequencies below 4Hz, the plant can not be considered to behave linear anymore, [32]. In Fig. 2.8, the value $\mu_{T_d}^{-1}(E_T)$ is plotted per frequency for the plant in physical coordinates $G_p(s)$, where $E_T = (G_p - \text{diag}\{G_p\})\text{diag}\{G_p\}^{-1}$, see Thm. 2.3.1. It is visible that, when the plant is controlled in physical coordinates, interaction limits the achievable bandwidth significantly. After applying decoupling transformations, the residual interaction is studied plotting $\mu_{T_d}^{-1}(E_{T,d})$, where $E_{T,d}$ models the residual interaction as multiplicative output perturbations. Realistic robustness considerations imply that $\bar{\sigma}(T_d) < 10\text{dB}$. Hence, as for closed loop stability we desire $\bar{\sigma}(T_d) < \mu_{T_d}^{-1}(E_{T,d}), \forall \omega$, it is visible that the elements of the decentralized controller can be designed independently if the bandwidth of each design is below 100Hz.

2.4.2 Pseudo SVD systems

It was shown that systems that are dyadic, allow frequency independent input output transformations so that the closed loop functions are decoupled at a particular

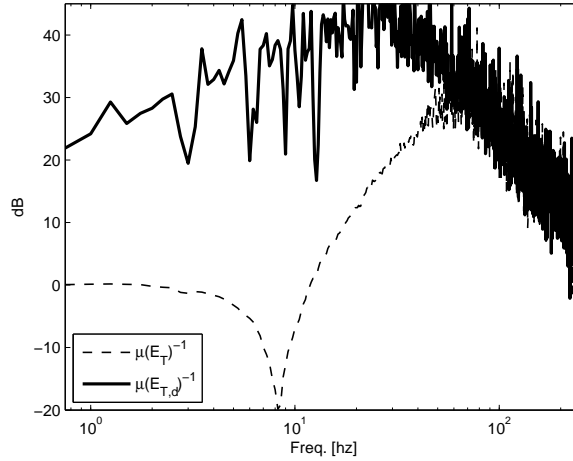


Figure 2.8: The value of $\mu_{T_d}(E_T)$ per frequency for the laboratory MIMO setup, $G_p(s)$, and after decoupling, $G(s)$

loop breaking point. This property is useful to achieve stability of multivariable systems. Even though the open loop is decoupled, it is still difficult to relate the directions of the open loop to the directions of closed loop functions. A specific class of systems that provides more insight in this, are systems that are dyadic and where additionally T_u, T_y are both orthogonal, they are called pseudo singular value decomposition (SVD) systems.

Definition 2.4.3. A square system $G_p(s)$ is called a pseudo singular value decomposition (SVD) system if there exist $U, V \in \mathbb{R}^{n \times n}$, $U^T = U^{-1}, V^T = V^{-1}$, so that the transfer function matrix,

$$G(s) = U^T G_p(s) V \quad (2.74)$$

is diagonal.

The class of pseudo singular value decomposition (SVD) systems arise naturally from design methods that rely on the singular value decomposition, see [63, 104]. This is because pseudo SVD systems have input (right) and output (left) principal directions that are constant for all frequencies. In [59, 146], the structural properties of pseudo SVD systems are exploited in robust control design. Furthermore, pseudo SVD systems are closely related to dyadic systems and mechanical systems, [4]. A dyadic system is a pseudo SVD system if the matrices T_u, T_y in Def. 2.4.1 are unitary matrices. If the plant $G_p(s)$ is a pseudo SVD system, decoupling is equivalent to defining a controller as $K_p(s) = V K(s) U^T$ where $K(s)$ is diagonal. The open loop at loop breaking point X, Fig. 2.5 is decoupled. So

that follows,

$$G_p K_p = UG(s)K(s)U^T, \quad K_p G_p = VK(s)G(s)V^T, \quad U^T U = I, V^T V = I \quad (2.75)$$

The output sensitivity function, input sensitivity function, output complementary sensitivity function and input complementary sensitivity function evaluated at X equal,

$$S_o = (I + GK)^{-1}, \quad S_i = (I + KG)^{-1} \quad (2.76)$$

$$T_o = GK(I + GK)^{-1}, \quad T_i = KG(I + KG)^{-1}, \quad (2.77)$$

which are all diagonal. However, the sensitivity functions in physical variables,

$$S_o^p = (I + G_p K_p)^{-1} = U S_o U^T, \quad T_o^p = U T_o U^T \quad (2.78)$$

$$S_i^p = (I + K_p G_p)^{-1} = V S_i V^T, \quad T_i^p = V T_i V^T, \quad (2.79)$$

are not diagonal. This shows that when the direction of an output disturbance d_o in physical variables is aligned with the first column of U , a single feedback loop can be tuned to reject this disturbance. The effect of that disturbance will be distributed onto the performance variables z with the gain of the elements of the first row of U , Fig. 2.5. Furthermore, it is visible that the input directions of $K_p(s)$ determine the input and output directions of S_o^p, T_o^p . The output directions of $K_p(s)$ are the input and output directions of S_i^p, T_i^p . For the control sensitivity and process sensitivity holds that,

$$K_p S_o^p = V K S_o U^T, \quad S_o^p G_p = U S_o G V^T. \quad (2.80)$$

Here it is visible that the input and output directions of these sensitivity functions can be different. Another useful property of pseudo SVD systems is that the decoupling transformations are norm invariant. Hence it follows that,

$$\bar{\sigma}(S_o^p) = \bar{\sigma}(S_o) \quad (2.81)$$

This shows that at a single frequency, the worst case disturbance rejection of the coupled closed loop system equals the disturbance rejection properties of one of the decoupled loops. Instead of only the worst case disturbance rejection, rejection in other directions can be designed as well. As all decoupled loops can be designed independently, disturbance rejection can be designed for each orthogonal direction at a time. This property will be exploited in Section 4.2. Pseudo SVD systems provide much insight into the directional aspects of multivariable control design. Because of the requirement of open loop decoupling, the input and output directions of the sensitivity functions can not be chosen freely. The consequences of this issue are discussed in detail in Section 4.3.

2.4.3 Mechanical systems

Some mechanical systems can be decoupled with frequency independent decoupling transformations. The dynamic behavior of motion systems is most often

dominated by mechanics. Therefore, physical interpretation of the mechanical systems can facilitate transparent multivariable control design and decoupling. From either finite element modeling, linearized first principle modeling, or reduced order continuous system descriptions, the following finite-dimensional, linear, multiple degree of freedom equations of motion can be derived, [31],

$$\begin{aligned} M\ddot{q} + D\dot{q} + Kq &= B_o u \\ y &= C_{oq}q. \end{aligned} \quad (2.82)$$

Herein, M, D, K are the mass matrix, viscous damping matrix and stiffness matrix respectively. In this model, only position measurements are considered. Extensions to include velocity and acceleration measurements can be found in [52]. We assume that the mass matrix is positive definite and the stiffness matrix is semi-positive definite. Several assumptions on the properties of D will be discussed shortly. The vector $q \in \mathbb{R}^{n_s}$ represents the displacement of the nodes of the lumped parameter system. From the undamped vibration problem, without input, the real mode shapes ϕ and eigen or natural frequency ω can be determined solving the following generalized eigenvalue problem,

$$K\phi = \omega^2 M\phi, \quad \phi \neq 0. \quad (2.83)$$

The zero valued eigen frequencies correspond to rigid body modes of the system. With p times multiplicity of eigen frequencies, there exists a set of p linearly independent eigen modes shapes. Then, these eigen mode shapes are not unique. Let the modal matrix Φ contain columns that span the directions of the mode shapes $\phi_i, i = 1, \dots, n_s$. Then, the equations of motion (2.82), can be expressed in *modal* coordinates,

$$\begin{aligned} M_m \ddot{\eta} + D_m \dot{\eta} + K_m \eta &= \Phi^T B_o u \\ y &= C_{oq} \Phi \eta, \end{aligned} \quad (2.84)$$

where $M_m = \Phi^T M \Phi$ and $K_m = \Phi^T K \Phi$ are diagonal. The matrix $D_m = \Phi^T D \Phi$ is only diagonal in special cases. For example, in case of Rayleigh or proportional damping, where it is assumed that, $D = \alpha M + \beta K$ with α, β nonnegative scalars, [31, p.303]. Also with modal or classic damping, D_m is diagonal, [31]. These damping models are often justified for structural analysis of lightly damped systems, [31, 52]. When D_m is diagonal and (2.84) is multiplied from the left with M_m^{-1} , one obtains,

$$\begin{aligned} \ddot{\eta} + 2Z\Omega\dot{\eta} + \Omega^2\eta &= M_m^{-1}\Phi^T B_o u \\ y &= C_{oq}\Phi\eta, \end{aligned} \quad (2.85)$$

where $\Omega^2 = M_m^{-1}K_m$, $Z = \text{diag}\{\zeta_i\}, i = 1, \dots, n_s$ are diagonal. We define,

$$y(s) = G_p(s)u(s), \quad (2.86)$$

where, $G_p(s)$ follows from (2.85). With the assumption that D_m is diagonal and defining $C_m = C_{oq}\Phi$, $B_m = M_m^{-1}\Phi^T B_o$, with Φ real valued, we write,

$$G_p(s) = C_m G_m(s) B_m, \quad (2.87)$$

with

$$G_m(s) = \text{diag}\{g_{m,i}(s)\}, \quad g_{m,i}(s) = \frac{1}{s^2 + 2\zeta_i\omega_i s + \omega_i^2}, i = \{1, \dots, n_s\}. \quad (2.88)$$

Then the following observation is evident,

Proposition 2.4.1. *A mechanical system is dyadic if D_m , in (2.84), is diagonal and both C_m, B_m are non-singular.*

Hence, the ability to decouple a mechanical system (with modal or proportional damping) depends on the actuator and sensor locations, the number of (dominant) modes and the alignment of mode shapes with the sensor and actuator matrices; dominant modes must be both in $\text{Ker}(C_m)^\perp$ and in $\text{Im}(B_m)$. Detailed procedures to design actuator and sensor locations for decoupling and control can be found in [52, 91].

If the system has rigid body modes in all six cartesian degrees of freedom, twelve eigenfrequencies will be equal to zero. Then, there exist a set of six linear independent eigenvectors. One may choose any orthogonal base to decouple the rigid body behavior of the system, [12]. Each axis of this base may be aligned with specific performance objectives or a particular disturbance direction, see Section 4.2. When the number of sensors and actuators exceed the number of rigid body modes, and C_m, B_m are invertible, in addition to rigid body decoupling, flexible modes may be decoupled, hence controlled independently, [12, 15, 115].

A mechanical system can be ϵ -approximately dyadic. Note that (2.87) can be written as a sum of rank one systems, each with a frequency independent input and output direction,

$$G_p(s) = \sum_{i=1}^{n_s} \frac{c_{m,i} b_{m,i}}{s^2 + 2\zeta_i\omega_i s + \omega_i^2}, \quad (2.89)$$

where $c_{m,i}$ and $b_{m,i}$ are real valued. Also, $c_{m,i}$ and $b_{m,i}$ are the i^{th} row of B_m and the i^{th} column of C_m respectively. Let us assume that the eigen frequencies are ordered as $\omega_1 \leq \omega_2 \leq \dots \leq \omega_{n_s}$. Then, a few modes with eigen frequencies $\omega_{n_l}, \dots, \omega_{n_h}$ that are well separated from the others, so that $\omega_{n_l-1} \ll \omega_{n_l}, \omega_{n_h} \ll \omega_{n_h+1}$ can be isolated as,

$$G_p(s) = \sum_{i=1}^{n_l-1} \frac{c_{m,i} b_{m,i}}{s^2 + 2\zeta_i\omega_i s + \omega_i^2} + \sum_{i=n_l}^{n_h} \frac{c_{m,i} b_{m,i}}{s^2 + 2\zeta_i\omega_i s + \omega_i^2} + \sum_{i=n_h+1}^{n_s} \frac{c_{m,i} b_{m,i}}{s^2 + 2\zeta_i\omega_i s + \omega_i^2}.$$

For the frequency region $\omega_{n_l-1} \ll \omega \ll \omega_{n_h+1}$ the plant can be approximated as,

$$G_p(s) \approx \sum_{i=1}^{n_l-1} \frac{c_{m,i} b_{m,i}}{s^2} + \sum_{i=n_l}^{n_h} \frac{c_{m,i} b_{m,i}}{s^2 + 2\zeta_i\omega_i s + \omega_i^2} + \sum_{i=n_h+1}^{n_s} \frac{c_{m,i} b_{m,i}}{\omega_i^2} \quad (2.90)$$

$$= \frac{1}{s^2} G_l + \sum_{i=n_l}^{n_h} \frac{c_{m,i} b_{m,i}}{s^2 + 2\zeta_i\omega_i s + \omega_i^2} + G_h. \quad (2.91)$$

In the case that,

$$G_{n_l, n_h}(s) = \sum_{i=n_l}^{n_h} \frac{c_{m,i} b_{m,i}}{s^2 + 2\zeta_i \omega_i s + \omega_i^2}, \quad (2.92)$$

is dyadic, input output transformations that decouple $G_{n_l, n_h}(s)$ may not necessarily result in decoupling of G_l and G_h . With the input and output transformations T_y, T_u that make $T_y G_{n_l, n_h}(s) T_u$ diagonal, we write,

$$G(s) = T_y G_p(s) T_u \quad (2.93)$$

$$\approx T_y G_{n_l, n_h}(s) T_u + T_y \left(\frac{1}{s^2} G_l + G_h \right) T_u, \quad (2.94)$$

and define,

$$E_T(s) = T_y \left(\frac{1}{s^2} G_l + G_h \right) T_u (T_y G_{n_l, n_h}(s) T_u)^{-1}. \quad (2.95)$$

This shows, by Def. 2.4.2, that a mechanical system is ϵ -approximately dyadic in frequency region $[\omega_{n_l}, \omega_{n_h}]$ only if $\bar{\sigma}(E_T(s)) < \epsilon$ for a sufficiently small value of ϵ . In this frequency interval, G_{n_l, n_h} dominates the dynamic behavior of the system over $\frac{1}{s^2} G_l$ and G_h . This can be used to construct additional sufficient conditions for stability and performance for the control design based on the dynamics of G_{n_l, n_h} , based on the framework in Section 2.3.1, [14].

Example 2.4.2. *Here, we focus on the control of linear time invariant electromechanical motion systems that have the same number of actuators and sensors as rigid body modes. Typical applications are high performance positioning stages used in semiconductor manufacturing, electron microscopy or component placement machines. The dynamics of such systems are often dominated by the mechanics, which are therefore constructed to be light and stiff, so that resonance modes due to flexible dynamics appear only at high frequencies.*

$$G_p(s) = \sum_{i=1}^{N_{rb}} \frac{c_i b_i^T}{s^2} + \sum_{i=N_{rb}+1}^N \frac{c_i b_i^T}{s^2 + 2\zeta_i \omega_i s + \omega_i^2}. \quad (2.96)$$

Herein, N_{rb} denotes the number of rigid body modes. The parameters ζ_i, ω_i are the relative damping and resonance frequency of the flexible modes. The vectors c_i, b_i span the directions of the i^{th} mode shapes and are constant for all frequencies. The resonance frequencies ω_i are high, hence the plant can be approximately decoupled using static input (and/or output) transformations, T_u, T_y respectively so that,

$$\begin{aligned} G_{yu}(s) &= T_y G_p(s) T_u \\ &= G(s) + G_{flex}(s), \quad G(s) = \frac{1}{ms^2} I, \end{aligned} \quad (2.97)$$

where $m \in \mathbb{R}^1$ and $G_{flex}(s)$ contains the flexible dynamics of the plant and is often non-diagonal. In many applications, the frequencies and damping of the resonance

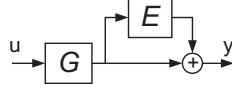


Figure 2.9: Multiplicative perturbation at the output of the plant to model influence of flexible dynamics.

modes changes in the life cycle of the plant and is sensitive to changes in position. Hence, inversion of these dynamics leads to robustness problems. The objective is to control the rigid body behavior of the plant with high fidelity. The influence of the flexible dynamics can then modeled as a multiplicative perturbation at the output of the plant $G(s)$,

$$G_{yu}(s) = (I + E(s))G(s), \quad (2.98)$$

with $E(s) = G_{flex}(s)G^{-1}(s)$, see also Fig. 2.9.

With a multivariable controller $K(s)$, the plant $G(s) = \frac{1}{ms^2}I$, and stable sensitivity function $S_o = (I + GK)^{-1}$, the closed loop system is stable when $\rho(E(j\omega)T_o(j\omega)) < 1, \forall \omega$, [56]. A sufficient condition for this is,

$$\bar{\sigma}(T_o(j\omega)) < \bar{\sigma}(E(j\omega))^{-1}, \forall \omega. \quad (2.99)$$

As $E(j\omega)$ is large at high frequencies, this shows that the flexible dynamics limit the bandwidth of the closed loop system. Hence, one is forced to make frequency wise tradeoffs if disturbances are to be rejected in motion systems.

The scaling of the plant can be interpreted as multiplication of the controller with a diagonal matrix. With this example, uncertain flexible dynamics can be translated into sufficient conditions on closed loop functions. These closed loop functions are designed considering a plant model with remarkable simple structure.

Example 2.4.3. In some high performance applications, see e.g., [143], systems are constructed to be light and stiff. Also, all contact to the world (friction, parasitic stiffness) is compensated for. In low frequencies, the rigid body dynamics are then dominant, and the contribution of the flexible dynamics at these frequencies can be modeled as,

$$G_{flex}(s)|_{s \rightarrow 0} = \sum_{i=1+n_{rb}}^{n_s} \frac{c_{m,i} b_{m,i}}{s^2 + 2\zeta_i \omega_i s + \omega_i^2} |_{s \rightarrow 0} = K_{flex}, \quad (2.100)$$

so that a model of the mid and low frequency behavior equals,

$$G_{LF}(s) = \frac{1}{s^2} K_{rb} + K_{flex}. \quad (2.101)$$

The rigid body dynamics are dyadic, so that constant input output transformations can be used to decouple this part of the dynamics. Due to the multiplicity of the

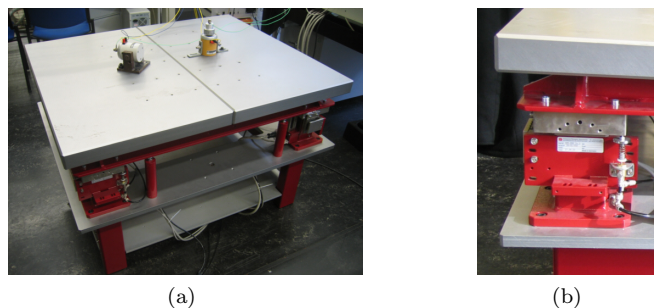


Figure 2.10: The active vibration isolation system (AVIS). *a*) Top view of the AVIS *b*) One passive isolator module of the AVIS.

rigid body modes, decoupling transformations are non-unique. This can be used to align decoupled loops with disturbances, performance objectives or K_{flex} . A design method for this is presented in Section 4.2. In tracking control problems, the contribution of the flexible dynamics at low frequencies can be compensated for using jerk derivative (snap) feedforward, as reported in [11] and published in [13, 16, 17, 18, 75, 76].

2.5 Decentralized control design for the AVIS

In this section, we illustrate some MIMO control design concepts by application to the industrial active vibration isolation system (AVIS), depicted in Fig. 2.10a. This system is used in industry to isolate delicate equipment from disturbances in the environment. Typical application areas are semi conductor industry, electron microscopy and biomedical engineering, [40]. The rejection of disturbances in such a system is a typical multivariable control problem. We show that, even after kinematic decoupling, the plant has significant interaction. The implications of interaction on the ability to apply independent decentralized control design will be discussed in this section.

2.5.1 The AVIS

The goal of the AVIS is to isolate the table from disturbances from the environment (floor) and to reject disturbances from acting directly on the table. In order to achieve this, a passive and an active suspension system are used in parallel. The passive vibration isolation system has four isolator modules containing pneumatic air-mounts and a mechanical leveling system, Fig. 2.10b. The passive isolator modules result in lightly damped suspension modes at low frequencies. The system is open loop stable. The active vibration isolation system can be

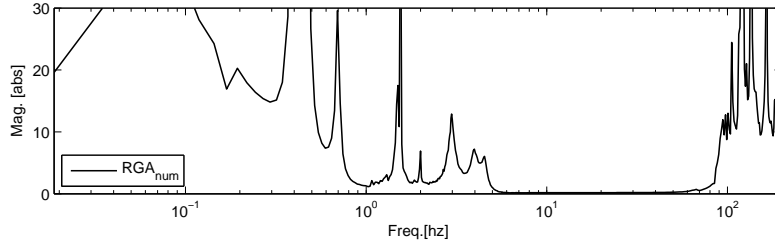


Figure 2.11: Relative gain array number of the AVIS after kinematic decoupling.

employed driving two linear motors in each of the four isolator modules while measuring the absolute velocity of the table by means of geophones. Three of the four isolator modules contain two geophones each. Therefore, the AVIS has eight inputs and six outputs. Using a kinematic model, the force of each actuator can be expressed as a contribution to forces and torques at the center of gravity. A similar relation can be derived for the sensors. These kinematic relations are used to approximately decouple the plant dynamics in the frequency region where the plant behaves as a rigid body, [111, 133]. The inputs and the outputs of the plant are then expressed at the center of gravity of the table in a six cartesian coordinates.

A frequency response of the kinematic decoupled plant is obtained by exciting each cartesian input at a time with multi-sines from 0.02 – 200Hz while measuring all cartesian outputs of the plant. The frequency response is shown in Fig. A.1. The suspension modes due to the passive isolator modules show up around 1.5 – 5Hz. As a result of limited mechanical stiffness of the connections between the isolator modules and the table, resonance dynamics appear above 70Hz. These modes may change slowly in time and are therefore treated as uncertainty. At frequencies below 0.1Hz, the system can not be considered to behave linear anymore due to friction dynamics. The plant interaction is significant, to get a first impression of the plant interaction, one may plot the *relative gain array number* per frequency, defined as, [125, p. 82],

$$RGA_{num}(\omega) = \|\Lambda_{RGA}(\omega) - I\|_{sum}. \quad (2.102)$$

Herein, $\Lambda_{RGA}(\cdot)$ is the relative gain array, see (2.41) and $\|\cdot\|_{sum}$ is the sum matrix norm, $\|A\|_{sum} = \sum_{i,j} |a_{ij}|$. At frequencies where interaction is small, the relative gain array approaches the identity matrix, hence the relative gain array *number* approaches zero. The relative gain array number of the plant after kinematic decoupling is shown in Fig. 2.11. The relative gain array itself is shown in Fig. A.2. It is visible that the interaction is small at frequencies between 5 – 70Hz, where the plant behaves as a rigid body, but is large elsewhere. The implications of interaction for the feedback control design of the active vibration isolation system are discussed in the following section.

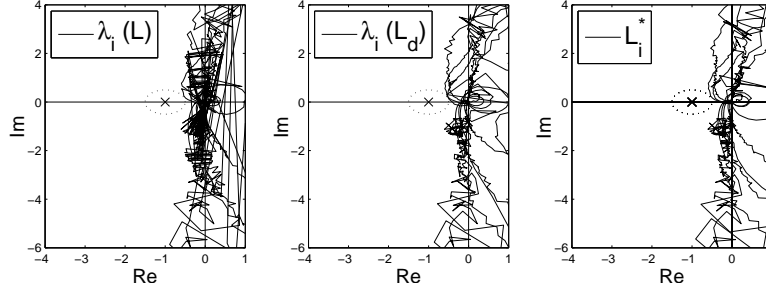


Figure 2.12: Characteristic loci of the open loop with a decentralized feedback controller. Left: characteristic loci of $L = GK$, Middle: characteristic loci of $L_d = G_d K$, Right: characteristic loci of each i^{th} single input single output equivalent open loop L_i^* .

2.5.2 Feedback control design

A decentralized feedback controller for the active suspension system is to be designed. The objective is to increase the damping of the passive suspension modes and minimize the influence of disturbances to the output of the plant. The disturbances are not specified, a more detailed discussion on this is presented in Chapter 3. As the plant dynamics above 70Hz are uncertain, the open loop should have sufficient roll-off at high frequencies. A common strategy to achieve those goals is to apply so called *sky-hook damping*, [61]. A similar strategy is followed in this control design.

For each cartesian axis, we design a controller with proportional gain and second order low-pass filter,

$$k_i(s) = k_p \frac{(2\pi f_{lp})^2}{s^2 + 2\zeta_{lp} 2\pi f_{lp} s + (2\pi f_{lp})^2}, \quad i = \{x, y, z, R_x, R_y, R_z\}, \quad (2.103)$$

so that the open loop will have at least two cross-over frequencies. Where necessary, a notch filter is designed to suppress narrow band resonance phenomena. Considering the Nyquist plot of the open loop function $L_d = G_d K$, where G_d holds the diagonal elements of G , it is visible that $S_d = (I + G_d K)^{-1}$ is stable, Fig. 2.12. Using the generalized Nyquist criterion, Def. 2.1.2, the characteristic loci of $L = GK$ are also shown in Fig. 2.12. As the characteristic loci of $L = GK$ do not encircle the point $(-1, 0)$, the feedback controller results in closed loop stability of the AVIS. This is a necessary and sufficient condition for closed loop stability. As the plant interaction is significant, redesign of a controller in a single axes may change any characteristic locus. More detailed analysis is required to make redesign of this given controller possible.

The role of individual feedback loops and the influence of interaction can be

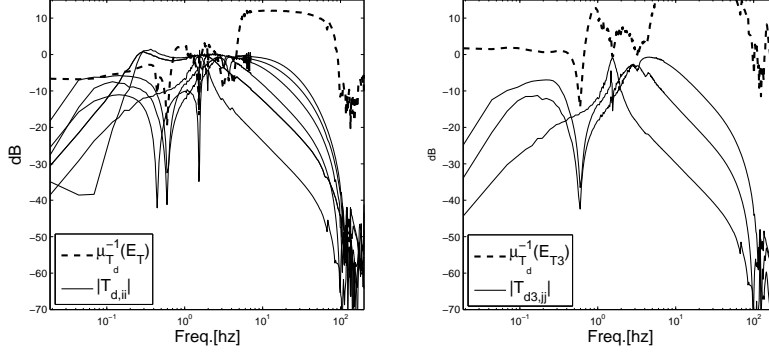


Figure 2.13: Graphical representation of the sufficient condition for closed loop stability. Left: independent decentralized control of all cartesian axis. Right: independent decentralized control in the y, z and R_y axis, while other loops are closed.

investigated using Thm. 2.3.1. Unfortunately, this is only a sufficient condition and may therefore lead to conservative designs. Theorem 2.3.1 states that the MIMO system is closed loop stable if G is stable, $(I + G_d K)$ is stable, and

$$\bar{\sigma}(T_d) < \mu_{T_d}^{-1}(E_T), \quad \forall \omega. \quad (2.104)$$

Herein, $E_T = (G - G_d)G_d^{-1}$ and $T_d = (I + G_d K)^{-1}G_d K$. As $\bar{\sigma}(T_d) = \max_i |T_{d,ii}|$, the contribution of each i^{th} independent closed loop function can be related to the bound $\mu_{T_d}^{-1}(E_T)$. In Fig. 2.13, it is shown that each closed loop function $T_{d,ii}$ crosses $\mu_{T_d}^{-1}(E_T)$ and therefore, the sufficient condition for closed loop stability is not achieved. Hence, the decentralized feedback controller cannot be designed in each cartesian axis independently. The effect of redesign of a single controller on the closed loop stability is not sufficiently transparent in this way.

As the desire to design a controller for each cartesian axis independently is not realistic for this application, one may use a sequential design strategy. Each i^{th} loop can be studied when all other loops are closed, defining the i^{th} equivalent open loop function,

$$L_i^* = \mathcal{F}_l(F_u(L, -I_{i-1}), -I_{n-i}), \quad (2.105)$$

see Fig. 2.14a, [118]. As each equivalent open loop does not encircle the point $(-1, 0)$ in the Nyquist plane, Fig. 2.12, it is shown that the closed loop MIMO system with the given controller is stable. With sequential design, the redesign of a single equivalent open loop may change all other equivalent open loops. Hence, there is no guarantee that the margins of other equivalent open loops are preserved. Commonly, this implies that the sequential design has to be iterated. For this application, this appears to be of minor concern. To illustrate this, both L

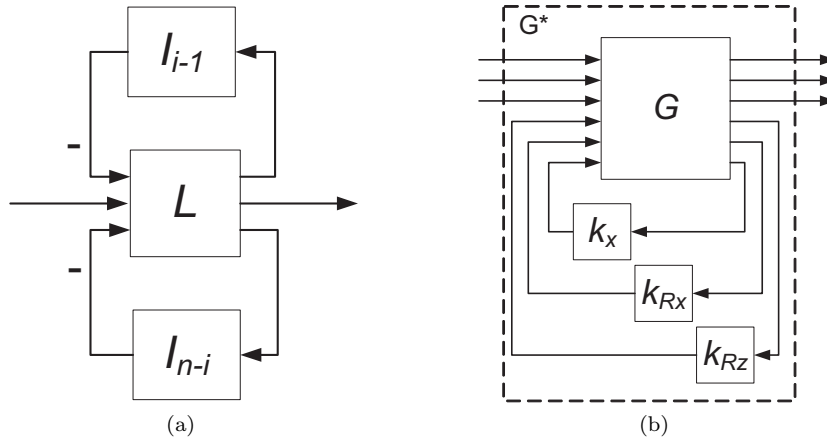


Figure 2.14: a) Equivalent open loop L_i^* . b) The equivalent plant G^* with three loops closed.

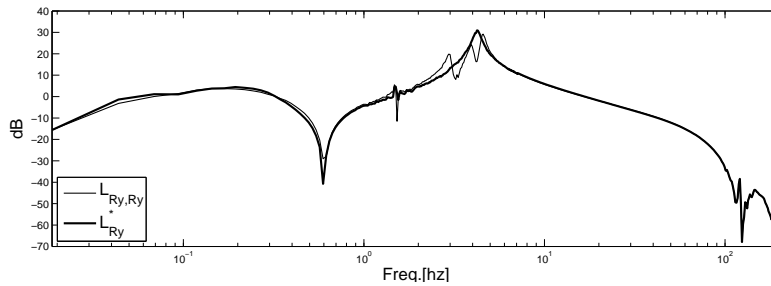


Figure 2.15: Thick: the equivalent open loop when all loops except the R_y loop are closed, $L_{R_y}^*$. Thin: the R_y, R_y element of the open loop $L = GK$.

and $L_{R_y}^*$ are shown in Fig. 2.15. It is visible that the modes at 1.5, 3, 4, 5Hz are damped. However, the general shape of $L_{R_y}^*$ is almost similar to L_{R_y, R_y} . This is also observed in other equivalent open loops. Therefore, sequential design for this application is rather intuitive. It is found that it is possible to increase the proportional gain for all controllers except the controller for the x -axis.

A third, alternative, design approach can be followed that combines the insights from sequential and independent decentralized control design. Herein, one can close certain loops, calculate the resulting equivalent plant and analyse if the inputs and outputs of this equivalent plant can be controlled independently. From the relative gain array, Fig. A.2, it is clear that suspension modes result in interaction at frequencies from 1 – 5Hz. Feedback control of a single loop may result in an equivalent plant that has considerable more damping in these suspension

modes. After many trial and error designs, it appears that the equivalent plant G^* with loops x, R_x and R_z closed, Fig. 2.14b, can be controlled independently. We define $E_{T3} = (G^* - G_d^*)(G_d^*)^{-1}$ where G_d^* holds the diagonal elements of G^* . The sufficient condition for closed loop stability then becomes,

$$\bar{\sigma}(T_{d3}) < \mu_{T_{d3}}^{-1}(E_{T3}), \quad \forall \omega. \quad (2.106)$$

This is shown graphically in Fig. 2.13 (right figure). As this condition is just satisfied, it is possible to design the decentralized controller for the loops, y, z and R_y independently while the loops x, R_x and R_z are closed.

2.5.3 Discussion

It is shown that the AVIS, with kinematic decoupling, has significant plant interaction that lead to typical multivariable issues for feedback control design. Frequency independent decoupling by means of a kinematic model resulted in small interaction in the frequency region where the plant behaves as a rigid body. At other frequency regions, interaction was large so that a feedback controller cannot be designed for each cartesian axis independently. Sequential design of the decentralized controller was shown to be a feasible approach. The drawbacks that usually come with sequential design (many iterations, ordering of the design sequence, etc.) turn out to be of minor concern for this particular application.

The AVIS is not a dyadic system as decoupling at one frequency range does not imply decoupling at another frequency range. The decoupling transformations used in this section are not unique. Alternatively, one may consider decoupling based on the mode shapes of the suspension modes. As the suspension modes have very low damping, the mode shapes are almost real. The inverse of the modal matrix, Section 2.4.3, will directly lead to the frequency independent decoupling transformations. Still, dynamics below 1Hz and above 70Hz may not be aligned with the suspension mode shapes, hence result in interaction. This alternative decoupling approach requires additional physical insight that may be obtained using modal analysis or more general identification techniques.

The output sensitivity function and process sensitivity function are shown in Fig. A.3, Fig. A.4 respectively. Compared to the AVIS with only the passive vibration isolation system (open loop), the active vibration isolation (closed loop) results in significantly less amplification of disturbances in the frequency range 1 – 5Hz, due to damping of the suspension modes. The output of the plant with and without feedback control is shown in Fig. 2.16. When we look more specifically to, for example, the R_z -axes, Fig. 2.17, it is visible that disturbances just outside the bandwidth are amplified. This is a typical implication of the Bode's integral formulae, Section 2.2. Hence, although vibrations due to the suspension mode at 2Hz are rejected, disturbances at low and high frequencies are more amplified than when the AVIS is operating in open loop. Therefore, depending on the disturbance characteristics, feedback control may or may not result in better

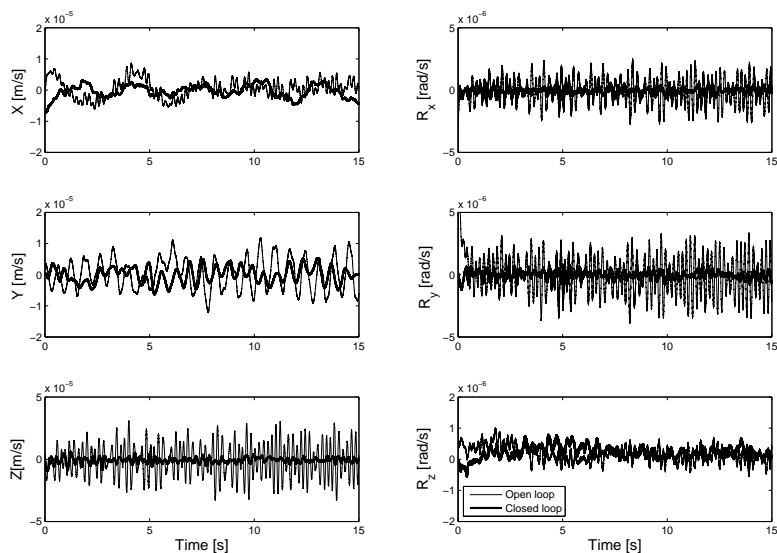


Figure 2.16: Output of the AVIS in open loop (thin) and closed loop (thick).

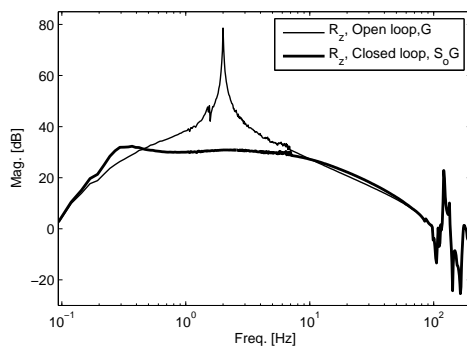


Figure 2.17: The R_z axis of the AVIS, plant G and process sensitivity $S_o G$.

time domain performance. This is shown in Fig. 2.18 where the AVIS is excited with a broad band disturbance at the input of the plant.

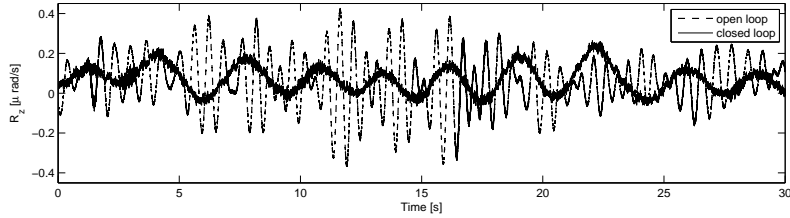


Figure 2.18: Output of the AVIS in open loop (thin) and closed loop (thick) in the R_z axis.

2.5.4 Conclusion

In this section, it was shown that the AVIS, with kinematic decoupling, has interaction that leads to some typical multivariable stability design issues. The same, decentralized, feedback controller was used to illustrate different tests for closed loop stability. The characteristic loci showed that the system is closed loop stable. However, the sufficient conditions for closed loop stability with independent decentralized control design were not achieved. The tests for sequential decentralized control design showed that the system was closed loop stable. The drawbacks of sequential design depend strongly on the application, but turned out to have little consequences for control design of the AVIS. It was shown that a combination of sequential and independent design can be used to isolate parts of the AVIS that can be controlled independently.

2.6 Disturbance rejection

In the previous sections, some of the complexity issues of MIMO control design are discussed. In some applications, one may use open loop decoupling transformations to isolate parts of the plant that can be stabilized independently. The controller, expressed in new variables, can be (block) diagonal so that relatively simple (SISO like) control techniques can be used to achieve closed loop stability. Transformations that factorize criteria for closed loop stability, based on (2.2), may not imply that the disturbance rejection control problem is simplified.

In multivariable systems, directions of exogenous signals play an important role. Directions of disturbances are determined by the ratio in which exogenous signals are dispersed over the controlled variables. From Section 2.4, we know that when a disturbance acts on a single physical variable of the plant, open loop decoupling transformations imply that this disturbance is distributed over many controlled variables. Then, the disturbance direction is determined by the decoupling transformations. In many applications, disturbances at each controlled variable, may

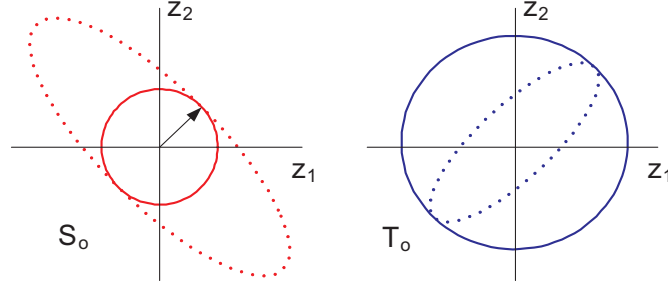


Figure 2.19: Rejection of disturbance in fixed direction at a single frequency using decentralized control (solid) and centralized control (dotted)

result from just a few physical causes (sources). Characterization of these sources and the way they are dispersed over the controlled variables may facilitate physical interpretation of the direction of disturbances.

To understand the role of directions in the disturbance rejection control problem, we consider the following relation,

$$z = S_o d_o - T_o n. \quad (2.107)$$

Herein, d_o, n , denote the output disturbance and sensor noise respectively. The objective is to keep the performance variable z as small as possible in presence of d_o and n . We study the rejection of d_o , which has direction \bar{d}_o ,

$$d_o(s) = \bar{d}_o v_d(s). \quad (2.108)$$

At a single frequency p , the singular value decomposition of $S_o(p)$ is $S_o(p) = U_{S_o} \Sigma_{S_o} V_{S_o}^H$. Then, $z(p)$ is small if the last column of V_{S_o} is aligned with \bar{d}_o , so that $v_d(p)$ is amplified with the smallest singular value of S_o . Hence, two issues rise immediately. First, the control designer must be able to shape V_{S_o} in such a way that a particular singular value related to a particular singular value of S_o is aligned with the disturbance. Therefore, one must be able to relate the feedback controller with the input space of closed loop functions. Second, the singular values of S_o that amplify the disturbance are to be designed sufficiently small. To achieve this, one must derive relations between the singular values of S_o and the feedback controller.

If high gain feedback is applied in all directions, the sensitivity function is small at all frequencies and in all directions. This results in high disturbance rejection performance. However, high gain feedback implies that other design objectives may be more difficult to achieve. This is illustrated in Fig. 2.19. Herein, the input space of the closed loop functions of a 2×2 system is depicted. An output disturbance, d_o , acts at two controlled variables z_1, z_2 . If the disturbance is considered to act independently on both variables z_1, z_2 , it is natural to apply a decentralized

controller to minimize the sensitivity function in the directions of the controller variables. As a consequence of the algebraic limitations, noise is amplified in both z_1 and z_2 directions, see right hand side of Fig. 2.19. Alternatively, if one has determined that d_o acts in one direction, one may apply centralized control, to minimize the sensitivity function in that direction and at the same time allow the sensitivity function in orthogonal directions to increase. The input principal direction of S_o , related to the minimum principal gain of S_o , is then aligned with the direction of d_o . The costs, as implied by the algebraic limitations, are then reduced as amplification of noise in the direction of d_o is increased but amplification of noise in directions orthogonal to that is not. Additionally, the analytical limitations discussed in Section 2.2, point out that minimization of the sensitivity function at one frequency range in one direction, implies that the sensitivity function increases at other frequencies in the same direction.

Hence, as specifications become tighter, it is required to minimize sensitivity functions only in the frequency ranges and the directions that are relevant for disturbance rejection. Therefore, it may be desired to design closed loop transfer functions with different gains in different directions (non-uniform gain). If the directions of disturbances and sensor noise are not canonical, def. 2.1.3, centralized controllers may be required and control design can be complicated. A technique to characterize disturbance directionality in multivariable systems is discussed in the next chapter. Herein, the AVIS is used as an illustrative example. In Chapter 4, methods are developed to design multivariable controllers that accommodate directions of disturbances.

Chapter 3

Characterization of disturbances in multivariable systems

Rejection of disturbances in multivariable systems poses challenges in many applications, due to the number of controlled variables, and the interaction between these controlled variables, [122]. Although in theory, solutions are readily available, [125], [84], it is widely recognized that practical application of this theory is far from trivial, [143],[102]. Therefore, the structure of plant dynamics is often exploited to either reduce the degrees of freedom, [48], or decouple controlled variables, [56], [59]. Even then, the multivariable nature of disturbances complicates performance system analysis. In this chapter, a method is developed to interpret the characteristics of multivariable disturbances. With this, the acquired physical insights into the disturbance situation can be used to simplify control design for multivariable systems.

Disturbances result from a combination of phenomena (sources, causes) that can not be measured individually. Only a mixture of these phenomena is observed, acting on many controlled variables at the same time. This problem typically emerges in motion control, where multiple degrees of freedom deviate from their intended position due to disturbances emanated from just a few sources, e.g., pump, floor, and machine vibrations. In these cases, performance of the multivariable system is determined by only a few dominant sources, often less than the number of controlled variables. Conventional disturbance modeling approaches result in white noise coloring filters to describe the spectral content of the observed disturbances. Examples of such approaches can be found in [81, 127, 131].

Although these approaches can straightforwardly be applied to model the multivariable aspects of disturbances, [133], most of these techniques are not aimed at identifying the number of causes that generate the observed multivariate disturbances. As the size of multivariable systems increases, it is more difficult to rely on physical insight to interpret and characterize the nature of these sources. Therefore, there is a strong desire to develop techniques to identify sources that generate disturbances in multivariable systems.

As no direct measures of the sources are available, one faces a *blind* identification problem. Blind identification problems can not be solved in general. Hence, assumptions on the expected model structure are required to find solutions for particular applications. In this work, it is assumed that the ratio in which a source propagates over the controlled variables (the direction) is fixed. Typical examples of this are disturbances that originate from sources that have a fixed physical location. Also, the control system architecture can give rise to fixed direction disturbances, see, e.g., [122]. This allows us to adopt techniques that are used in the field of information theory, direction of arrival problems and array processing. See [24], [30] for a survey. A common approach is the use of independent component analysis (ICA) techniques to solve these blind identification problems within some inherent indeterminacies, [137]. ICA was applied in diagnostics of chemical processes [134], [80, 134], rotating machinery monitoring [152], and fault detection [120, 135]. The ICA signal model, that is used to model the disturbances, assumes no particular (e.g. consecutive) ordering of the observations (disturbances). Consequently, one must assume that the sources are mutually statistically independent. Then, higher order statistics (skewness, kurtosis, etc.) of the observations can be used in ICA solvers. Estimates of higher order statistics have large variance, and are notorious to be sensitive to outliers, [106]. Also, as higher order statistics of Gaussian signals are zero, ICA is not able to identify sources that are Gaussian. In some applications, it is argued that the assumption of statistical independence in the basic ICA signal model is not justified, [5].

In our identification problem, the observed disturbances are collected as consecutive samples in the time domain. Also, it is justified to assume that sources are either temporal non-white or non-stationary. Hence, the time structure of the observed disturbances can be exploited to solve the blind identification problem within indeterminacies. Instead of using general ICA, one can use methods that rely on a set of second order statistics of the observations, like the Second Order Blind Identification (SOBI) method of [7]. As no higher order statistics are required, sources are allowed to be Gaussian and statistically dependent, [106]. A contribution of this work is to illustrate that the signal model assumptions of SOBI are naturally justified in the disturbance identification problem. The consequences of these assumptions differ from the original field of application and are therefore discussed in greater detail.

A related problem is to determine how many dominant phenomena contribute

to the observed disturbances. This is especially challenging in the presence of small interfering, noisy, signals. In literature on basic ICA, this problem is often attacked with a pre-processing step using principal component analysis (PCA), [65], or Karhunen-Loève analysis, [93]. These techniques assume a particular spatial structure of the noise signals [8], [25], which is not always justified in our identification problem. It is shown that PCA can be naturally integrated in the SOBI method. But it is also shown that such approaches may fail dramatically, especially when sources act almost in the same direction. It is illustrated that post-processing of the results from SOBI leads to a much more reliable estimate of the number of dominant sources.

The theory is applied to an identification problem of the 6×6 MIMO active vibration isolation system discussed in Section 2.5. This system is controlled in six cartesian axes. All controlled loops suffer from only a few synthetically added sources. Only the error of the feedback system is used in identification. It is shown how the SOBI method can be applied to blindly identify the sources, the number of dominant sources and obtain structural information of disturbances. It is illustrated that results from SOBI facilitate physical interpretation of directions of disturbances in this multivariable system. Furthermore, it is demonstrated how the structural information of disturbances can be used to track down the location of sources without performing additional measurements. This facilitates procedures to eliminate dominant sources in multivariable system design. Also, a design tool is proposed to assist multivariable control system design. With this, the disturbance rejection problem can be condensed to analysis of only a few dominant sources, so that complexity in multivariable control problems can be reduced significantly. Control design methods that make specific use of insights obtained in this chapter are proposed in Chapter 4.

This chapter is organized as follows. In Section 3.1, it is shown how to retrieve multivariate disturbances from closed loop measurements and which assumptions are made in the SOBI signal model. Next, the blind identification method used in this work is introduced in Section 3.2. Section 3.3 illustrates how the identification method can be used to identify physical sources in an active vibration isolation platform. Furthermore, Section 3.4 illustrates how allocation of these physical sources can be realized. Next, Section 3.5 shows the development of a design tool that uses the results from identification to assist multivariable feedback control system design. Finally, concluding remarks are made in Section 3.6.

3.1 Multivariate disturbance identification

A plant G with n inputs and n outputs is considered, that is controlled by a feedback controller K in the architecture depicted in Fig. 3.1. The disturbances are modeled as additive, vector valued signals $d \in \mathbb{R}^n$ that enter at the input of the plant, comprising all disturbances acting on the system. We assume that the

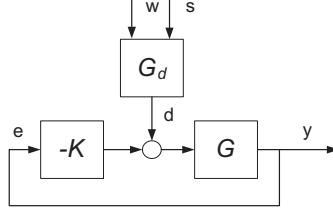


Figure 3.1: Feedback control structure. G is the plant, K the controller, G_d the disturbance model.

plant is invertible and known within negligible uncertainties. Hence, disturbances at the output of the plant can be considered at the input of the plant (and vice versa). The error e equals

$$e = S_o G d, \quad (3.1)$$

where $S_o = (I + GK)^{-1}$ is the output sensitivity function. It is assumed that the transfer function $S_o G$ is known and is invertible. A batch of observations of the servo error can then be obtained, $e(t) \in \mathbb{R}^n$ for $t = 0, \dots, T_s N$, where T_s denotes the sample time and $N + 1$ is the number of samples. Hence, the disturbance $d(t)$ can be reconstructed using the (stable approximate) inverse of $S_o G$. The disturbance at each plant input, namely $d_i(t)$, $i = 1, \dots, n$, result from a mixture of sources $s_j(t)$, $j = 1, \dots, m$ that are to be identified. We restrict ourselves to cases where $m \leq n$. We introduce a framework where the designer has the ability to identify only a few sources. The rest of the signals that generate disturbances, but are not identified, are called interfering signals or noise signals, $w_l(t)$, $l = 1, \dots, p$ with $p \leq n$. The consequences of the separation of $d(t)$ into $s(t)$ and $w(t)$ are discussed in detail in Section 3.2.3.

The following signal model is used,

$$d(t) = \underbrace{\begin{bmatrix} G_s & G_w \end{bmatrix}}_{G_d} \begin{bmatrix} s(t) \\ w(t) \end{bmatrix}, \quad (3.2)$$

where $G_s \in \mathbb{R}^{n \times m}$ and $G_w \in \mathbb{R}^{n \times p}$. The τ -lagged covariance matrix at time t is defined for a multivariate signal $x(t)$,

$$R_x(t, \tau) = E\{x(t)x(t - \tau)^T\} \quad (3.3)$$

where $E\{\cdot\}$ is the statistical expectation. The components of $x(t)$ are uncorrelated if $R_x(t, \tau)$ is diagonal. If the signal $x(t)$ has non-stationary power, the covariance $R_x(t, \tau_f)$ at a fixed τ_f varies with the time t . For non-white signals $x(t)$, $R_x(t, \tau)$ varies for different values of $\tau \neq t$. Without loss of generality, it is assumed throughout this paper that all signals have zero mean.

For the blind identification method presented in this work, the following assumptions are made.

A 1. The matrix G_d is constant and has full column rank.

A 2. The sources $s_j(t), j = 1, \dots, m$ are mutually temporally uncorrelated.

A 3. The time lagged autocorrelation of each source $s_j(t)$ is different for, at least, one lag $\tau > 0$, or, the source has different (non-stationary) power for, at least, one time instant t .

Assumption A1) implies that the mixture of the source and noise signals is instantaneous (only direct feed-through) and does not vary with time. For narrow band disturbances, this assumption holds when the mixture is constant in the frequency region of the disturbances. This is natural in the case that the physical location of the sources is fixed by means of the architecture of the plant (e.g., a pump that has a fixed location in a building). Assumptions A2) and A3) are naturally justified if sources are due to different phenomena, e.g., pump vibrations and acoustic disturbances. In our identification procedure, the sources are arranged in descending order. This ordering may change if the scaling of the inputs or outputs of the plant G in Fig. 3.1 is changed. We therefore assume that the inputs and outputs of the plant are scaled appropriately and the scaling does not change, see e.g. [125, p.5]. For non-white sources, the blind identification technique presented here uses the covariance function (3.3) for different time lags τ ,

$$R_d(0, \tau) = G_s R_s(0, \tau) G_s^T + G_w R_w(0, \tau) G_w^T. \quad (3.4)$$

In the following, we work out the case where it is assumed that the sources are non-white. As the second order statistics vary for different time lags τ we write for ease of notation $R_d(\tau) = R_d(0, \tau)$. The same line of reasoning can be followed in case that it is assumed that sources have non-stationary power by just replacing $R_d(\tau)$ with $R_d(t)$ for fixed τ and varying t , [106]. In that case, one can use $R_d(t) = R_d(t, 0)$ for varying t .

The objective is now to identify the sources $s(t)$ and the matrix G_d from the observed disturbances $d(t)$ only. As we do not know the mixing matrix G_d and have no knowledge about the sources $s(t)$, we face a *blind* identification problem. This will be discussed in the next section.

3.2 Blind identification

As both the matrix G_d and the sources are to be identified, one faces a blind identification problem. The blind identification problems can be solved up to a few indeterminacies [136]: the scaling between the matrix G_d and the sources and the ordering of the sources. These indeterminacies are expressed in a diagonal scaling matrix Λ and permutation matrix P respectively.

Definition 1. The pair $(A, s(t))$ and the pair $(\hat{A}, \hat{s}(t))$ are said to belong to the same equivalence class \mathcal{S} if there exists a diagonal matrix $\Lambda > 0$ and permutation matrix P so that $\hat{A} = AP\Lambda$, $\hat{s}(t) = \Lambda^{-1}P^T s(t)$.

Signals that belong to the same equivalence class have similar statistical properties [136]. Also, all signals in the equivalence class have the same “waveform”, that is, the same shape in the time domain. Furthermore, the ratio in which sources contribute to the observed disturbances is the same for all signals in the same equivalence class. The objective of blind identification is to identify the matrix and the signals that represent the equivalence class that contains the true matrix G_d and the true sources $s(t)$.

As the disturbances are consecutive samples in the time domain, statistics of neighboring time samples can be used to solve the blind identification problem. The method presented here, is worked out for the case of non-white sources although the same line of reasoning can be followed in case one assumes that sources have non-stationary power. For clarity of presentation, the method is presented for the case that $m = n$ and noise is absent, $w(t) = 0$. The influence of noise will be discussed later.

At $\tau = 0$ the covariance matrix of the observed disturbances equals,

$$R_d(0) = G_s R_s(0) G_s^T, \quad (3.5)$$

whereas at $\tau > 0$ the τ lagged covariance matrix equals,

$$R_d(\tau) = G_s R_s(\tau) G_s^T. \quad (3.6)$$

As the sources are uncorrelated A2), both $R_s(0)$ and $R_s(\tau)$ are diagonal. As, for now, we assumed that $m = n$, G_s is square and invertible. With (3.5) and the inverse of (3.6), we find that,

$$R_d(\tau)^{-1} R_d(0) = G_s R_s(0) R_s(\tau)^{-1} G_s^{-1}, \quad (3.7)$$

so that,

$$R_d(\tau)^{-1} R_d(0) G_s = G_s R_s(0) R_s(\tau)^{-1}. \quad (3.8)$$

Finding G_s is equivalent to solving a standard generalized eigenvalue problem [106]. The eigenvalues are the terms of the diagonal matrix $R_s(0)R_s(\tau)^{-1}$ and the corresponding columns of G_s are the eigenvectors. As in any eigenvalue problem, the ordering of the eigenvalues and the scaling between the eigenvalues and the eigenvectors is arbitrary. In fact, these are exactly the inherent indeterminacies of the blind identification problem. Therefore, we define the matrix with eigenvectors, obtained with solving (3.8), as \hat{G}_s . So that the estimated sources are $\hat{s}(t) = \hat{G}_s^{-1} d(t)$. Then, the pair $(\hat{G}_s, \hat{s}(t))$ where $\hat{s}(t) = \hat{G}_s^{-1} d(t)$, belongs to the same equivalent class as the pair $(G_s, s(t))$, the mixing matrix and the sources

respectively.

A regular solution to the generalized eigenvalue problem exists if the product $R_s(0)R_s(\tau)^{-1}$ has non-zero, distinct diagonal terms [53]. As the sources are not known beforehand, it is non trivial to guarantee that such a regular solution exists for a particular choice of (τ) in $R_d(\tau)$. This will be discussed later in this section.

In literature, there is an extensive amount of work on solving generalized eigenvalue problems [53]. Often a two step solution is proposed. Here, we refer to these two steps as the following,

Step 1) whitening

Step 2) unitary diagonalization

In the whitening (or principal component analysis) step the observations are expressed in the smallest orthogonal signal space. This serves as a preprocessing step for unitary diagonalization. In the unitary diagonalization step, special attention is paid to finding regular solutions for the generalized eigenvalue problem. Herein, A3) plays an important role. A dedicated unitary diagonalization procedure can be used to increase numerical robustness. The two steps are discussed for the case that the noise signals are absent. In the last part of this section, the implications of preprocessing the signal space in the presence of noise signals $w(t)$ is discussed.

3.2.1 Whitening

The objective of the whitening step is to find a minimal number of m uncorrelated components $z(t) \in \mathbb{R}^m$ that represents the observed disturbances $d(t)$. Hence, an orthogonal whitening matrix $W \in \mathbb{R}^{m \times n}$ is to be found so that

$$z(t) = Wd(t), \quad (3.9)$$

with $R_z(0) = I$ and $m \leq n$. From (3.5), one can take the singular value decomposition [53] of $R_d(0)$, so that,

$$R_d(0) = [U_{ds} \mid U_{ns}] \left[\begin{array}{c|c} \Sigma_{ds} & 0 \\ \hline 0 & 0 \end{array} \right] \left[\begin{array}{c} U_{ds}^T \\ U_{ns}^T \end{array} \right]. \quad (3.10)$$

Here m , the number of non-zero singular values, Σ_{ds} , represent the size of the source signal subspace. Using (3.9) the whitening matrix W must equal

$$\begin{aligned} R_z(0) &= WR_d(0)W^T \\ &= WG_sR_s(0)G_s^TW^T \\ &= WU_{ds}\Sigma_{ds}U_{ds}^TW^T = I. \end{aligned} \quad (3.11)$$

By A2), $R_s(0)$ is diagonal. As the scaling between the estimate of G_d and the estimate of the sources is an indeterminacy, one can choose $R_s(0) = I$ without loss of generality. It follows from (3.11) that,

$$W = \Sigma_{ds}^{-\frac{1}{2}} U_{ds}^T, \quad (3.12)$$

which columns are orthogonal. All signals in the subspace orthogonal to W , signals in the image of U_{ns} , are not considered in the next step of the blind identification procedure. Substitution in (3.9) then gives the m principal components $z(t)$ that are present in the observed disturbances $d(t)$. The directions of the disturbances are contained in U_{ds} . Note that $R_z(0)$ does not change when $z(t)$ is transformed with any unitary matrix U . Hence, the matrix \hat{G}_s , (3.8), is recovered up to an unknown matrix U . Due to this freedom, the signals $z(t)$, also called *principal components*, can still result from a mixture of the sources with an unknown unitary matrix U ,

$$z(t) = Us(t). \quad (3.13)$$

In general, the matrix U can not be written as the product of a permutation matrix P and a diagonal scaling matrix Λ . Hence, the signals $z(t)$ do not belong to the same equivalence class as the sources $s(t)$. The second step in the blind identification procedure is to reduce this freedom by using a stronger condition, namely by simultaneous diagonalization of a set of lagged covariance matrices.

3.2.2 Unitary diagonalization

In order to find signals that are in the same equivalence class as the sources, the whitening step was shown to be insufficient. By not only diagonalizing a single second order statistic, but using additional diagonalization requirements, a stronger condition can be obtained that reduces the class of solutions. The additional statistics that are used here, are based on the assumption that the sources are non-white, A3) so that (3.4) can be exploited and not only $R_d(0)$. The same line of reasoning holds for the case where one assumes that the sources have non-stationary power, [106], [107]. In order to solve the blind identification problem, one still has to determine a unitary matrix U so that

$$R_s(\tau) = U^T R_z(\tau) U \quad (3.14)$$

is diagonal for $\tau > 0$. By (3.13) and A2) $R_z(0) = I$ and $R_z(\tau), \tau > 0$ are diagonal. Recall that the generalized eigenvalue problem, (3.8), has a regular solution if the diagonal terms of the lagged covariance matrix of the sources, namely $R_{s,ii}(\tau)$, are mutually distinct. As $R_s(\tau)$ is not known a-priori, it is not trivial to choose a lag τ to guarantee solvability of the blind identification problem. An approach to overcome this difficulty is to *simultaneously* diagonalize a set of covariance matrices for $\tau_k \in \{\tau_j > 0 | j = 1, \dots, N_k\}$. Then, all vectors $\kappa_i = [R_{s,ii}(\tau_1), \dots, R_{s,ii}(\tau_{N_k})]$, $i = 1, \dots, n$ must be distinct in order to find a regular solution [7]. The vectors κ_i are already distinct if for a single value of i , the

diagonal terms $R_{s,ii}(\tau_i)$ are distinct.

In the case of sample statistics, and the presence of noise, exact simultaneous unitary diagonalization is practically not feasible. Hence an approximate simultaneous unitary diagonalization must be formulated instead. Here, the approach of [25] is followed, that makes use of the following measure. See [126] for an alternative approach. For an $n \times n$ matrix M , with entries M_{ij} , we define

$$\mathbf{off}(M) = \sum_{i,j=1,i \neq j}^n |M_{ij}|^2. \quad (3.15)$$

The set of matrices $R_z(\tau_k) = \{R_z(\tau_1), \dots, R_z(\tau_{N_k})\}$ are approximately diagonalized by an $n \times n$ unitary matrix \hat{U} , when the following criterion is minimized,

$$\mathcal{J}(R_z(\tau_k), \hat{U}) = \sum_{j=1, \dots, N_k} \mathbf{off}(\hat{U}^T R_z(\tau_j) \hat{U}). \quad (3.16)$$

which solution,

$$\hat{U} = \arg \min \mathcal{J}(R_z(\tau_k), \hat{U}) \quad (3.17)$$

can be obtained by means of a generalized iterative Jacobi technique [25]. An alternative formulation of this criterion is a weighted nonlinear least squares problem [147]. Herein, one may include additional information about the expected nature of the sources [151]. For large problems, methods based on recursive splitting of subspaces are proposed in [155].

Finally, the results of whitening, (3.12), and unitary diagonalization, (3.17), are used to recover the signals that are in the same equivalence class as the true sources as,

$$\hat{s}(t) = \Lambda P s(t) = \hat{U}^T W d(t). \quad (3.18)$$

The estimate of the matrix G_s is $\hat{G}_s = W^\dagger \hat{U}$. In the whitening step, it was chosen to define $R_s(0) = I$. This implies that all scalings of the sources are contained in \hat{G}_s . Alternatively, one may choose to scale the columns of \hat{G}_s to unity, this is just a matter of convention and does not play any role in further use of this disturbance model.

3.2.3 Influence of noise signals

Often a few dominant sources are to be identified in the presence of many other interfering phenomena. These phenomena, defined as noise signals $w(t)$ in (3.2) may deteriorate the performance of the blind identification procedure. This holds for second order blind identification as well as the basic ICA approaches in literature, [65]. In the case that $m + p \leq n$, the first $m + p$ principal components

of $d(t)$ can be used in blind identification so that each noise signal is identified as an additional source. Problems arise when $m + p > n$ as the blind identification method can not identify more sources than observations. This can be illustrated considering the signal model defined in (3.2). Herein the covariance of the disturbances equals,

$$R_d(0) = G_s R_s(0) G_s^T + G_w R_w(0) G_w^T \quad (3.19)$$

where $R_s(0), R_w(0)$ are symmetric. The objective is to determine the structure at the right hand side of this equation while only knowing $R_d(0)$. The singular value decomposition of the covariance of $d(t)$ equals

$$\begin{aligned} R_d(0) &= U_d \Sigma_d U_d^T \\ &= [U_{ds} \mid U_{dw}] \left[\begin{array}{c|c} \Sigma_{ds} & 0 \\ \hline 0 & \Sigma_{dw} \end{array} \right] \left[\begin{array}{c} U_{ds}^T \\ U_{dw}^T \end{array} \right]. \end{aligned} \quad (3.20)$$

Each element in Σ_d belongs to a single principal component, the contribution of each principal component to the variance of the observed disturbances can be measured. Note that when the scaling of the inputs or outputs of the plant is changed, the contribution of these principal components may change as well. In contrast with (3.10), each principal component contains contributions from source and noise signals. Hence the values of Σ_d cannot be used to determine the dimensions of the source and noise signal space. The Σ_{ds} in the decomposition of (3.20) is not equal to the Σ_{ds} in the decomposition (3.10). Only in the case that one knows beforehand that G_s and G_w are orthogonal, one may select the appropriate columns of U_d to isolate the sources from the noise. In general G_s and G_w are not orthogonal, hence additional assumptions on the nature of the noise signals must be made.

A commonly used assumption, [65], is that the noise space orthogonal to the source space can be approximated as $\Sigma_{dw} \approx \rho^2 I_{n-m}$, and one can assume, e.g., on physical grounds, that $\Sigma_{ds} = \Sigma_s + \rho^2 I_m$, the variance of the spatially white noise space equals $\rho^2 \approx \frac{1}{n-m} \text{tr}(\Sigma_{dw})$. Hence, an unbiased estimate of the source variances can be obtained using $G_s R_s(0) G_s^T \approx U_{ds} (\Sigma_{ds} - \rho^2 I_m) U_{ds}^T$. This strategy is justified in the special case that $G_w = I_n$ and $R_w(\tau) = \rho^2 I_n \delta_{t,\tau}$. The simultaneous diagonalization procedure can be performed on the lagged covariance matrices with $\tau > 0$ as $R_w(\tau) = 0, \tau > 0$. This special structure is often justified in array processing applications, [24]. Here, all sensors in the array are assumed to suffer from interference of sensor noise signals each having the same covariance. In control applications, these assumptions may be reasonable when all channels (e.g., all sensors) have the same noise variance. This is a crude assumption in most applications.

In general however, one does not know m, p exactly and coping with interfering phenomena remains a weakness of the blind identification procedure. Even

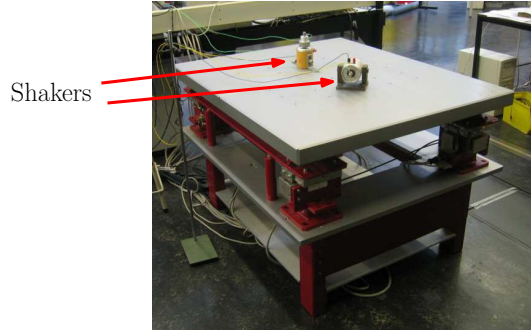


Figure 3.2: Active vibration isolation platform. Shakers mounted at the table surface generate disturbances.

if one assumes that the noise is small compared to the $m < n$ source signals, problems may still occur in estimating the number of sources. As the singular values of $R_d(0)$ are non-zero, one cannot determine the number of sources in the whitening step. This is particularly true if the matrix G_s is ill conditioned, e.g., if sources act in almost the same direction. The best approach in that case, is to carry out the unitary diagonalization for the whole signal space of the observations and the noise and source signal must be isolated a posteriori. This means that no dimension reduction is applied during the whitening step, but is only possible after the complete blind identification procedure has been carried out. This means that the assumptions, A1), A2), and A3), must hold for all signals that generate the disturbances.

3.3 Identification results

The second order blind identification method is used to identify sources of disturbances in the 6×6 MIMO active controlled vibration isolation platform depicted in Fig. 3.2. The platform consist of an actively mounted table driven with Lorentz actuators. The velocity of the table is measured by means of geophones. The position of the table is to be isolated from disturbances from the environment and disturbances that act on the table. The plant is decoupled in six cartesian degrees of freedom, the origin coincides with the center of gravity (COG) of the table. Each axis is independently controlled by a single input single output controller. Two sources are added synthetically to the system, by means of two shakers placed at the surface of the table. Both the location and the time behavior of the shakers are considered to be unknown. For validation purposes, the acceleration of the shakers is measured by means of piezo elements attached to the moving parts of the shakers. The objective is to recover estimates of the sources that are in the same equivalence class as the measured signals from the shakers.

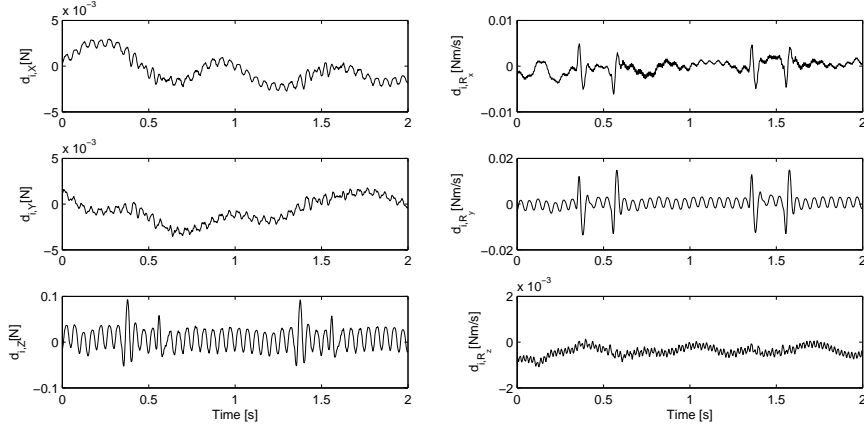


Figure 3.3: Reconstructed input disturbance of the active vibration isolation platform.

The first step is to reconstruct the disturbances from measurements of the error of the feedback controlled system, Fig. 3.1. The transfer function between the acceleration of the shakers, x , and the observed error equals,

$$e = G(I + KG)^{-1}G_dG_x x \quad (3.21)$$

Herein, G_x denotes the transfer function between forces acting on a certain location of the table and the acceleration of the shakers x . The transfer function matrix G_x is constant and diagonal, $\text{diag}(G_x) = [g_{x1}, g_{x2}]^T$. As the disturbances are above the bandwidth of the feedback controlled loops in each axes, $(I + KG)^{-1} \approx I$. Also, the plant behaves rigid and is decoupled so that the plant dynamics can be approximated at each i^{th} diagonal term by, $G_{ii}(s) = \frac{1}{s}g_{ii}, g_{ii} \in \mathbb{R}^1$. As scaling is an indeterminacy of the blind identification method, the derivative of the identified sources (in terms of velocities) can be compared to the acceleration of the shakers to validate the blind identification method. From a batch of observed servo errors $e(t)$, the disturbances $d(t) \in \mathbb{R}^6$, for $t = 0, \dots, T_s N$ can be reconstructed. Herein, $T_s = 1 \times 10^{-3}$ denotes the sample time and $N + 1 = 1 \times 10^3$ the number of samples. The disturbances at each controlled axis are depicted in Fig. 3.3. The following estimator for the covariance at time $t = 0$ for lag τ is used,

$$\hat{R}_d(\tau) = \frac{1}{N} \sum_{t_i=0}^N d(t_i)d(t_i - \tau)^T. \quad (3.22)$$

It is assumed that the sources are non-white, A3), hence N_k estimates of the $\tau_k \in \{\tau_j > 0 | j = 1, \dots, N_k\}$ lagged covariance matrices are used in the blind

identification method. The choice of N_k is rather arbitrary as no information about the sources is available beforehand. From practical experience $N_k = 20$ is a satisfactory tradeoff between statistical averaging and computation time. After blind identification both $\hat{s}(t)$ and \hat{G}_s are determined, so that

$$d(t) = \hat{G}_s \hat{s}(t) + d_w(t). \quad (3.23)$$

Herein, $d_w(t) = G_w w(t)$, see (3.2), is the part of the disturbance that results from noise signals. The matrix G_w and the signals $w(t)$ are not identified in the blind identification procedure. As shown earlier, blind identification cannot determine whether scaling is contained in the sources or in the mixing matrix. In the whitening step it was therefore assumed that the sources have unit variance, $R_s(0) = I$. All scaling is then contained in the estimated mixing matrix. One may express this scaling in a diagonal matrix Γ . Then, the directions, normalized to unity, equal the columns of the matrix \overline{G}_s so that the following holds,

$$\hat{G}_s = \overline{G}_s \Gamma. \quad (3.24)$$

The ratio in which each j^{th} source contributes to the observed disturbance in each channel is then contained in each j^{th} column of \overline{G}_s . The diagonal terms of the matrix Γ indicate the relative contribution of each source to the observed disturbances.

Blind identification is performed for two cases; 1) identification with a PCA-like (whitening) pre-processing step to identify only a few dominant sources $m < n$, 2) identification of as many sources as observed disturbances $m = n$.

3.3.1 Case 1, $W \in \mathbb{R}^{2 \times 6}$

The first case illustrates how one can use the whitening step in SOBI to identify only a few dominant sources, $m < n$. The number of dominant sources is estimated by studying the contribution of each principal component to the total variance of the observed disturbances, as measured by the singular values of $\hat{R}_d(0, 0)$,

$$\text{diag}(\Sigma_d) = 1 \times 10^{-3} \begin{bmatrix} 0.5667 \\ 0.0126 \\ 0.0017 \\ 0.0013 \\ 0.0002 \\ 0.0001 \end{bmatrix}. \quad (3.25)$$

Herein, $\text{diag}(\cdot)$ stacks the diagonal terms of (\cdot) as a column vector. The relative contribution of each principal component is depicted in Fig. 3.4. It is visible that the first principal component is responsible for 97 percent of the variance of the observed disturbances. Hence, solely on the basis of the principal components,

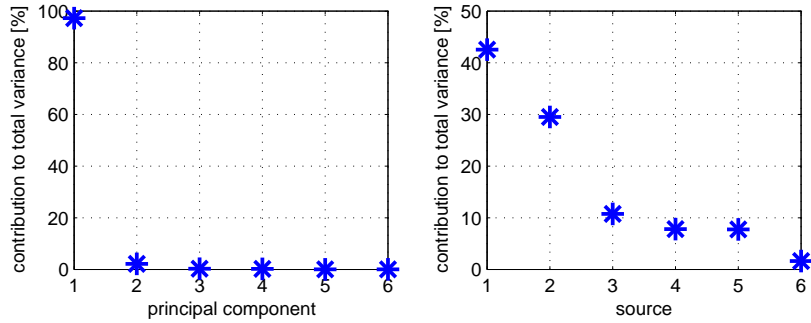


Figure 3.4: Percentage of contribution to the variance of the observed disturbances. Left, per principal component, Case 1). Right, per identified source, Case 2)

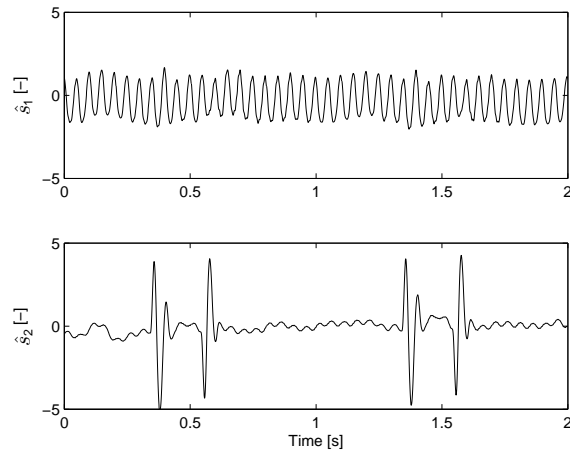
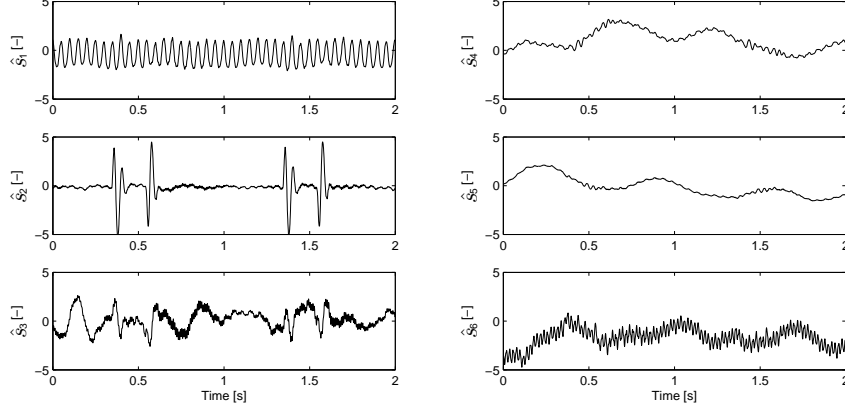


Figure 3.5: The two identified sources recovered from the observed disturbances, Case 1).

one could conclude that there is one single dominant source responsible for the observed disturbances. Here, we choose $m = 2$, so that the whitening matrix becomes $W \in \mathbb{R}^{2 \times 6}$. One may choose higher m if more sources are to be identified. After unitary diagonalization, the estimated sources are obtained as depicted in Fig. 3.5. The matrix $\hat{G}_s = \overline{G}_s \Gamma$ is estimated as,

Figure 3.6: All six identified uncorrelated sources \hat{s} in Case 2).

$$\bar{G}_s = \begin{bmatrix} -0.0161 & 0.0052 \\ -0.0164 & -0.0025 \\ -0.9933 & 0.9827 \\ -0.0183 & -0.0753 \\ -0.1122 & -0.1692 \\ -0.0011 & 0.0013 \end{bmatrix}, \text{diag}(\Gamma) = \begin{bmatrix} 0.0183 \\ 0.0155 \end{bmatrix}. \quad (3.26)$$

3.3.2 Case 2, $W \in \mathbb{R}^{6 \times 6}$

In this approach, the signal space is not reduced in the whitening step, hence $m = n$ sources are identified. The number of dominant sources is estimated after applying SOBI. The whitening matrix is a square transformation and the unitary diagonalization problem, (3.17), is solved simultaneously for N_k lagged covariance matrices, each with size (6×6) . The estimated sources are shown in Fig. 3.6. The matrices $\hat{G}_s = \bar{G}_s \Gamma$ equal,

$$\bar{G}_s = \begin{bmatrix} -0.0161 & 0.0059 & -0.0277 & 0.0785 & 0.0469 & 0.7055 \\ -0.0100 & -0.0050 & -0.0705 & 0.3416 & 0.0265 & 0.2330 \\ -0.9955 & 0.9738 & 0.9942 & 0.9352 & -0.9237 & 0.0226 \\ -0.0126 & -0.0664 & -0.0581 & -0.0370 & 0.3624 & -0.6509 \\ -0.0923 & -0.2173 & -0.0110 & 0.0138 & 0.1118 & -0.1519 \\ 0.0015 & -0.0018 & 0.0474 & 0.0321 & -0.0042 & 0.0260 \end{bmatrix}, \quad (3.27)$$

$$\text{diag}(\Gamma) = \begin{bmatrix} 0.0190 \\ 0.0132 \\ 0.0048 \\ 0.0035 \\ 0.0035 \\ 0.0007 \end{bmatrix}. \quad (3.28)$$

The values of Γ indicate the contribution of the identified sources to the disturbance. The contribution of each of the six estimated sources is depicted in Fig. 3.4. It is visible that the first two estimated sources are responsible for more than 70 percent of the observed disturbances. Comparing these results to the left side of Fig. 3.4, it is clear that the first five estimated sources contribute mostly to the first principal component. Hence, using blind identification, we are able to estimate sources of disturbances even if those sources act almost in the same direction.

3.3.3 Validation and interpretation of results

The results from Case 1), show that the identified sources contain components from different phenomena. Also, the number of dominant sources was estimated incorrectly. This demonstrates that estimates from PCA can be misleading in cases where sources act in almost the same directions (z -direction in this case). Figure 3.5 shows that SOBI is not able to separate the first two sources. The results from Case 2) are much more satisfying. From the post-analysis, it is concluded that indeed two sources are responsible for most of the observed disturbances. The i^{th} row element of the j^{th} column of \bar{G}_s shows the dominance of the j^{th} source on the i^{th} disturbance. It appears that the first two sources act mostly in z direction. Also, both sources contribute to disturbances in R_y and R_x -direction. This is supported by physical insight; the shakers are at some distance from the center of gravity of the table. The third source that is identified is recognized as the undamped suspension mode of the plant in z -direction. The fourth source is likely to result from floor vibrations (z -direction). The fifth and sixth source have no clear physical interpretation.

To validate the first two identified sources of Case 2), measurements from the acceleration of the shakers are used. Figure 3.7 shows that measured acceleration of moving parts of the shakers. The time derivative of the estimated sources for Case 1) and Case 2) are shown in Fig. 3.8a and Fig. 3.8b. In Fig. 3.9, the spectra of the shakers and the first two identified sources of Case 2) are shown. Again, it is visible that the sources are identified up to arbitrary scaling and permutation.

Using the results from blind identification, the disturbance model (3.23) is con-

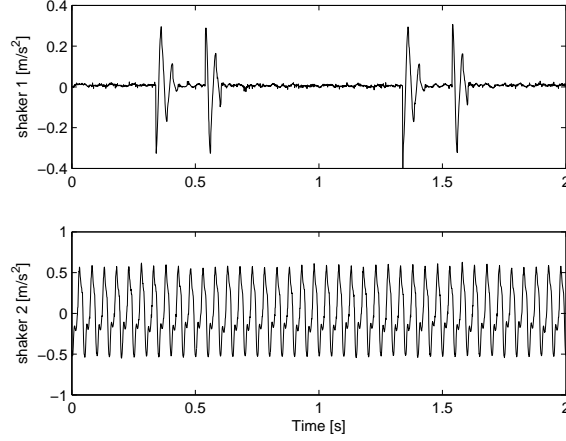


Figure 3.7: Measured acceleration of the shakers.

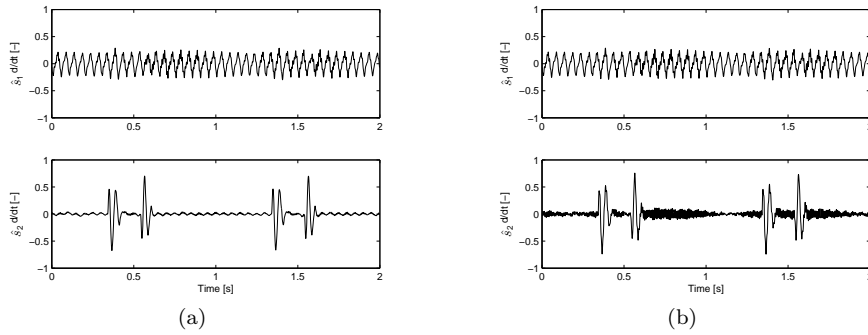


Figure 3.8: Left: time derivative of the estimated sources of Case 1). Right: time derivative of the estimated sources of Case 2).

structured as,

$$\begin{aligned}
 d(t) &= \hat{G}_s \hat{s}(t) + d_w(t) \\
 &= \sum_{j=1}^m d_{s_j}(t) + d_w(t)
 \end{aligned} \tag{3.29}$$

Herein, the contribution of each j^{th} source, $s_j(t)$ can be studied. The closed loop transfer function, (3.1), can be used to decompose the servo error in contributions of each source. This indicates the priority of eliminating or rejecting a particular source. Several approaches may then be followed to reduce the influence of the sources on the performance of the multivariable system. In the following sections it is shown how the results from blind identification can be used for 1) allocation

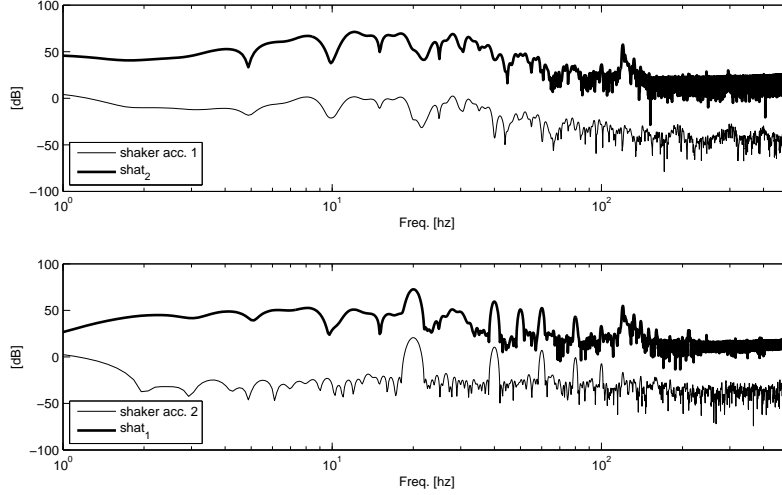


Figure 3.9: Spectrum of the acceleration measurements of the shakers and the time derivative of the first two blindly identified sources. Scaling and permutation are indeterminacies of the identification procedure.

of the sources and 2) as a design tool in multivariable feedback control design.

3.4 Localization of sources

In order to eliminate a source, finding its location is a challenging issue. In this section, it is illustrated that the results from blind identification in combination with a kinematic model can be used to allocate dominant sources. The following three additional assumptions are required,

A 4. *The table behaves rigid in the frequency region of interest*

A 5. *The sources act as point forces*

A 6. *The sources act on the table surface.*

The disturbance d_{sj} due to the source s_j is decomposed in cartesian coordinates.

$$d_{sj} = [d_{sx}^j, d_{sy}^j, d_{sz}^j, d_{Rxx}^j, d_{Ryy}^j, d_{Rz}^j]^T \quad (3.30)$$

The active vibration isolation platform is controlled in cartesian coordinates with the origin at the center of gravity of the table, hence each disturbance $d_{sj}, j =$

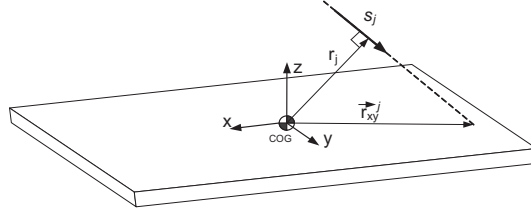


Figure 3.10: Multi body model to find the location of the j^{th} independent component from the disturbance forces acting on the center of gravity.

$\{1, \dots, m\}$ is expressed as a disturbances acting on the center of gravity of the table. By assumption A5), allocation of the source boils down to finding the vector from the center of gravity to the point where the source acts, see Fig. 3.10. As the table is assumed to be rigid, A4), one can use to following relation, $\vec{M}_{COG} = \vec{r} \times \vec{F}_{COG}$, see for example [64], to show that,

$$\begin{bmatrix} d_{Rx}^j \\ d_{Ry}^j \\ d_{Rz}^j \end{bmatrix} = \begin{bmatrix} 0 & d_z^j & -d_y^j \\ -d_z^j & 0 & d_x^j \\ d_y^j & -d_x^j & 0 \end{bmatrix} \begin{bmatrix} r_x^j \\ r_y^j \\ r_z^j \end{bmatrix}. \quad (3.31)$$

The matrix at the right hand side of this equation has rank 2, hence it is only possible to find the shortest distance r_j to a line on which the j^{th} source is located. Using assumption A6), r_z^j becomes zero see Fig. 3.10, and the vector \vec{r}_{xy}^j from the center of gravity to the source location can be uniquely determined, as (3.31) reduces to,

$$\begin{bmatrix} d_{Rx}^j \\ d_{Ry}^j \end{bmatrix} = \begin{bmatrix} 0 & d_z^j \\ -d_z^j & 0 \end{bmatrix} \begin{bmatrix} r_x^j \\ r_y^j \end{bmatrix}. \quad (3.32)$$

Herein, the matrix at the right hand side is full rank. In (3.31), it shows that only the *ratio* between the elements in d_{sj} (3.30) matters. Hence, it suffices to take in account only the direction of d_{sj} , which equals the j^{th} column of \vec{G}_s , (3.28). Therefore, the indeterminacies, that are inherent to the blind identification problem, have no influence on this procedure.

By using the first two identified sources in (3.28) the location of the actual sources can be recovered. For ten subsequent experiments, the estimated locations are depicted in Fig. 3.11. The actual location of the shakers is marked with the diamonds. It is clear that the location of the sources can be recovered with acceptable accuracy. Once the source is tracked down, possibilities can be investigated to eliminate the source or to eliminate the impact on the performance by redesign of the plant.

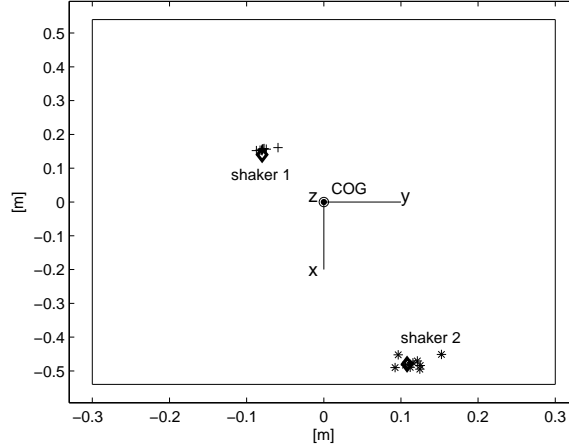


Figure 3.11: Top view of table surface. Estimated location of the sources for ten experiments, \hat{s}_1 (+), \hat{s}_2 (*) and actual location of the shakers \diamond .

3.5 Disturbance driven multivariable feedback control

If the sources cannot be eliminated, or the plant cannot be redesigned, multivariable feedback control may be employed to reject the influence of the source on the performance of the system. As (3.23) provides a multivariable disturbance model, model based techniques can be applied for the synthesis of multivariable controllers, see e.g. [125], [84]. Here, we focus on a specific property of multivariable systems, namely the role of the *direction* of the disturbances. Directions play an important role in multivariable system design, [125],[94]. In Section 2.2, it was shown how directions determine the achievable performance of control systems as a result of inherent limitations. In practical cases, it is very difficult to give a physical interpretation to multivariate disturbances, hence the directionality of disturbances can not always be exploited. Here, it is shown how the results from SOBI provide a physical interpretation of directions of disturbances in the active vibration isolation platform. Also, the performance of two candidate feedback controllers is evaluated using a measure of performance that makes use of the identification results of SOBI.

From (3.29) and Fig. 3.1 follows,

$$e = GS_i(\hat{G}_s \hat{s} + d_w), \quad (3.33)$$

where $S_i = (I + KG)^{-1}$ is the *input* sensitivity. Using SOBI, the directions of the disturbances due to each j^{th} source are obtained as the j^{th} column of \hat{G}_s ,

(3.29). In the spirit of error budgeting techniques, [68], one may use Equation (3.33) to study the contribution of each estimated source \hat{s}_j to the servo error. For example, we may study,

$$\|e(\omega)_j\|_2 = \|GS_i(j\omega)d_{sj}(\omega)\|_2, \quad (3.34)$$

per frequency ω . Herein, $d_{sj}(\omega)$ is the disturbance as a result of the j^{th} source and $\|x(j\omega)\|_2$ is the Euclidean norm of x evaluated at each frequency ω . This measure expresses the size of the servo error $e(\omega)$ resulting from a sinusoidal disturbance $d_{sj}(\omega)$ that is generated by the source $s_j(\omega)$. The contribution of each source to the final servo error can be studied in this way. Hence, disturbance rejection performance of a multivariable control system can be decomposed in disturbance rejection performance per physical disturbance cause (source).

Another measure can be derived that specifically takes into account the directional aspects of disturbances. If the direction of the disturbances are aligned with input directions that correspond to small singular values of S_i , attenuation of disturbances is high. Hence, the alignment between each column of \hat{G}_s and the relevant closed loop transfer function is a measure of how well d_{sj} , the disturbance that originates from source s_j , is rejected. We define,

$$\alpha_j(\omega) = \frac{\|G(j\omega)S_i(j\omega)d_{sj}(\omega)\|_2}{\|d_{sj}(\omega)\|_2}, \quad (3.35)$$

which can be considered as a closed loop variation of the *disturbance condition number* discussed in [122]. If $\alpha_j(\omega)$ is small, the closed loop function is said to be well-aligned with the disturbance direction of disturbances that are due to the source s_j . This measure can be used to select controllers that result in better disturbance alignment. As the disturbances can now be decomposed in contributions per source, alignment can be given a physical interpretation.

We illustrate these measures on the active vibration platform. The disturbance rejection performance for two feedback control designs is studied. The first controller, K_1 , was discussed extensively in Section 2.5. The second controller, K_2 , equals K_1 , except in the z -axis. In this axis, the crossover points are changed from 0.6Hz, 10Hz to 0.5Hz, 20Hz. In Fig. 3.12 the measure, (3.34), is depicted. The top figure shows $\|e\|_2$ as a function of all the input disturbances. These disturbances contain contributions of all sources. At frequencies below 20Hz, the controller K_2 results in better disturbance rejection than the design with controller K_1 . At frequencies above 20Hz, disturbance rejection with K_2 is worse than the lower bandwidth design K_1 . As 20Hz is the maximum bandwidth frequency, it is clear that this is caused by the waterbed effect, Section 2.2. The same tradeoff seems to apply for the middle and bottom figure, that shown $\|e\|_2$ as a result of only the first and second identified sources. As these sources act almost exactly in z -direction, see the first two columns of \hat{G}_s in (3.27), the high bandwidth controller for the z -axes, K_2 , results in more high frequency amplification of the disturbances due to the shakers. Using the same measure, we can investigate how much performance can be gained by eliminating the sources by system redesign. This

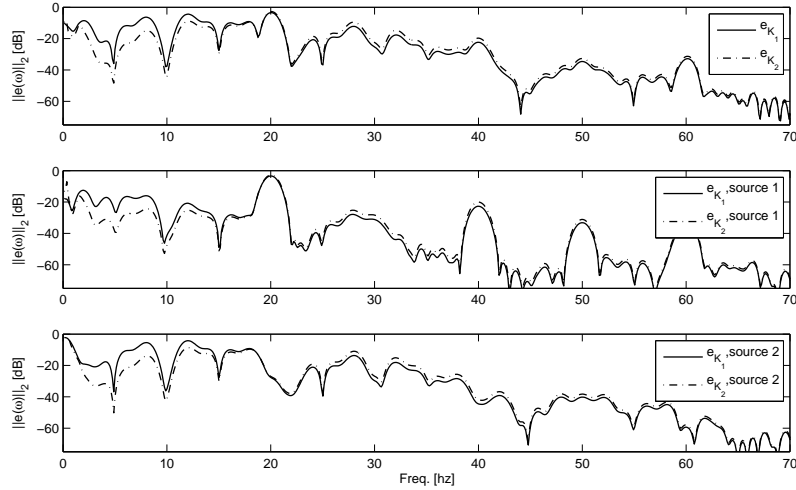


Figure 3.12: Norm of the servo error with two control designs with K_1, K_2 . Top: as a result of all disturbances, Middle: as a result of disturbances due to \hat{s}_1 . Bottom: as a result of disturbances due to \hat{s}_2 .

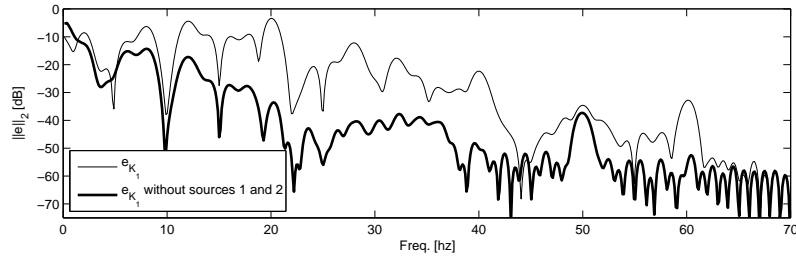


Figure 3.13: Norm of the servo error in the original situation and the error without the contributions of the first two estimated sources.

is shown in Fig. 3.13 where we depicted $\|e\|_2$ for the original case (same as top figure in Fig. 3.12) and the predicted value of $\|e\|_2$ is the disturbances due to the first two blindly identified sources are removed.

The closed loop disturbance alignment measure $\alpha(\omega)$ is shown in Fig. 3.14. In the top figure, $\alpha(\omega)$ is shown as a function of all disturbances. Reducing the sensitivity function in the z -axis implies that the process sensitivity function has low gain for disturbances that act in z -direction. As most disturbances appear to act in z -direction, see \bar{G}_s in (3.27), the controller K_2 results in better disturbance alignment at frequencies within the bandwidth. At frequencies above

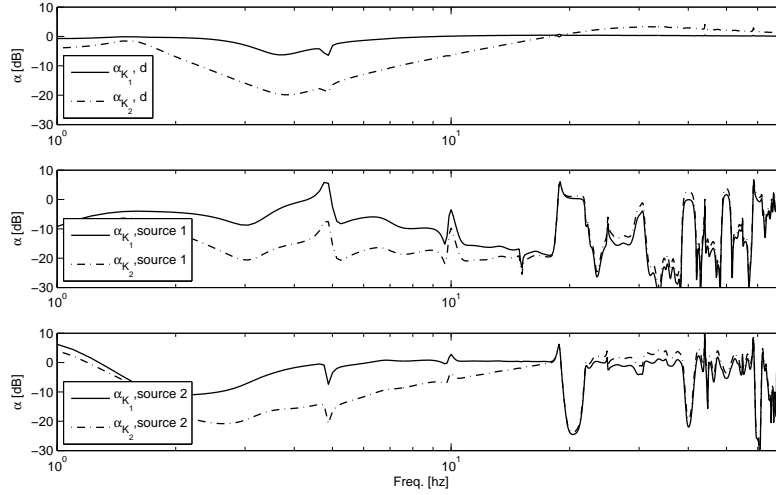


Figure 3.14: Disturbance alignment condition number $\alpha(\omega)$ with two control designs with K_1, K_2 . Top: for all disturbances, Middle: for disturbances due to \hat{s}_1 . Bottom: for disturbances due to source \hat{s}_1

the bandwidth, K_1 has smaller sensitivity in z -direction and therefore results in better disturbance alignment than K_2 . In the middle and bottom figure $\alpha(\omega)$ is shown for disturbances due to the first two blindly identified sources, \hat{s}_1 and \hat{s}_2 . As they act mostly in z -direction, it is clear that disturbance alignment is mostly determined by the controller in the z -axis.

In conclusion, we find that the controller K_2 outperforms K_1 in rejecting the low frequency disturbances that are generated by the shakers. If disturbance rejection at high frequencies is important, the low bandwidth design with K_1 is to be preferred. As the disturbances due to the shakers act mostly in z -direction, the multivariable disturbance rejection problem can be simplified to redesign of the controller of the z -axis. As we determined the contribution of each source to the input disturbances of the AVIS, we are able to predict the performance of the system for the case that the first two sources are eliminated.

3.6 Conclusion

In this chapter, a blind identification method is used to find root causes (sources) of disturbances in multivariable control systems using closed loop measurements of the error. The proposed identification method successfully identifies dominant sources in an industrial active vibration isolation platform. Also, the location of

sources can be determined, without any additional measurements. Furthermore, a design indicator, that uses the results from identification, provides insight in the disturbance rejection performance of multivariable controllers. It is shown that the proposed identification method can be used to estimate the number of sources in multivariable disturbances, even in cases where the sources act almost in the same direction.

An example was presented where insights from blind identification can be used to evaluate disturbance rejection performance of different multivariable controllers. In this application, it is shown that the multivariable control (re)design of the MIMO 6×6 active vibration isolation system can be reduced to (re)design of the controller in only a single direction. It was found that disturbance rejection in this direction is mostly determined by control design in a single axis. Hence, control design complexity is reduced significantly. In more general cases, disturbance directions are not aligned with only a single controlled axis. The same identification method can be applied, but control (re)design, to reject disturbances in exactly those directions that are related to the sources, is generally more involved. This is discussed in the following chapter.

Chapter 4

Directionality in multivariable control design

Once disturbances and noise are characterized, accommodating directions of disturbances and noise in feedback control design is desirable. In this chapter, several directionality driven feedback control design methods are proposed. From the unit feedback configuration, Section 2.1, we found the following relates noise n and output disturbances d_o with the performance variable z ,

$$z = S_o d_o - T_o n \quad (4.1)$$

where $S_o = (I + L)^{-1}$ is the output sensitivity function and $T_o = LS_o$ is the output complementary sensitivity function. As the objective is to keep z as small as possible in presence of d_o and n , the sensitivity function must have low gain in the frequencies and directions where d_o is large. For noise rejection, the complementary sensitivity function must have low gain at frequencies and directions where n is large. If closed loop functions are to be designed with different gains in different directions (non-uniform gain), the following design issues arise immediately.

First, non-uniform gain closed loop functions imply that the open loop function has non-uniform gain. Then, relations between open and closed loop functions as derived in Section 2.1.3, do not provide much insight for control design. Second, the input and output directions of the open loop depend strongly on the alignment between plant and controller. Hence, it is not intuitive to shape the input and output directions of the open loop by (re)tuning the controller parameters. Third, recall from (2.11), that,

$$\begin{aligned} \kappa(G)^{-1} \sigma_i(S_o) &\leq \sigma_i(S_i) \leq \kappa(G) \sigma_i(S_o) \\ \kappa(K)^{-1} \sigma_i(S_o) &\leq \sigma_i(S_i) \leq \kappa(K) \sigma_i(S_o). \end{aligned} \quad (4.2)$$

This implies that if either $\kappa(K) \gg 1$ or $\kappa(G) \gg 1$, the singular values at one loop breaking point do not have to be equal to the singular values at another loop breaking point. Therefore, robustness margins at one loop breaking point may significantly differ from robustness margins at the other loop breaking point. These issues shown that, compared to the decoupling approaches in Section 2.4, design complexity of multivariable controllers is increased significantly.

In motion control applications, there are situations that the plant can be decoupled and scaled so that $\kappa(G) = 1$ at some frequencies. This typically occurs in plants that have free rigid body modes or plants that have stiff connections to the environment. Then, at least at low and intermediate frequencies, dominant dynamics can be considered as $G(s) = g(s)I$. If a centralized (non-diagonal) controller K is designed, the input and output directions of the open loop are completely determined by the controller. Furthermore, as $\kappa(G) = 1$, (4.2) shows that $\sigma_i(S_o) = \sigma_i(S_i)$, so that robustness margins are the same at different loop breaking points. The only issue that is left to resolve, is to relate input directions of the sensitivity and complementary sensitivity function to specific design choices of the feedback controller. This is investigated in this chapter.

This chapter is organized as follows. In the next section, it is discussed how the results from blind identification of fixed direction disturbances can be used to choose weighting filters for norm based design. Section 4.2, proposes a loop shaping method to reject disturbances in specific, non-canonical, directions. In the third section, it is studied how directions of both disturbances and sensor noise can be introduced in manual and norm based design. The class of plants that is considered in this chapter does not include the AVIS discussed in Section 2.5 and Section 3.3. To illustrate the concepts developed in this chapter, direction dependent control design is applied to an industrial atomic force microscope in Section 4.4.

4.1 Norm based design

The generalized plant framework provides a way to formulate many practical control design issues. In Section 2.3, this framework was used for analysis of multivariable control systems. Using operator norms on the generalized plant, control design objectives can be expressed. If a parametric model of the generalized plant is available, controllers can be synthesized with respect to these design objectives, [36].

Common operator norms used in control synthesis methods are the \mathcal{H}_∞ or \mathcal{H}_2 norm. We are particularly interested in the frequency domain loopshaping aspects of norm based control design. Minimizing the \mathcal{H}_∞ norm corresponds to minimizing the largest peak of the largest singular value of a system, [38, 128]. Therefore, the transmission of signals with the worst direction at the worst frequency is pe-

nalized. By careful design of weighing filters, certain directional aspects of the closed loop function can be shaped. A great advantage of this, is that the system \mathcal{H}_∞ norm satisfies the multiplicative property. Hence, the system \mathcal{H}_∞ norm of the generalized plant can be shaped by studying the system \mathcal{H}_∞ norm of particular closed loop functions and the system \mathcal{H}_∞ norm of weighting filters.

Alternatively, \mathcal{H}_2 synthesis can be applied. Minimizing the system \mathcal{H}_2 norm corresponds to minimizing the sum of squares of all singular values of the system over all frequencies, [128]. The result is that the response in “average” directions and “average” frequencies is shaped, [125, p.159]. The system \mathcal{H}_2 norm does not satisfy the multiplicative property. Hence, (re)design of weighting filters is not intuitive, [34], and it can be more difficult to minimize a closed loop function in a small frequency interval and in a particular direction from a practical point of view.

On the basis of these observations, we choose \mathcal{H}_∞ control synthesis for frequency domain loopshaping control design. When time domain interpretations are preferred, one may reconsider our choice for \mathcal{H}_∞ control synthesis. Minimizing the systems \mathcal{H}_2 norm minimizes the root mean square response of the system due to unitary white noise inputs. Minimizing the systems \mathcal{H}_∞ norm minimizes the worst case gain for sinusoidal inputs at any frequency. As MIMO stochastic disturbance models can be obtained quite straightforwardly, [133], \mathcal{H}_2 synthesis can be preferred. More signal interpretations of system norms can be found in [125, p. 539] and references therein.

To shape the principal gains of closed loop transfer functions at different loop breaking points, weighting filters are to be designed that translate the design specifications. As was discussed in Section 1.2.2, the choice of sensible weighting filters for such a design can be non-trivial, especially for multivariable systems. With the insight and information obtained with procedures to characterize disturbances, it is now investigated how weighting filters can be chosen for norm based multivariable control design. To illustrate different choices of weighting filters, an \mathcal{H}_∞ design example is studied where a decoupled plant is subjected to disturbances that have fixed directions. As weighting filters are not necessarily diagonal, norm based synthesis typically results in centralized controllers. Different disturbance model choices give rise to different weighting filters, the implications of these are illustrated.

4.1.1 Disturbance rejection with \mathcal{H}_∞ control design

A generalized plant, including plant, controller, interconnections, and weighting filters, relates exogenous signals w to performance variables z ,

$$z = Mw, \quad M = \mathcal{F}_l(P, K). \quad (4.3)$$

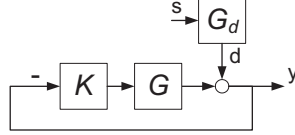


Figure 4.1: Block diagram of controller architecture. The disturbance d enters the loop at the output of the plant G . A feedback controller K is to be designed.

The objective is to minimize the transfer from w to z , by design of a stabilizing controller K , so that in,

$$\|M\|_\infty = \max_{\omega} \bar{\sigma}(M(j\omega)) \quad (4.4)$$

$$= \max_{\|w\|_2 \neq 0, \omega} \frac{\|M(j\omega)w(\omega)\|_2}{\|w(\omega)\|_2} \leq \gamma \quad (4.5)$$

γ is minimized. In the case that no model uncertainty is taken into account, the controller resulting from \mathcal{H}_∞ synthesis approaches that of frequency weighted \mathcal{H}_2 synthesis when γ approaches infinity, [23, p. 375]. The formulation of the generalized plant, with interconnections and weighting filters, is a delicate issue. Several examples are provided in [125]. We focus on the disturbance rejection problem discussed in Section 1.2. Herein, the issue is to find a stabilizing controller K so that, among other objectives, the transfer function from exogenous disturbances d to performance variable z is minimized. For the rejection of disturbances, the following weighted output sensitivity function,

$$\|S_o V\|_\infty \quad (4.6)$$

is to be minimized. Herein, V is a rational, stable, minimum phase, frequency dependent weighting filter that represents the frequencies and directions of the output disturbances. The choice of V is often non-trivial, especially in multivariable systems where aside from frequency dependence, directions are to be taken into account. Here, we will focus on the disturbance rejection for which the fixed direction disturbance model from Chapter 3 holds. We consider only sources, no interfering noise signals, hence with $G_d = G_s$,

$$d(t) = G_d s(t). \quad (4.7)$$

The columns of the matrix G_d hold the directions of the disturbances and $s_i(t)$ are mutually statistical independent but unmeasurable sources. As $s(t)$ can not be measured directly, conventional control design approaches consider $d(t)$ without detailed knowledge of G_d and $s(t)$. With the results from the blind identification procedure outlined in Chapter 3, we study how estimates of the sources and the matrix G_d can be used in control design and how they improve on the approach using $d(t)$ only.

Firstly, principal component analysis (or whitening) can be used to recover uncorrelated components $z(t)$ and the whitening matrix W . Then, the following disturbance model can be formulated,

$$d(t) = W^{-1}Us(t) = W^{-1}z(t). \quad (4.8)$$

This shows that the sources are recovered up to an unknown unitary matrix, U . The directions of disturbances due to each uncorrelated component are contained in the columns of W^{-1} .

Secondly, the Second Order Blind Identification (SOBI) procedure, estimates independent components $\hat{s}(t)$, so that the following disturbance model holds,

$$d(t) = W^{-1}\hat{U}P\Lambda s(t) = \hat{G}_d\hat{s}(t). \quad (4.9)$$

Herein, both $\hat{s}(t)$ and $s(t)$ are statistically independent. Furthermore, Λ is an arbitrary diagonal matrix with $\Lambda > 0$ and P is a permutation matrix. Both Λ and P can not be determined with the blind identification procedure. These indeterminacies have no influence on the spectra of the estimated sources, $\hat{s}(t)$. Hence the spectra of the estimated sources equal the spectra of the true sources. SOBI determines the unitary matrix \hat{U} , so that $\hat{G}_d = W^{-1}\hat{U}$. In the whitening step, it was assumed that $R_s(0) = I$, which implies that all scalings of the sources are contained in \hat{G}_d . Alternatively, one may choose to scale the columns of \hat{G}_d to unity. This is just a matter of convention.

This shows, that quite some detail of the disturbance model is gathered using blind identification techniques. With this in mind, three approaches to choose V are studied. Namely, designs with 1) disturbance direction fixed, sources unknown, V_d , 2) disturbance direction not fixed, hence worst case design, V_{wc} , 3) disturbance direction fixed and sources blindly identified, $V_{\hat{s}}$.

Disturbance direction fixed, sources unknown

In this design approach, no information from blind identification is used. In the case that the plant is decoupled, a common practical approach is to consider the disturbance $d(t)$ as an exogenous signal acting on each controlled variable independently. The relations between disturbances at each controlled variable are neglected. Hence, the disturbance at each controller variable is, rather naively, modeled without taking into account any mutual information. This approach is incorrect in general and does not provide any guarantee for the achievable performance. However, we would like to demonstrate its implications. Therefore, a diagonal weighting filter in (4.6), is chosen so that $V = V_d$,

$$V_d(j\omega) = \text{diag}\{V_{d,i}(j\omega)\} \quad (4.10)$$

where $V_{d,i}(j\omega)$ is designed to satisfy

$$|V_{d,i}(j\omega)| \geq |\sqrt{\Phi_{d_i}(j\omega)}|. \quad (4.11)$$

Herein, $\Phi_{d_i}(j\omega)$ is the (univariate) power spectrum of the output disturbance on each i^{th} output of the plant (the controller variable). As the disturbances $d(t)$ are a mixture of source signals $s(t)$, it is expected that an upper bound, (4.11), may introduce conservatism and may fail to model the multivariable disturbance at all.

Disturbance direction not fixed, hence worst case

Another approach is to model the largest disturbance that may result from a linear combination of the sources. We refer to this disturbance as the worst case disturbance. The alignment between output sensitivity function and the direction of this largest disturbance determine if this disturbance leads to a worst case disturbance rejection performance. In this approach, the objective is to design a controller that rejects this worst case disturbance in any direction. The results from whitening (principal component analysis) can be used to construct a weighting filter V for (4.6). As the first principal component equals the worst case disturbance, $d_{wc}(t)$, it follows from $d(t) = W^{-1}z(t)$ that,

$$d_{wc}(t) = \tilde{w}_1 z_1(t), \quad (4.12)$$

where \tilde{w}_1 is the first column of W^{-1} . Without loss of generality, we choose to normalize the columns of \tilde{w}_1 to unity and move all scaling to the signal $z_{wc}(t) = \|\tilde{w}_1\|_2 z_1(t)$, $\tilde{w}_{wc} = \tilde{w}_1 \|\tilde{w}_1\|_2^{-1}$, so that,

$$d_{wc}(t) = \tilde{w}_{wc} z_{wc}(t). \quad (4.13)$$

In order to weight for the worst case disturbance in all directions, the following weighting filter $V = V_{wc}$ is chosen as,

$$V_{wc}(j\omega) = V_{z,wc}(j\omega) I, \quad (4.14)$$

where $V_{z,wc}(j\omega)$ is a scalar weighting filter so that

$$|V_{z,wc}(j\omega)| \geq |\sqrt{\Phi_{z_{wc}}(j\omega)}| \quad (4.15)$$

is satisfied. Herein, $\Phi_{z_{wc}}(j\omega)$ is the power spectrum of $z_{wc}(t)$. The first principal component is generally a mixture of the sources, hence the spectra of $z_{wc}(t)$ contains components from the sources. In practical control design, weighting filters have limited order. Therefore, with design of an upper bound, conservatism may be introduced. Furthermore, using the same weight in all directions, (4.14), can be unnecessarily pessimistic.

Disturbance direction fixed, blindly identified

When SOBI is used, the independent components $\hat{s}(t)$ and the constant matrix \hat{G}_d are recovered. With this information, it is demonstrated how a weighting filter

V can be constructed for norm based control design. Without loss of generality, one may normalize the columns of \hat{G}_d to unity. A diagonal scaling matrix $\Lambda = \text{diag}\{\lambda_i\}$, with $\lambda_i = \|\hat{g}_{d,i}\|_2^{-1}$ the inverse of the norm of the i^{th} column of \hat{G}_d is defined. Now, $\hat{G}_d = \tilde{G}_d\Lambda$ and,

$$d(t) = \tilde{G}_d\tilde{s}(t) \quad (4.16)$$

where $\tilde{s}(t) = \Lambda\hat{s}(t)$. Herein, \tilde{G}_d contains the directions of each independent component whereas all magnitude information is held by $\tilde{s}(t)$. We define the total weighting filter $V = V_{\tilde{s}}$ as the transfer function matrix,

$$V_{\tilde{s}}(j\omega) = \tilde{G}_dV_{\tilde{s}}(j\omega). \quad (4.17)$$

Herein, $V_{\tilde{s}}(j\omega)$ is diagonal ($V_{\tilde{s}}(j\omega)$ is non diagonal if \tilde{G}_d is non-diagonal) with on each i^{th} diagonal element a weighting filter for the power spectrum of the i^{th} (scaled) independent component, namely,

$$|V_{\tilde{s}_i}(j\omega)| \geq |\sqrt{\Phi_{\tilde{s}_i}(j\omega)}|, \quad i = 1, \dots, n \quad (4.18)$$

The indeterminacies of the blind identification solution only imply the exchange of gain, sign and permutation between $\hat{s}(t)$ and the columns of \hat{G}_d . Therefore, each weighting filter in (4.18) bounds the spectrum of each independent source. This may result in less conservative upper bounds, especially when the order of the weighting filter is restricted. Also, from an engineering perspective, more insight can be obtained as weighting filters have a physical meaning. As the directions of the actual sources are taken into account, one is able to design weighting filters in only those directions that are relevant.

4.1.2 Simulation Example

The design of weighting filters for disturbances is illustrated on a model of a two degrees of freedom manipulator. The plant is diagonal, so that the plant can be controlled independently in each direction. We choose a diagonal plant for illustration purposes, the norm based control design framework is able to handle more general plants. The plant is defined as,

$$G(s) = \begin{bmatrix} \frac{k_1}{s^2} & 0 \\ 0 & \frac{k_2}{s^2} \end{bmatrix}. \quad (4.19)$$

Here, $k_1 = k_2 = 4 \times 10^3$, which results in a magnitude of $0dB$ at $10Hz$ for each controlled axis. The plant dynamics are uncertain at frequencies above $100Hz$. The output disturbances are shown in Fig.4.3. As the plant has uncertain dynamics above $100Hz$, roll-off is desired. This requirement is expressed by weighting the control sensitivity KS_o with W_{ks} . Also, we have a low frequency objective, expressed by a weight W_s on the output sensitivity. These two objectives are

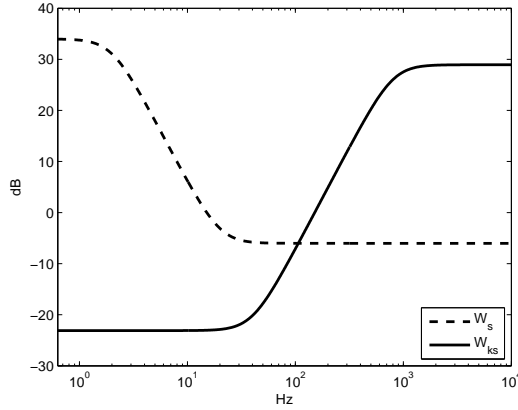


Figure 4.2: Frequency response (magnitude only) of the elements of the weighting filters (diagonal) for the sensitivity function W_s (dashed) and the control sensitivity function W_{ks} (solid).

formulated in a standard \mathcal{H}_∞ mixed sensitivity problem, see, e.g., [125]. Now a stabilizing controller K is to be found that minimizes,

$$\left\| \begin{array}{c} W_s S_o V \\ W_{ks} K S_o V \end{array} \right\|_\infty. \quad (4.20)$$

The weighting filters W_s, W_{ks} are chosen diagonal, with the same gain in all directions. The frequency response of the elements of W_s, W_{ks} is shown in Fig. 4.2. These weighting filters are the same for all examples. The weighting filter V expresses the characteristics of the output disturbances. Choosing a particular V , the relevant frequencies and directions of the disturbances can be taken into account. The initial design is $V = I$. Alternative choices of V are studied, each using a different disturbance model. All designs are targeted to achieve the same closed loop bandwidth with the same robustness margins.

Blind identification

The Second Order Blind Identification method from Chapter 3 is used to characterize the observed output disturbances, d_1, d_2 , shown in the left hand side of Fig. 4.3. From the whitening procedure the uncorrelated components $z(t), d(t) = W^{-1}z(t)$, are determined. The whitening matrix equals,

$$W^{-1} = \begin{bmatrix} -4.21 & -0.35 \\ -3.57 & 0.41 \end{bmatrix}. \quad (4.21)$$

The uncorrelated components are shown in the middle plot of Fig. 4.3. It is clear that these uncorrelated components do not allow straightforward physical

interpretation. Using joint diagonalization, the independent components $\hat{s}(t)$ are recovered

$$\hat{s}(t) = \hat{G}_d^{-1}d(t) = \hat{U}^T W d(t) \quad (4.22)$$

where \hat{G}_d is determined as

$$\hat{G}_d = \begin{bmatrix} -3.01 & -2.97 \\ -3.01 & -1.97 \end{bmatrix}. \quad (4.23)$$

For this example, the true (but unknown) matrix was

$$G_d = \begin{bmatrix} 3 & 3 \\ 3 & 2 \end{bmatrix} \quad (4.24)$$

so that the indeterminacy of the blind identification method implies that the sign of the recovered mixing matrix (and the same change of sign in the recovered sources) can not be identified. The independent components are shown in the right plot of Fig. 4.3. Clearly, a step sequence and a combination of harmonics

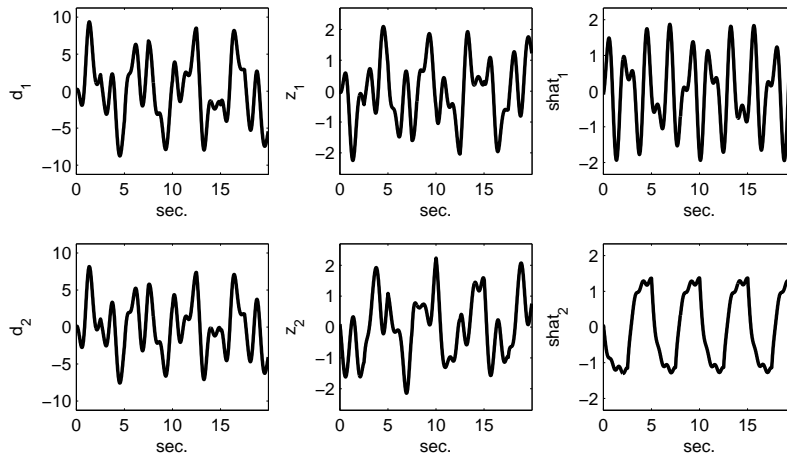


Figure 4.3: Left: output disturbances $d(t)$, Middle: uncorrelated components $z(t)$, Right: independent components $\hat{s}(t)$

can be distinguished. In a practical situation, one may interpret this as sources from physical phenomena (other machines in a factory, pumps, etc.). With these results, control design with several different choices of the weighting filter V are considered.

Weighting filter design

We choose to have the same bandwidths (first 0dB crossing of principal gains of the output sensitivity function) and the same margins in all designs. This is no

limitation in the theory presented here, but allows more transparent comparison of the sensitivity functions. In order to obtain the same bandwidths in all designs, the weighting filter V is designed to equal the identity matrix at frequencies close to the bandwidth. We restrict ourselves to fourth order weighting filters V , hence in all three designs, each power spectrum is bounded with a second order weighting filter.

The first control design considers a weighting filter, $V = V_d$, that bounds the square root of the power spectra of $d(t)$ at each controlled variable. Each of these power spectra contain contributions of both sources. A second order weighting filter is designed to bound each spectrum from above, Fig. 4.4. In the second

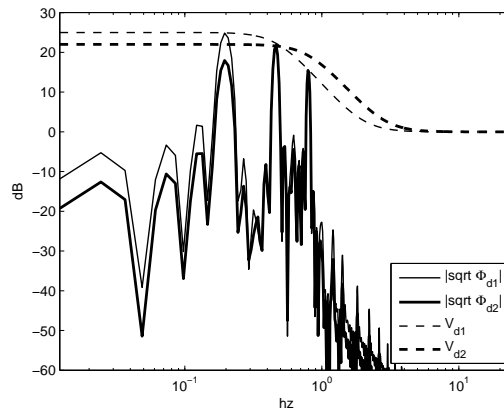


Figure 4.4: Weighting filter design based on the power spectrum of the output disturbances.

design, a weighting filter, $V = V_{wc}$, is constructed that bounds the power spectrum of the worst case disturbance (the first principal component). The worst case disturbance contains contributions of both sources. A second order weighting filter is used to bound the power spectrum from above, Fig. 4.5. This weighting is applied in all directions, see (4.14). The third design uses the information from blind identification to construct a weighting filter $V = V_{\hat{s}}$. The power spectra of $\tilde{s}(t)$, that is $\hat{s}(t)$ scaled with Λ , are calculated. The estimated sources are independent, hence their spectra are separated. Second order low pass weighting filter bounds the power spectrum of each estimated source, $\hat{s}(t)$, from above, Fig. 4.6. As the total weighting filter must be equal to the identity matrix at frequencies around the bandwidth we choose,

$$V_{\hat{s}}(j\omega) = \tilde{G}_d V_{\tilde{s}}(j\omega) - I. \quad (4.25)$$

Herein, $V_{\tilde{s}}$ is diagonal and $V_{\hat{s}}$ is non-diagonal. The designs are discussed in detail in the following section.

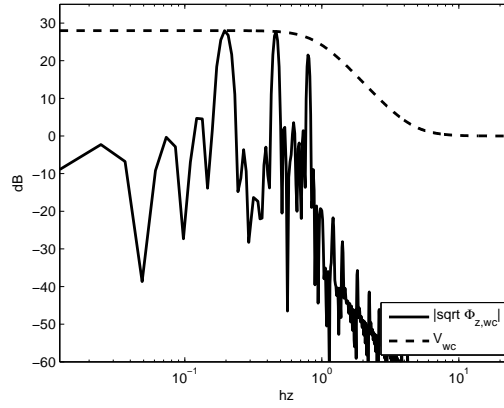


Figure 4.5: Weighting filter design based on the power spectrum of the worst case disturbance.

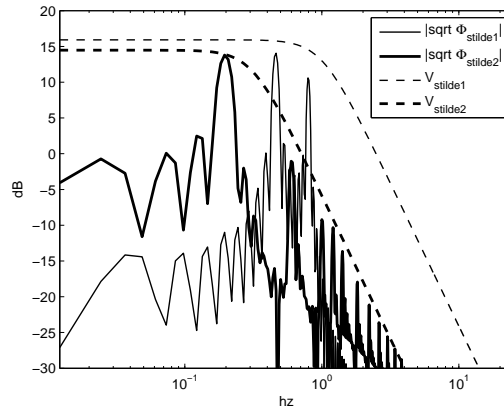


Figure 4.6: Weighting filter design based on the power spectrum of the independent components.

Discussion

Each design approach resulted in a different weighting filter and therefore a different sensitivity function. Here, the differences between those sensitivity functions are discussed. We have the initial design with $V = I$ and the three designs with specific models of the disturbances, V_{wc} , V_d and $V_{\tilde{s}}$ respectively. Ideally, weighting filters describe the spectrum of the disturbances perfectly. In practical situations however, the order of the transfer functions of the weighting filters is restricted. Then, weighting filters are tuned to upper bound the square root of the power

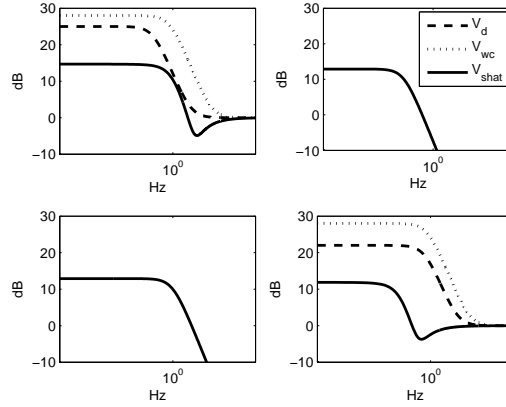


Figure 4.7: Bode magnitude plot of all three weighting filters, V_d (dashed), V_{wc} (dotted), $V_{\hat{s}}$ (solid)

spectrum. If the order of the transfer functions of the weighting filters is small, conservatism is introduced in upper bounding the power spectra. This conservatism may be significant when the power spectra contain contributions of more sources, as in the case of V_d, V_{wc} . In the design with $V_{\hat{s}}$, the spectra of each source is distinct and weighting filters can be chosen to describe the contribution of each source independently. Then, conservatism due to the restricted order of the weighting filters may be reduced. As each estimated source can be related to a physical cause of the disturbance, transparent design of (non-diagonal) weighting filters is facilitated. The bode magnitude plot of all three weighting filters is depicted in Fig. 4.7. Herein, it is shown that both V_{wc} and V_d are diagonal and $V_{\hat{s}}$ is non-diagonal. The principal gains of each weighting filter are depicted in Fig. 4.8. Both V_d and V_{wc} have high gains in all principal directions. As the disturbances only act in a few directions, V_d and V_{wc} weight the sensitivity function in directions that are not relevant from a disturbance perspective. In contrast, the weighting filter $V_{\hat{s}}$ weights only in the relevant directions and at the same time, reduces weight in orthogonal directions. Furthermore, as the spectra of $\hat{s}(t)$ describes each source independently, design of weighting filters may be more intuitive and less conservatism may be introduced in cases where the order of the weighting filter is restricted.

The weighting filter choices result in different output sensitivity functions. The bode magnitude of the output sensitivity functions is shown in Fig. 4.9. Only the design with weighting filter $V_{\hat{s}}$ results in a sensitivity function with large off-diagonal terms. These off-diagonal terms are required to reject disturbances in only a particular direction. In this case, this also implies that the diagonal terms of the sensitivity function are significantly larger compared to the designs with V_{wc} and V_d . The principal gains of the sensitivity functions are shown in

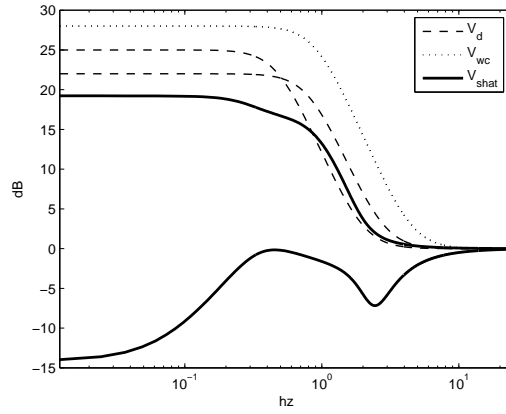


Figure 4.8: Principal gains of the weighting filters V_d (dashed), V_{wc} (dotted) and $V_{\hat{s}}$ (solid).

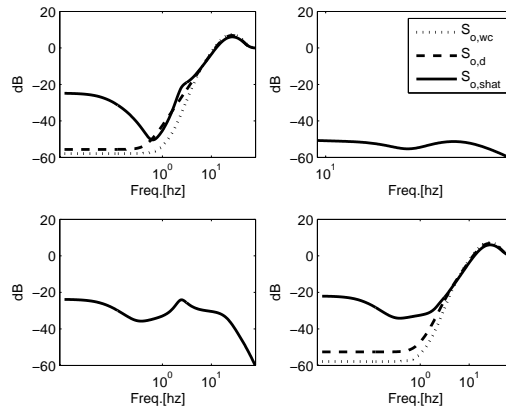


Figure 4.9: Bode magnitude plot of the output sensitivity functions resulting from design with V_{wc} , V_d and $V_{\hat{s}}$ respectively.

Fig. 4.10. The designs with V_d and V_{wc} result in sensitivity functions that are smaller in all directions compared to the initial design $V = I$. The sensitivity function with the design with $V_{\hat{s}}$, has small sensitivity function in the directions of the disturbances, but is allowed to increase in orthogonal directions. In this case, the costs of disturbance rejection in the design with weight $V_{\hat{s}}$ turns out to be equal to the initial design with weight $V = I$. From Cor. 2.2.1, we know that

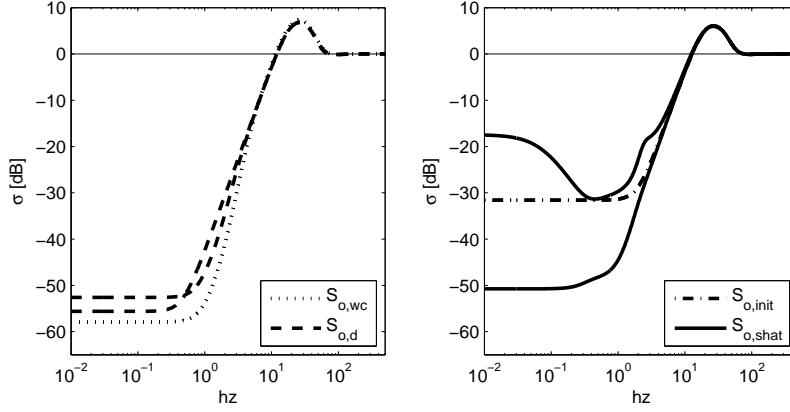


Figure 4.10: Principal gains of output sensitivities with four choices of V . Left: design with weight filter based on the output disturbances (dashed) and design for worst case disturbance in all directions (dotted). Right: initial design with $V = I$ (dash dot) and design based on the independent components (solid).

Table 4.1: Cumulative sum of the area, in $\text{dB} \times \text{Hz}$, below $\ln \sigma_i(S_o)$

	$O_{\sigma_1 < 0\text{dB}}$	$O_{\sigma_2 < 0\text{dB}}$	$O_{\sigma_1 > 0\text{dB}}$	$O_{\sigma_2 > 0\text{dB}}$	$O_{\text{sum}\sigma_i > 0\text{dB}}$
$V = I$	-212	-212	210	210	421
$V = V_d$	-232	-251	243	236	479
$V = V_{wc}$	-271	-271	268	268	536
$V = V_{\hat{s}}$	-181	-246	214	210	425

the following integral relation holds,

$$\sum_{i=1}^n \int_0^{\infty} \log \sigma_i(S_o(j\omega)) d\omega = \sum_{i=1}^n F_i = 0. \quad (4.26)$$

For all four designs, the singular values of the output sensitivities are calculated over a linear frequency grid $f = [0.01 \text{ } 1e3][\text{Hz}]$ with 1×10^4 points. Then, the area is calculated between each principal gain and 0dB for the intervals where the principal gains are below and above 0dB respectively. The results are listed in Table 4.1. Here, $O_{\sigma_i < 0\text{dB}}$ denotes the area between $\sigma_i(S_o)$, and 0dB when $\sigma_i(S_o)$ is below 0dB , $O_{\sigma_i > 0\text{dB}}$ denotes above. The total area between $\sigma_i(S_o)$ and 0dB when $\sigma_i(S_o)$ is above 0dB , is denoted as $O_{\text{sum}\sigma_i}$.

For the design with $V = I$ and V_{wc} , the terms F_i in (4.26) appear to be zero. As in the designs V_d and $V_{\hat{s}}$, the terms F_i are non-zero, one is able to tradeoff the

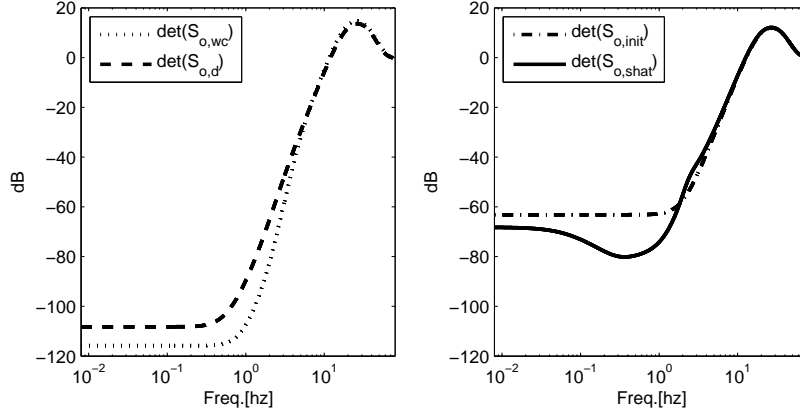


Figure 4.11: Determinant of the output sensitivity functions per frequency of all four designs.

disturbance rejection properties between principal gains. For these designs, the principal directions that belong to those principal gains change per frequency. It is therefore difficult to relate a specific input/output of the sensitivity to those principal gains. The design with $V_{\hat{s}}$ has the same amplification at high frequencies as the design with $V = I$, the term $O_{sum\sigma_i > 0dB}$ is almost the same in the two designs. Another useful relation to show this, is the integral relation of the determinant of the sensitivity function,

$$\int_0^{\infty} \log |\det(S_o(j\omega))| d\omega = 0. \quad (4.27)$$

The determinant of the sensitivity functions per frequency is plotted in Fig. 4.11. The designs with V_d and V_{wc} result in much smaller values at low frequencies than the design with $V = I$. As a result of (4.27), the area of the sensitivity function above $0dB$ increases. The design with $V = V_{\hat{s}}$ results in values that are smaller or larger than the initial design at low frequencies. The total area below $0dB$ is the same as in the design with $V = I$, hence the area above $0dB$ does not increase. As this measure relies on the determinant of the sensitivity function, it does not provide information for frequency wise tradeoffs of individual input output relations.

Using the integral relation from Theorem 2.2.3, it can be studied how a frequency wise tradeoff from a single (linear combination of the) input to a single (linear combination of the) output of the sensitivity function works out. For the design with $V_{\hat{s}}$, the transfer function from the first estimated source to the output of the first controlled axes equals, $S_{uv} = e_1^T S_o \tilde{g}_{d1}$, with \tilde{g}_{d1} the first column of \tilde{G}_d , and $e_1 = [1, 0]^T$. To reject the influence of the first source on the first controlled axes, the single input single output transfer function S_{uv} must be minimized. In Fig.

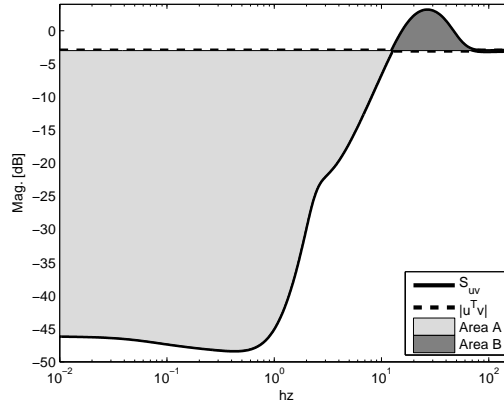


Figure 4.12: Bode magnitude plot of S_{uv} and $|u^T v|$ and the area below and above $|u^T v|$.

4.12, both S_{uv} and $|u^T v|$ are shown. As a result of Theorem 2.2.3, the area A must be equal to the area B when S_{uv} is plotted against linear scale (not shown here), hence a frequency wise tradeoff similar to that of scalar systems exists for this input/output combination.

These integral relations show that the design with $V_{\hat{s}}$ takes into account only those disturbance directions that are relevant. In directions orthogonal to those of the disturbances, the sensitivity function is allowed to increase. The alternative designs, V_d and V_{wc} , result in sensitivity functions that are reduced in more directions than required. As a result, unnecessary costs appear as increase of the sensitivity function at other frequencies. As $S_o + T_o = I$, the complementary sensitivity function increases, see Fig. 4.13. It is visible that the singular values of $T_{o,wc}, T_{o,d}$ are almost 2dB larger in this region than the singular values of $T_{o,init}, T_{o,shat}$. The singular values of $T_{o,init}, T_{o,shat}$ are almost the same in this frequency region. This is also illustrated in the time domain. In Fig. 4.14, the response of $z = S_o d$ is shown for the four designs. It is visible that the design with V_d, V_{wc} have better disturbance rejection performance than the design with $V = I, V_{\hat{s}}$. The design with $V_{\hat{s}}$ has better disturbance rejection performance than the initial design. To illustrate the costs of disturbance rejection in the time domain, we study the response to sensor noise, $z = T_o n$. Herein, we choose $n(t)$ as a sum of sinusoids in the frequency range 20 – 40Hz. The response of the design with $V_{\hat{s}}$ is equal to the design with $V = I$, Fig. 4.15. The amplification of sensor noise for the designs with V_{wc}, V_d is a factor $1.25 \approx 2\text{dB}$ higher than with the design $V_{\hat{s}}$.

In order to reject disturbances only in relevant directions, the sensitivity function can have non-zero non-diagonal terms. If the plant is diagonal, a centralized

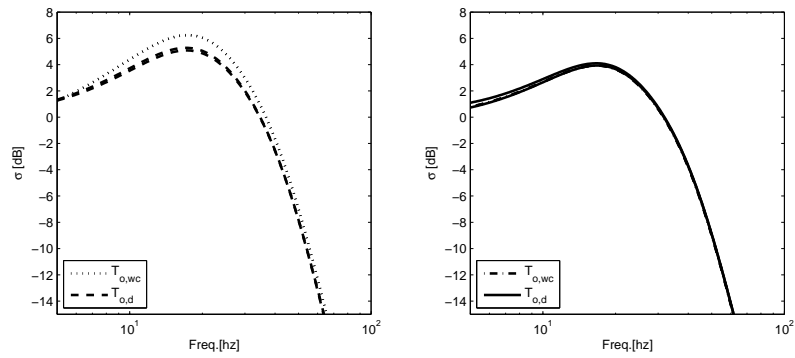


Figure 4.13: Singular values of the complementary sensitivity function for all four designs.

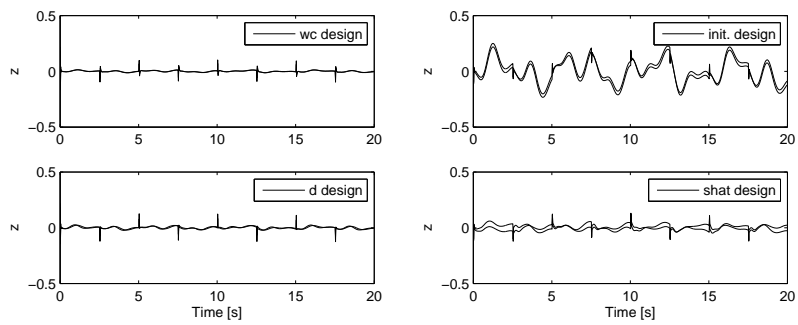


Figure 4.14: Response of the performance variable z to the disturbance d , see (4.7).

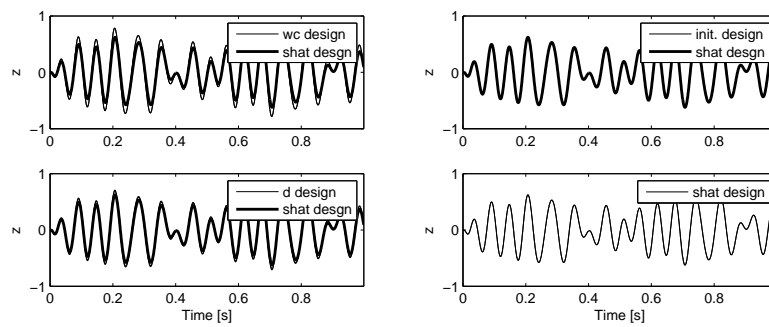


Figure 4.15: Response of the performance variable z to sensor noise at 20 – 40Hz.

controller is required. The \mathcal{H}_∞ synthesis method naturally generated these centralized controllers. It is interesting to investigate how similar results can be obtained using manual loop shaping design.

4.1.3 Conclusion

In this section, it was shown how the insight and information from the blind identification method can be exploited in the choice of weighting filters for \mathcal{H}_∞ control design. A non-diagonal weighting filter was used to shape the sensitivity function in such a way that only relevant disturbance directions are taken into account. In orthogonal directions, the sensitivity function was allowed to increase, leading to less severe frequency wise performance tradeoffs. The blind identification techniques unmix the spectra of the sources. If the order of the transfer functions of the weighting filters is small, it may be preferable to design the weighting filters on the unmixed spectra. As the estimated sources have the same spectra as the physical sources, a transparent and physically motivated choice of non-diagonal weighting filters is facilitated. In the next sections, loop shaping techniques, that only require non-parametric models, are developed to design centralized controllers for the rejection of fixed direction disturbances.

4.2 Disturbance decoupling design

In this section, a method will be proposed to design a feedback controller to reject disturbances with strong directional dependence. The inherent tradeoffs in feedback control, see Section 2.2, can then be made for each disturbance direction independently. The resulting controller will have a centralized structure. The method is restricted to a specific class of plants. We only discuss rejection of disturbances with orthogonal directions. To illustrate the design method, a parametric model of an industrial high performance positioning system, called a waferstage, is used. A competing controller is designed using \mathcal{H}_∞ synthesis. It is shown that the proposed design method can be used to reverse engineer, hence interpret, a (centralized) MIMO \mathcal{H}_∞ controller.

We focus on the rejection of output disturbances that can be represented by the following transfer function matrix,

$$V_{d_o}(s) = UV_d(s). \quad (4.28)$$

Herein, $V_d(s)$ is a square diagonal transfer function matrix and U is a non-singular matrix with constant elements for all frequencies. In the following, we restrict ourselves to the case where U is an orthogonal matrix. A few remarks on more general choices of U will be given at the end of this section.

The class of plants to which this method is restricted are plants where the directions do not change under orthogonal pre- and post multiplication. Then, $\kappa(G) = 1$, see (4.2), and $GK = KG$, so that control design is simplified. We can describe those plants as,

$$G(s) = g(s)I, \quad (4.29)$$

where $g(s)$ is scalar. By using the framework presented in Section 2.3, unmodeled dynamics can be taken into account and the class of plants can be extended to systems that are of the form,

$$G_p(s) = (I + E(s))G(s), \quad G(s) = g(s)I \quad (4.30)$$

where E is stable. An example of systems that can be described this way are motion systems with rigid body behavior, Section 2.4.3 and Example 2.4.2. An industrial motion control application without rigid body modes that can also be represented in this way is discussed in Section 4.4. From Section 2.3, a sufficient condition for closed loop stability can be deduced that states that when $S_o = (I + GK)^{-1}$ is stable and,

$$\bar{\sigma}(T_o(j\omega)) < \frac{1}{\bar{\sigma}(E(j\omega))}, \quad \forall \omega, \quad (4.31)$$

where $T_o = I - S_o$, the closed loop MIMO system is stable. In systems with rigid body modes, the term $\bar{\sigma}(E(j\omega))$ is large at high frequencies, hence the bandwidth of the feedback system is constrained. The challenge is to develop a control design method to reject disturbances exploiting their directionality. Then, one has the freedom to make the frequency wise tradeoffs discussed in Section 2.2 per orthogonal disturbance direction.

4.2.1 Control design in disturbance directions

Originally, the plant is defined in the *control coordinates*. A coordinate transformation $y_d = U^T y$ so that, $U^T d_o(s) = V_d(s)$, can be used to express the variables in *disturbance coordinates*. This is equivalent to choosing a controller $K(s) = UK_d(s)U^T$, with $U \in \mathbb{R}^{n \times n}$, $U^T U = I$ and $K_d(s)$ a diagonal matrix with scalar transfer functions. For the class of plants considered here holds that, $G(s) = g(s)I$. Hence, the transfer functions at the right hand side of (2.107), become,

$$\begin{aligned} S_o &= US_o^d(s)U^T \\ T_o &= Ug(s)K_d(s)S_o^d(s)U^T \\ S_o G &= US_o^d(s)g(s)U^T \end{aligned} \quad (4.32)$$

where $S_o^d(s) = (I + g(s)K_d(s))^{-1}$, is the (diagonal) sensitivity function in disturbance coordinates. Therefore, all relevant closed loop transfer functions are

decoupled in the disturbance coordinates. This means that a disturbance with direction aligned to a column of U^T , is only affected by a single controller on the diagonal of $K_d(s)$. Also, by Corollary 2.2.4, the frequency domain tradeoff, implied by rejecting such a disturbance, only manifests itself in the diagonal element of $S_o^d(s)$ corresponding to the diagonal element of $K_d(s)$. At the same time, a single element of $K_d(s)$ can change more elements of $S_o(s)$, which is in control coordinates.

Considering the influence of the flexible dynamics, modeled as a multiplicative perturbation $E(s)$, Fig. 2.9, the transformation implies that the multiplicative perturbation in disturbance coordinates equals $E_d(s) = U^T E(s) U$. As U is orthogonal, $\bar{\sigma}(E_d) = \bar{\sigma}(E)$ and the same upper bound as shown in (4.31) has to be satisfied for all elements of the diagonal complementary sensitivity function in disturbance coordinates, $T_o^d(s)$.

The same coordinate transformation can be performed with any invertible matrix U , so that $K(s) = U K_d(s) U^{-1}$. However, the consequence is that the bound on $T_o^d(s)$ induced by E , can be conservative if the condition number of U increases as $\bar{\sigma}(U E U^{-1}) \leq \bar{\sigma}(E) \kappa(U)$, where $\kappa(U) = \bar{\sigma}(U) / \underline{\sigma}(U)$ is the condition number. Likewise, specifications as the peak value of the sensitivity functions are difficult to carry over to disturbance coordinates if $\kappa(U)$ is large.

As the rejection of fixed direction disturbances is studied in coordinates where the disturbances are decoupled, frequency domain tradeoffs are more transparent. Because the controller and all closed loop transfer functions in disturbance coordinates are diagonal, scalar design techniques, such as manual loopshaping see e.g. [129], can be facilitated. The resulting controller in control coordinates, $K(s)$, will in general be non-diagonal as the input directions of the sensitivity function in control coordinates $S_o(s)$ will be aligned to the disturbance directions (that can be non-canonical). The following example will show how the proposed method can be used in a practical design problem.

4.2.2 Application example

As a demonstration of the theory, a model of a waferstage is studied. This is a high precision positioning stage. A detailed description of the plant can be found in [97, 143]. The objective is to regulate the position of this stage in the presence of environmental disturbances, e.g., floor vibrations, machine oscillations, pumps, etc. We consider the case where the reference position of the stage is fixed and the location of the origin of disturbance is fixed. Then, the directions of the disturbances are fixed. Identification of the direction and the origin of such disturbances is discussed in Chapter 3. The stage has six degrees of freedom, here only the outputs y_x, y_y, y_z (and interaction in between) are studied. These outputs are in cartesian coordinates. It is a requirement that the plant is expressed in these cartesian coordinates. The Bode magnitude diagram of $G_{yu}(s)$ is shown in

Fig. 4.16. Frequencies that are discussed in this work are indicated by numbers. Following the approach of Example 2.4.2, the plant model that is used for control design equals,

$$G(s) = \frac{1}{ms^2}I \quad (4.33)$$

where $m \in \mathbb{R}^1$, Fig. 4.17. Flexible dynamics $G_{flex}(s)$, Fig. 4.17, limit the achievable bandwidth as the inverse of the maximum singular value of $E(s) = (G_{yu}(s) - G(s))G(s)^{-1}$ upperbounds the allowable complementary sensitivity, see Fig. 4.21. For robustness purposes it is required that $\bar{\sigma}(S_o) < 6\text{dB}$. We study the rejection of three artificial sinusoids in orthogonal directions. Each harmonic is described by a scalar model $V_{di}(s), i = \{1, 2, 3\}$, representing the harmonic at frequency 1, 2, 3[–] respectively. The disturbance at the output of the plant is modeled by the transfer function matrix,

$$V_{d_o}(s) = UV_d(s) \quad (4.34)$$

where $V_d(s) = \text{diag}\{V_{d1}(s), V_{d2}(s), V_{d3}(s)\}$ and U is a constant orthogonal matrix,

$$U = \frac{1}{3} \begin{bmatrix} 2 & -2 & 1 \\ 1 & 2 & 2 \\ 2 & 1 & -2 \end{bmatrix} \quad (4.35)$$

which columns span the directions of the disturbances. Here, we chose U artificially. However, U may be constructed using the results of the identification procedure discussed in Chapter 3. In the next subsections, three design approaches are considered that are designed to have the same level of rejection of these disturbances.

Multiloop SISO design in control coordinates

If the plant is sufficiently decoupled, a common approach is to design a decentralized feedback controller by choosing SISO controllers for each cartesian axis. This is often called a *multiloop SISO* control design, [125]. Manual design typically uses a combination of lead lag, second order lowpass elements, see, e.g., (2.103). In order to achieve disturbance rejection at specific frequencies, the SISO controllers are augmented with a collection of inverted notches (bandpass filters) tuned at the components of the disturbances at the output of the plant, Fig. 4.18. As in this approach, the directions of the disturbances are not taken into account explicitly, the disturbances at each j^{th} output of the plant are then modeled as,

$$d_{o,j}(s) = \sum_{i=1}^3 U_{j,i} V_{di}(s) \quad (4.36)$$

where $U_{j,i}$ denotes the j, i^{th} element of U . With this approach, for this particular application example, it turns out to be very difficult to reject these disturbances

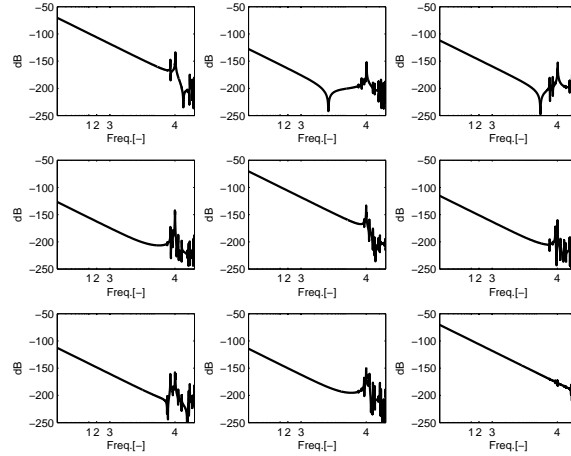
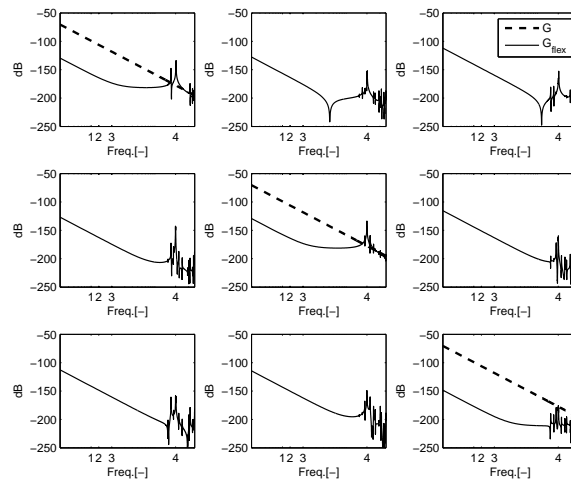


Figure 4.16: Bode magnitude diagram of the high precision positioning stage.

Figure 4.17: Bode magnitude diagram of G and G_{flex} .

while at the same time satisfying the other design requirements, $\bar{\sigma}(S_o) < 6[dB]$, $\bar{\sigma}(T_o) < \bar{\sigma}(E)^{-1}$. Rejection of the disturbances is only possible if either the sensitivity peak increases, or the complementary sensitivity function crosses the bound induced by the flexible dynamics, Fig. 4.21. This typical limitation can be explained as in Fig. 4.22 it is visible that the sensitivity function is reduced in

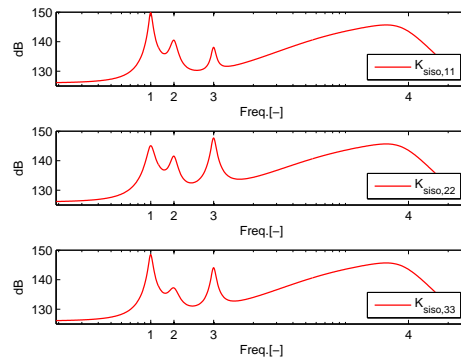


Figure 4.18: Bode magnitude diagram of the diagonal terms of the multiloop SISO controller (in control coordinates).

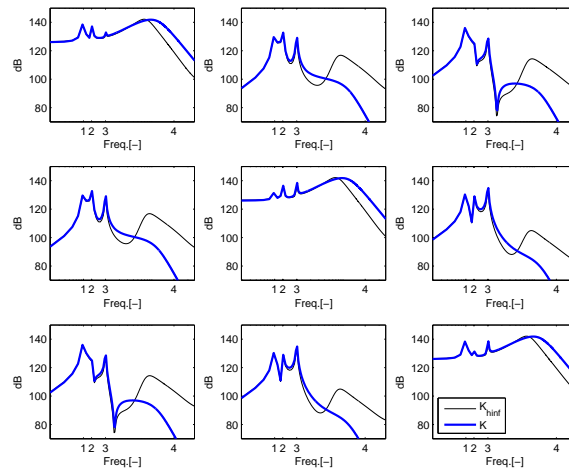


Figure 4.19: Bode magnitude diagram of the controller in control coordinates, K_{hinf} and K .

directions that are not relevant for this design case. Hence the sensitivity function is increased more than necessary. This design approach does not result in a satisfactory solution for this problem.

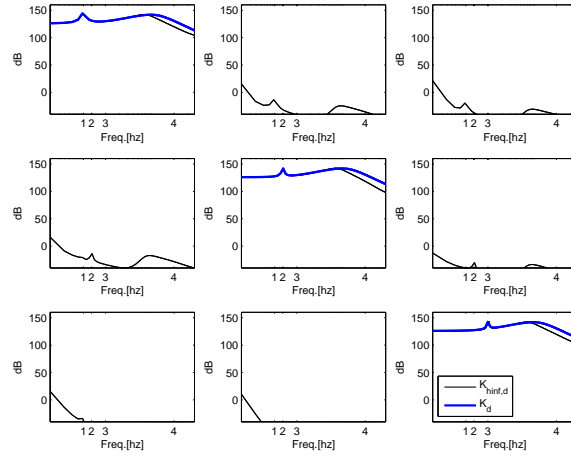


Figure 4.20: Bode magnitude diagram of the controller in disturbance coordinates, $K_{hinf,d}$ and K_d .

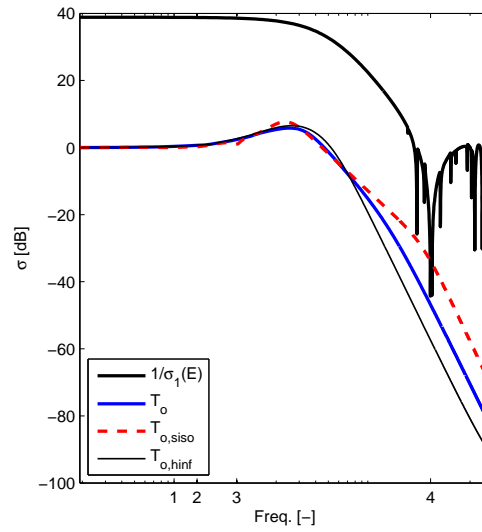


Figure 4.21: Maximum singular value of complementary sensitivity for \mathcal{H}_∞ design, SISO design and design in disturbance coordinates compared to the bound induced by $E(j\omega)$.

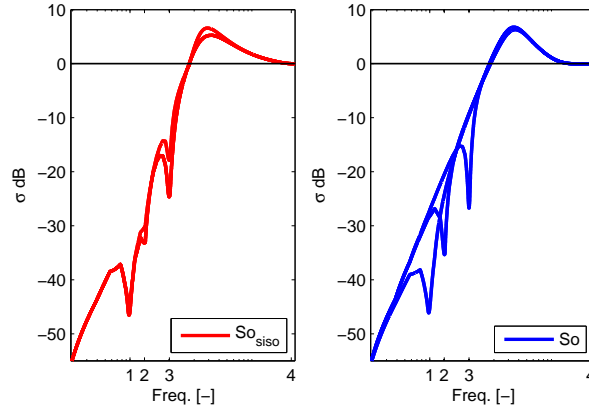


Figure 4.22: Principal gains of the output sensitivity function. Multiloop SISO design (left) and design in disturbance coordinates (right).

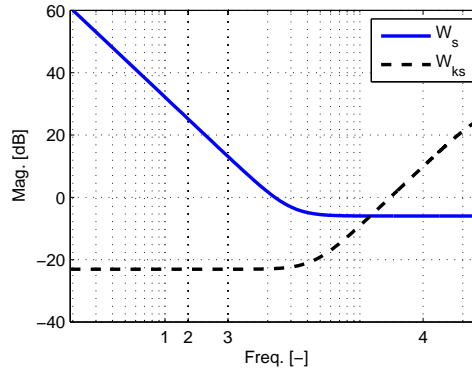


Figure 4.23: Weighting filters used in \mathcal{H}_∞ design.

Design in disturbance coordinates

A 3×3 MIMO controller is designed in disturbance coordinates, following the approach in Section 4.2.1. Each element of the (diagonal) controller in disturbance coordinates affects a single (diagonal) term of $S_o^d(s)$, that has to be small at frequencies where $V_{di}(s)$ is large. A lead lag controller with second order low pass filter is designed for each loop. The harmonic disturbance is rejected using a single inverted notch (band pass) filter, tuned to a single frequency, 1, 2, 3 [-], for each loop respectively. The bandwidth is limited by $\bar{\sigma}(E)$, Fig. 4.21, which was shown to be invariant under orthogonal coordinate transformation. The bode magnitude diagram of the controller, $K_d(s)$, is depicted in Fig. 4.20. The controller in control

coordinates equals $K(s) = UK_d(s)U^T$ and is shown in Fig. 4.19. In Fig. 4.22 it is visible that each principal gain is small at only one frequency of the disturbance. Hence, the sensitivity function is small only in the directions that are relevant for this disturbance model.

\mathcal{H}_∞ design in control coordinates

The objective is to design a 3×3 MIMO controller using \mathcal{H}_∞ -synthesis, that takes into account the directions of the disturbances. The design is formulated in control coordinates. Synthesis of the \mathcal{H}_∞ controller is based on the following mixed sensitivity formulation,

$$\min_{\text{stab. } K_{\text{hinf}}} \left\| \begin{array}{c} W_s S_o V \\ W_{ks} K S_o V \end{array} \right\|_\infty. \quad (4.37)$$

Herein, $W_s(s)$ and $W_{ks}(s)$ are chosen diagonal, see Fig. 4.23. The weighting filters are parameterized as a function of bandwidth, see [143]. The weight $V(s)$ models the disturbances at the output of the plant and equals,

$$V(s) = UV_d(s) \quad (4.38)$$

where $V_d(s)$ is the diagonal transfer function matrix from (4.34). Note that as $V(s)$ is non-diagonal, the generalized plant becomes coupled, and there is no reason why the resulting \mathcal{H}_∞ controller should be diagonal. In fact, we expect that the resulting \mathcal{H}_∞ controller is non-diagonal to accommodate the directionality of the disturbances. The resulting \mathcal{H}_∞ controller indeed turns out to have large non-diagonal terms, see Fig. 4.19. However, if the same \mathcal{H}_∞ controller is transformed to disturbance coordinates using, $K_{\text{hinf},d} = U^T K_{\text{hinf}}(s)U$, it is visible, Fig. 4.20, that \mathcal{H}_∞ synthesis comes up with the same solution as our manual loopshaping design in disturbance coordinates, at least in the frequency region of the disturbances. The \mathcal{H}_∞ controller has a different roll off at higher frequencies. This leads to better roll off of the singular values of T_o , but seems to result in larger cross-terms of the complementary sensitivity function at these frequencies.

4.2.3 Discussion

Only the \mathcal{H}_∞ control and the manual loopshaping control design in disturbance coordinates are shown to provide feasible solutions to this disturbance rejection problem. This is explained as in both approaches the sensitivity function is reduced only in directions that are relevant. A conventional multiloop design approach was shown to be overly conservative and hence dictates frequency domain tradeoffs that made it impossible to satisfy the design requirements. For comparison, each SISO controller in the multiloop approach was designed using \mathcal{H}_∞ -synthesis (results not shown here). As these designs still have to face

the same frequency domain tradeoffs, no feasible control design could be obtained.

The design in disturbance coordinates, has spectral radius $\rho(E(j\omega)T_o(\omega)) = 0.70$, which is achieved at frequency 4[-], see also Fig. 4.21. And $\rho(E(j\omega)T_o(\omega)) = 0.19$, $\rho(E(j\omega)T_o(\omega)) = 3.13$ for the \mathcal{H}_∞ controller and multiloop respectively. This again shows that the multiloop design is not able to satisfy the design requirements. The order of the \mathcal{H}_∞ controller is 42. The SISO design must duplicate notches in each loop and has order 27. The controller designed in disturbance coordinates has order 15. Aside from this advantage, the design in disturbance coordinates is more transparent as a controller can be designed for each harmonic independently. Also, this approach resulted in approximately the same controller as the \mathcal{H}_∞ design, at least at the frequency region where disturbances are rejected.

Although the manual design in disturbance coordinates is only applicable for a limited class of plants, it does illustrate how rejection of fixed direction disturbances can be achieved in a transparent way. As this example shows that the results from \mathcal{H}_∞ synthesis can be interpreted, design using non-diagonal weighting filters is illustrated. In this example, the bandwidths of the controllers in disturbance coordinates were chosen equal. If there are directions where disturbances are small, bandwidth may be reduced. In those directions, robustness margins can be increased and amplification of high frequency sensor noise is decreased. Hence, both disturbances and sensor noise can be rejected when they act in orthogonal subspaces. This will be discussed in more detail in the next section.

4.2.4 Conclusions

It is discussed and illustrated that rejection of disturbances in only the relevant directions is important in design problems with tight specifications. Exploiting the structure of a class of electromechanical systems, a coordinate transformation can be applied that allows transparent, even manual, design of multivariable controllers to reject disturbances only in the relevant directions. If the same issue is approached with \mathcal{H}_∞ design, and the resulting MIMO \mathcal{H}_∞ controller is transformed to the same coordinates, the \mathcal{H}_∞ controller is shown to do exactly the same.

4.3 Non uniform noise and disturbance rejection

In this section, it is studied how one can design multivariable controllers if in addition to the frequency wise separation of noise and disturbances, directions of noise and disturbances are taken into account. This is an extension of the control design in disturbance coordinates proposed in Section 4.2. We show that if the gain related to specific input directions of both S_o and T_o is to be designed, one requires that the open loop L has different input and output directions. Even

for the specific class of plants considered in Section 4.2, it can be complicated to design controllers with manual loopshaping techniques.

A similar problem arises in the control design for ill-conditioned plants, studied in [42]. Herein, approximate algebraic relations are derived between non-uniform gain open loop and closed loop transfer function matrices. With this in mind, one can deduce insights to facilitate manual loopshaping of centralized non-uniform gain controllers. By means of comparison, controllers are designed using model based \mathcal{H}_∞ -synthesis. Herein, non-diagonal weighting filters take into account the directional aspects of disturbances and sensor noise.

4.3.1 Analysis of non-uniform gain controllers

In Section 2.1.3, it was shown that when the gain of the open loop transfer function is the same in all directions (uniform gain), straightforward relations can be derived between different closed loop transfer functions. This can be considerably more complicated when the open loop has high gain in only some directions and low gain in others. For this case, we can study the singular value decomposition of the open loop function evaluated at a single frequency,

$$\begin{aligned} L(j\omega) &= U\Sigma V^H \\ &= U_1\Sigma_1V_1^H + U_2\Sigma_2V_2^H, \end{aligned} \quad (4.39)$$

with $U_1, V_1 \in \mathbb{C}^{n \times k}$, $U_2, V_2 \in \mathbb{C}^{n \times (n-k)}$. Herein, $U_1\Sigma_1V_1^H$ denotes the part with high gain, and $U_2\Sigma_2V_2^H$ denotes the part with low gain, $\underline{\sigma}(\Sigma_1) \gg \bar{\sigma}(\Sigma_2)$. The objective is to study how the high and low gain subsystems effect the closed loop gain and directions at that particular frequency ω .

A useful concept in the study of directions using the singular value decomposition is that of principal angles, [63]. This provides a measure of alignment between subspaces and can be used later to study system properties. The principal angles θ_j are defined in the following, [53],[46].

Definition 4.3.1. *The principal angles $\theta_j \in [0, \frac{\pi}{2}]$ between subspaces \mathbf{V}_i and \mathbf{U}_i are defined recursively as,*

$$\cos \theta_j = \max_{v \in \mathbf{V}_i} \max_{u \in \mathbf{U}_i} |v^H u| = \tilde{v}_j^H \tilde{u}_j, \quad j = 1, \dots, k \quad (4.40)$$

with $\|u\| = \|v\| = 1$ and $u^H \tilde{u}_i = 0$, $v^H \tilde{v}_i = 0$ for $i = 1, \dots, j-1$ and $\bar{\theta} = \theta_k \geq \theta_{k-1} \geq \dots \geq \theta_1 = \underline{\theta}$.

The subspaces \mathbf{V}_i and \mathbf{U}_i are said to be aligned, when $\theta_j = 0, \forall j$. They are misaligned, orthogonal, when $\theta_j = \frac{\pi}{2}, \forall j$. Given an orthogonal basis in \mathbf{V}_i respectively \mathbf{U}_i , the principal angles can be calculated straightforwardly using the singular value decomposition. Considering the decomposition in Equation 4.39,

Table 4.2: Approximate algebraic relations between open loop and closed loop functions in case of ill-conditioned open loop, [42].

Case	condition	$S_{o,app}$	$T_{o,app}$
a	$\underline{\sigma}(\Sigma_2) \gg 1$	$V_1 \Sigma_1^{-1} U_1^H + V_2 \Sigma_2^{-1} U_2^H$	$I - L^{-1}$
b	$\underline{\sigma}(\Sigma_1) \gg 1$	$V_2 (U_2^H V_2 + \Sigma_2)^{-1} U_2^H$	$I - S_{o,app}$
c	$\underline{\sigma}(\Sigma_1) \gg 1 \gg \bar{\sigma}(\Sigma_2)$	$V_2 (U_2^H V_2)^{-1} U_2^H$	$U_1 (V_1^H U_1)^{-1} V_1^H$
d	$\bar{\sigma}(\Sigma_2) \ll 1$	$I - T_{o,app}$	$U_1 \Sigma_1 (I_k + V_1^H U_1 \Sigma_1)^{-1} V_1^H$
e	$\bar{\sigma}(\Sigma_1) \ll 1$	$I - L$	L

the orthogonal bases of the input and output subspaces are determined. In the case of $2k \leq n$, it follows that,

$$\cos \theta_j = \sigma_j(V_1^H U_1), \quad j = 1, \dots, k, \quad V_1 \in \mathbf{V}_1, U_1 \in \mathbf{U}_1. \quad (4.41)$$

So that $\bar{\theta} = \arccos \underline{\sigma}(V_1^H U_1)$ and $\underline{\theta} = \arccos \bar{\sigma}(V_1^H U_1)$. For $2k \leq n$, the matrix $V_2^H U_2$ has k singular values which are identical to those of $V_1^H U_1$ plus an additional $n - 2k$ singular values which are equal to one. If $2k > n$, the roles of $V_2^H U_2$ and $V_1^H U_1$ are interchanged. The first k singular values of $V_2^H U_2$ equal unity, the arc cosines of the remaining singular values equal the principal angles between the subspaces \mathbf{V}_1 and \mathbf{U}_1 . With the relations shown in Appendix B, we find that the principal angles can also be calculated as,

$$\begin{aligned} \sin \theta_j &= \sigma_j(V_1^H U_2) \\ &= \sigma_j(V_2^H U_1), \quad j = 1, \dots, k. \end{aligned} \quad (4.42)$$

This shows that only k principal angles are required to describe the alignment of all the relevant subspaces in (4.39). When the principal angles are not all zero, there is interaction between the subsystems in (4.39). As will be shown next, this interaction in the open loop can have considerable effect on closed loop performance.

Five different frequency regions can be distinguished, for which different asymptotic relations can be derived between the decomposition of Equation 4.39 and closed loop functions, $S_o(j\omega) \approx S_{o,app}$, $T_o(j\omega) \approx T_{o,app}$. The approximations are listed in Table 4.2, a proof is presented in [46] and [42]. An example for a frequency region where each of these cases apply, is shown in Figure, 4.24. The Case (a) refers to the high gain in all directions. Then, the approximation is straightforwardly, $S \approx L^{-1} = V_1 \Sigma_1^{-1} U_1^H + V_2 \Sigma_2^{-1} U_2^H$. Case (e) applies to a frequency range where the gain is small in all directions, the approximation is again straightforward in this case. Case (b) and Case (d) are both valid for a frequency range where the singular values of low, respectively high, gain subsystem cross $0dB$. The Case (c), describes the intermediate frequency region, where the alignment of the subspaces determine a great deal of the closed loop performance. In

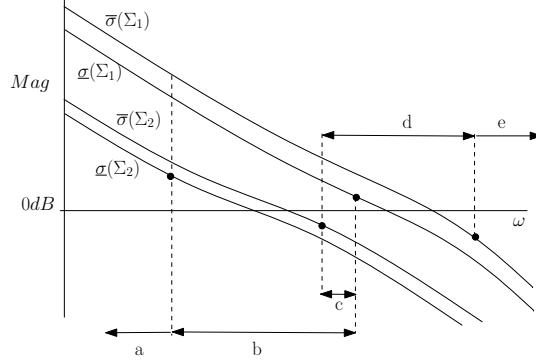


Figure 4.24: Example of frequency ranges where approximate cases apply.

this region, it follows that,

$$\bar{\sigma}(S_o) \approx \frac{1}{\underline{\sigma}(U_2^H V_2)} = \frac{1}{\cos \bar{\theta}}. \quad (4.43)$$

This shows, that the sensitivity peak in the intermediate frequency region is directly related to the misalignment of the subspaces of V_2, U_2 , as measured by $\bar{\theta}$. Or equivalently, the misalignment of V_2, U_1 , see (4.41) and (4.42). Although a small misalignment is tolerable as $\cos(\bar{\theta})$ is nonlinear in $\bar{\theta}$. For example, $\bar{\theta} \leq 60^\circ$, implies that $\bar{\sigma}(S_o) < 6dB$. This shows that a controller with non-uniform gain can be designed even in cases where input and output subspaces are not perfectly aligned.

However, one must be careful when $\bar{\theta}$ is large and all subsystems have approximately the same gain. This is demonstrated in Figure 4.25, where the maximum singular value of the sensitivity function is depicted together with the maximum singular value of the asymptotic relations from Table 4.2. As the difference in crossover regions becomes smaller, the approximations fail to predict the maximum singular value of the sensitivity function in the intermediate frequency region.

In low and high frequency region however, the approximate relations reveal how directions of sensitivity and complementary sensitivity function are related to the input and output directions of the open loop. In the case that the noise and disturbances are strongly direction dependent, it can be investigated how this can be exploited with the design of a non-uniform gain controller. This will be discussed in the next section.

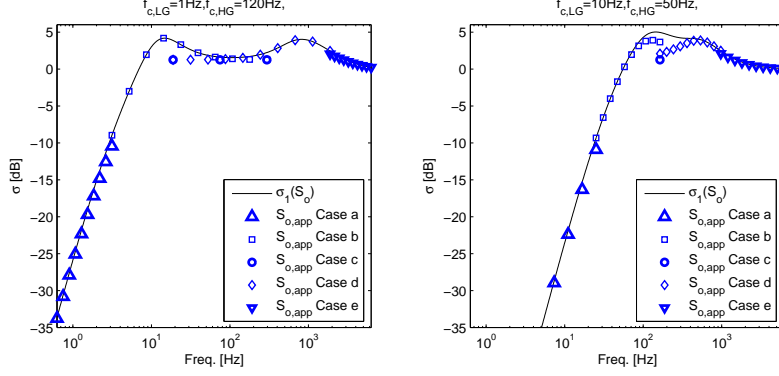


Figure 4.25: Maximum singular value of S_o and approximations for $\beta = \frac{\pi}{3}$. Left: $f_{bb,lg} \ll f_{bb,hg}$. Right: $f_{bb,lg} < f_{bb,hg}$.

4.3.2 Disturbance rejection

Here, the issue is investigated where disturbances and noise are not only dominant in different frequencies, but also in different directions. In that case, the output disturbances can be decomposed in large disturbances that act in the subspace \mathbf{D}_1 and small disturbances that act in the subspace $\mathbf{D}_2 \perp \mathbf{D}_1$. Likewise, sensor noise can be decomposed in large signals that act in the subspace \mathbf{N}_1 and small noise signals that act in the subspace $\mathbf{N}_2, \mathbf{N}_2 \perp \mathbf{N}_1$.

As the objective is to reject both noise and disturbances, the complementary sensitivity function should be small in the directions of the dominant noise and the sensitivity function should be small in the directions of the dominant disturbances. In the case that $\mathbf{D}_1 \perp \mathbf{N}_1$ and $\dim(\mathbf{D}_1) + \dim(\mathbf{N}_1) \leq n$, the disturbance decoupling method discussed in Section 4.2 can be followed. In the more general situation that \mathbf{D}_1 is not orthogonal to \mathbf{N}_1 , rejection of disturbances and noise is more involved.

From the approximations of Table 4.2, it is visible that the *right* singular subspaces of L determine the direction of the rejected noise and the *left* singular subspaces determine the direction of the rejected disturbances. Likewise, the *left* singular subspace of L determines the subspace of the outputs of $S_{o,app}$ that are affected by disturbances. The *right* singular subspaces of L determine the subspace of the outputs of $T_{o,app}$ that are affected by noise. Thus, the objective is to choose the gain and the directions of the open loop so that,

$$\mathbf{D}_1 \subseteq \mathbf{U}_1, \quad \mathbf{N}_1 \subseteq \mathbf{V}_2. \quad (4.44)$$

In that case, the large noise signals act on low gain subsystem, and the disturbances act on the high gain subsystem. This shows that, by choosing the directions for noise and disturbance rejection, the output directions of S_o and T_o

are determined, because, $\mathbf{U}_1 \perp \mathbf{U}_2$, $\mathbf{V}_1 \perp \mathbf{V}_2$. The closed loop functions are then aligned with the dominant disturbance and noise directions. In general, this will lead to centralized controllers. The ability to choose the space \mathbf{U}_1 different from \mathbf{V}_2 is greatly determined by the role of the misalignment at intermediate frequencies, Case (c). Next, it is shown how the asymptotic approximations from Table 4.2 can be used to support manual loopshaping design or norm based design like \mathcal{H}_∞ -design.

Manual loopshaping design

In this manual loop shaping design method, the goal is to combine the insights of SISO manual loop shaping with the asymptotic algebraic relations for non-uniform gain controllers presented earlier. In this way, non-uniform gain closed loop functions can be designed that exploit the non-uniform gain of noise and disturbances. In general, centralized controllers will result. As will be shown, achieving performance and stability is not trivial. In order to reduce complexity, the input and output directions of the controller are chosen constant for all frequencies. The open loop transfer function matrix can then be decomposed as,

$$L(s) = U_{HG}L_{HG}(s)V_{HG}^T + U_{LG}L_{LG}(s)V_{LG}^T, \quad (4.45)$$

with $U_{HG}^{n \times k}$ and $\underline{\sigma}(L_{HG}(s)) \gg \bar{\sigma}(L_{LG}(s))$. Note the strong analogy with (4.39), as, in the case that $L_{HG}(s)$ is decoupled, at a frequency ω_o we have $\Sigma_1 = \text{diag}\{\sigma_i(L_{HG}(j\omega_o))\}$. For a uniform gain plant, e.g., $G(s) = g(s)I_n$, the directions of the open loop are determined by the controller. Hence, the controller to be designed has the structure,

$$K(s) = U_{HG}K_{HG}(s)V_{HG}^T + U_{LG}K_{LG}(s)V_{LG}^T, \quad (4.46)$$

with $\underline{\sigma}(K_{HG}(s)) \gg \bar{\sigma}(K_{LG}(s))$. For the orthogonal bases U_{HG}, V_{LG} holds that $U_{HG} \in \mathbf{U}_{HG}$ and $V_{LG} \in \mathbf{V}_{LG}$ with $\mathbf{D}_1 \subseteq \mathbf{U}_{HG}$, $\mathbf{N}_1 \subseteq \mathbf{V}_{LG}$. The maximum principal angle equals $\bar{\theta} = \arccos \underline{\sigma}(V_{HG}^T U_{HG})$. For achieving stability, the open loop can be evaluated at different loop breaking points. Hence, for $G(s) = g(s)I_n$, alternatively to shaping (4.45), one can study,

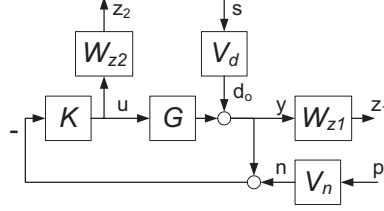
$$L'(s) = G'(s)K'(s), \quad (4.47)$$

with,

$$G'(s) = g(s) \left[\begin{array}{c|c} V_{HG}^T U_{HG} & V_{HG}^T U_{LG} \\ \hline V_{LG}^T U_{HG} & V_{LG}^T U_{LG} \end{array} \right], K'(s) = \left[\begin{array}{c|c} K_{HG}(s) & 0 \\ \hline 0 & K_{LG}(s) \end{array} \right]. \quad (4.48)$$

Both K_{HG} and K_{LG} must have uniform gain in order to preserve the directions of the open loop. One may design K_{HG} and K_{LG} independently, when $G'(s)$ is block diagonal dominant. Using Def. 2.3.1, $G'(s)$ is generalized (block) diagonal dominant if,

$$\mu_{T'}(E')^{-1} < 1, \quad (4.49)$$

Figure 4.26: Augmented plant used for the \mathcal{H}_∞ -design

with $T' = G'_d K'(I + G'_d K')^{-1}$, G'_d the block diagonal of G' , and,

$$E' = (G'(s) - G'_d(s))G_d'^{-1}(s) \quad (4.50)$$

$$= \begin{bmatrix} O & V_{HG}^T U_{LG} (V_{LG}^T U_{LG})^{-1} \\ V_{LG}^T U_{HG} (V_{HG}^T U_{HG})^{-1} & O \end{bmatrix}, \quad (4.51)$$

so that,

$$\begin{aligned} \mu_{T'}(E') &= \bar{\sigma}(V_{LG}^T U_{HG} (V_{HG}^T U_{HG})^{-1}) \\ &= \tan(\underline{\theta}), \end{aligned} \quad (4.52)$$

which is constant for all frequencies. Hence, $G'(s)$ is not block diagonal dominant when $\underline{\theta} > \frac{\pi}{4}$. Then, K_{HG} , K_{LG} cannot be designed independently. Alternatively, K_{HG} and K_{LG} can be designed by means of sequential loop closing. Again, typical multivariable issues arise if $\underline{\theta}$ increases. This will be illustrated later in the example.

\mathcal{H}_∞ design

A generalized plant is formulated to take into account the directions and frequency content of both noise and disturbances. If either noise or disturbances are to be modeled, one may use the signal based \mathcal{H}_∞ -design framework discussed in [125]. With the augmented plant, M ,

$$\begin{bmatrix} z_1 \\ z_2 \end{bmatrix} = M \begin{bmatrix} s \\ p \end{bmatrix}, \quad M = \begin{bmatrix} W_{z_1} S_o V_d & -W_{z_1} T_o V_n \\ -W_{z_2} K S_o V_d & -W_{z_2} K S_o V_n \end{bmatrix}, \quad (4.53)$$

the input spaces of both S_o and T_o can be shaped independently. With this interconnection structure we do not model exogenous signals between the controller and the plant. Therefore, there is no guarantee for internal stability with this design approach. However, we may check for internal stability after control synthesis. This appears to be of no concern in our examples. The variable z_2 , is added for numerical reasons. A block diagram of the augmented plant is shown in Figure 4.26. The weights on z_1, z_2 are $W_{z_1} = I$, $W_{z_2} = \rho I$ with $0 < \rho \ll 1$,

respectively. Then, it holds that,

$$\max\{\bar{\sigma}(S_o V_d), \bar{\sigma}(T_o V_n)\} \leq \bar{\sigma}(M) \leq \sqrt{2} \max\{\bar{\sigma}(S_o V_d), \bar{\sigma}(T_o V_n)\}, \quad (4.54)$$

[125, p.522]. As the case is studied where disturbances act mostly at low frequencies and noise dominates at high frequencies, this relation can be used to relate $\|M\|_\infty$ with the weighted closed loop functions. Furthermore, the weighting filters V_d, V_n contain the directional characteristics of the noise and disturbances. Following the partition of the disturbance and noise spaces from Section 4.3.2,

$$\begin{aligned} V_d(s) &= [V_{d1} \mid V_{d2}] \text{diag}\{v_{d1}(s)I_k, v_{d2}(s)I_{n-k}\} \\ V_n(s) &= [V_{n1} \mid V_{n2}] \text{diag}\{v_{n1}(s)I_{n-k}, v_{n2}(s)I_k\}, \end{aligned} \quad (4.55)$$

where $V_{d1} \in \mathbf{D}_1$ and $V_{n1} \in \mathbf{N}_1$ and $V_{d2}^T V_{d1} = 0$ and $V_{n2}^T V_{n1} = 0$. The scalar frequency dependent weights are chosen to characterize the disturbances and noise. As the gain of noise and disturbances is direction dependent,

$$\begin{aligned} |v_{d1}(j\omega)| &\ll |v_{d2}(j\omega)|, & \omega &\ll \omega_{bb_1} \\ |v_{n1}(j\omega)| &\gg |v_{n2}(j\omega)|, & \omega &\gg \omega_{bb_2}. \end{aligned}$$

Where $\omega_{bb_1}, \omega_{bb_2}$ is the cross over frequency of the desired low and high gain subsystem respectively. In the frequency region $\omega_{bb_1} < \omega < \omega_{bb_2}$, the weighting filters are tuned to enforce robustness margins.

4.3.3 Example

In this example, the issue is studied when noise is dominant at high frequencies, and disturbances are dominant at low frequencies. In addition to this conventional frequency wise characteristic, the direction of dominant noise and disturbances is taken into account. The objective is to design a feedback controller, by either manual or \mathcal{H}_∞ loopshaping, that minimizes the effect of disturbances and noise on the performance variables, z .

The plant, $G(s) = g(s)I_2$, is subjected to disturbances at the outputs with direction, \tilde{d} . The sensor noise has direction, \tilde{n} .

$$\tilde{d} = [\cos \alpha, \sin \alpha]^T, \quad \tilde{n} = [\cos(\alpha + \beta), \sin(\alpha + \beta)]^T, \quad \alpha = \frac{\pi}{3}. \quad (4.56)$$

Two different alignments between the noise and disturbance directions are studied. The directions are parameterized by $\beta = \{\frac{\pi}{3}, \frac{\pi}{6}\}$. The output disturbance direction is non-canonical, and the noise direction is non-canonical. The difference of the two cases is the (mis)alignment between dominant noise and disturbances. The directions of the noise and disturbance are plotted in the space of the controlled variables in Figure 4.27. Both manual and \mathcal{H}_∞ loopshaping are considered for the two cases.

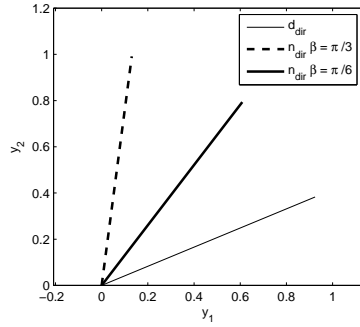


Figure 4.27: Directions of the sensor noise and disturbances in the space of the controlled variables y .

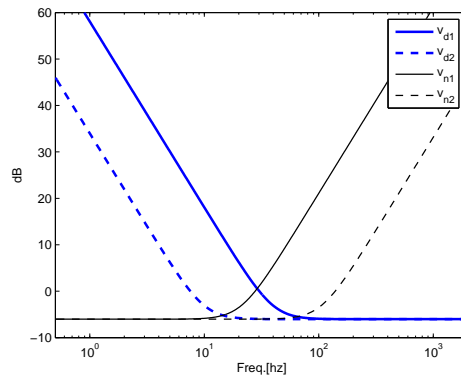


Figure 4.28: Bode magnitude plot of scalar frequency dependent weighting filters to characterize non-uniform disturbances and noise in the \mathcal{H}_∞ design example.

The \mathcal{H}_∞ design is performed for both alignments, $\beta = \{\frac{\pi}{3}, \frac{\pi}{6}\}$. The principal gains of the weighting filters V_d , V_n are shown in Figure 4.28. Furthermore, $W_{z_1} = I_2$, $W_{z_2} = \rho I_2$, $\rho = 1 \times 10^{-5}$. The directions of the weighting filters are chosen following Equation 4.55. The resulting closed loop system is internally stable. More details are discussed in Section 4.3.4.

The manual loopshaping design is more involved. Because the plant is 2×2 , scalar high and low gain loops can be designed. The input and output directions of the controller are chosen following Equation 4.46. Two PD feedback controllers with second order lowpass filter, resulting in a cross-over frequency of 10Hz and 50Hz, are designed sequentially. In each design step, the margins on

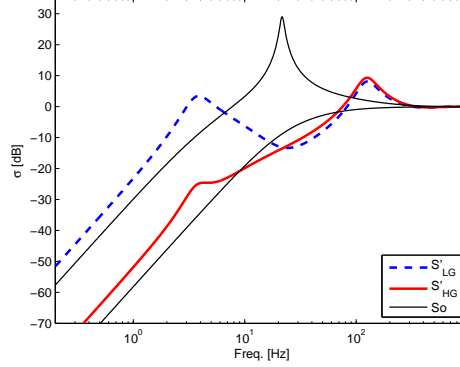


Figure 4.29: Principal gains of scalar sensitivity functions (sequential design) and the final 2×2 sensitivity function S_o of the manual design.

the equivalent open loop, the open loop with the other controller closed,

$$\begin{aligned} L_{HG}(s)' &= G'_{HG}(s)K_{HG}(s) \\ L_{LG}(s)' &= G'_{LG}(s)K_{LG}(s), \end{aligned}$$

with,

$$\begin{aligned} G'_{HG}(s) &= g(s)\{V_{HG}^T U_{HG} \\ &\quad - V_{HG}^T U_{LG} K_{LG} (I_{n-k} + g(s)V_{LG}^T U_{LG} K_{LG}(s))^{-1} V_{LG}^T U_{HG}\} \\ G'_{LG}(s) &= g(s)\{V_{LG}^T U_{LG} \\ &\quad - V_{LG}^T U_{HG} K_{HG} (I_k + g(s)V_{HG}^T U_{HG} K_{HG}(s))^{-1} V_{HG}^T U_{LG}\}, \end{aligned}$$

following Equation 4.48, are inspected. Closed loop stability can be achieved in this way, although robustness margins of the final closed loop may become arbitrarily small. For each design step, the principal gains of the sensitivity functions, $S_{LG} = \frac{1}{1+L'_{LG}}$, $S_{HG} = \frac{1}{1+L'_{HG}}$, are shown in Figure 4.29, together with the principal gains of the total sensitivity function $S_o = (I + GK)$ for $\beta = \frac{\pi}{6}$. Although the sensitivity functions S_{LG}, S_{HG} result in acceptable margins, the final resulting sensitivity function S_o is unacceptably large in the intermediate frequency range. This appears to be independent on the sequence in which S_{LG}, S_{HG} are designed. It is not straightforward to reduce the sensitivity function in this frequency region. This supports the expectations as the misalignment between the noise and disturbance directions is smaller than $\frac{\pi}{4}$. For $\beta = \frac{\pi}{3}$ the manual loopshaping method results in satisfactory performance, see Figure 4.30, Figure 4.31, Figure 4.32.

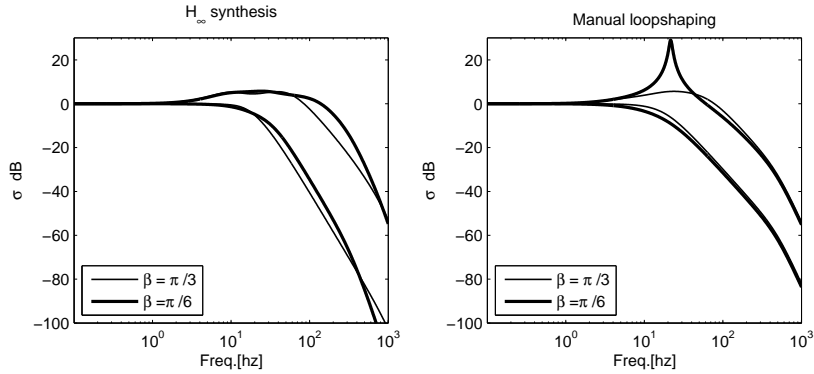


Figure 4.30: Principal gains of complementary sensitivity function for two different directions of the sensor noise

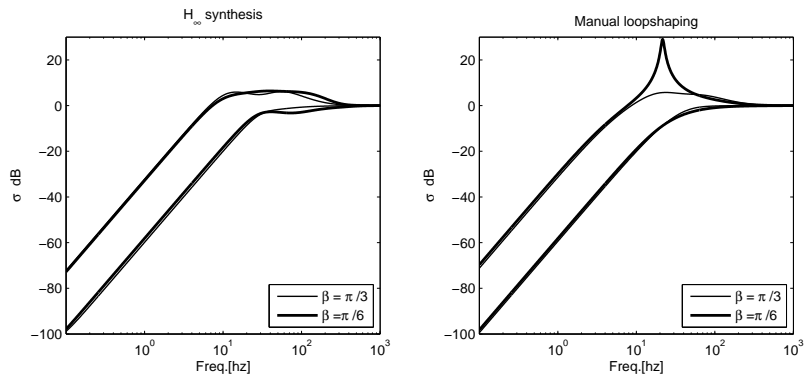


Figure 4.31: Principal gains of sensitivity function for two different directions of the sensor noise

4.3.4 Discussion

The approximate relations between closed loop and open loop transfer functions facilitate the design of centralized controllers with both manual loopshaping and norm based control design. The application of the manual loopshaping method proposed here, is limited to cases where noise and disturbances are strongly misaligned and the difference between the high and low gain subsystem is sufficiently large. It was demonstrated that for a 2×2 uniform plant, high and low gain subsystems can be designed either sequentially or independently if the noise and disturbances are sufficiently misaligned. If noise and disturbances are more aligned, the manual loopshaping method does not guarantee to achieve satisfactory robustness margins.

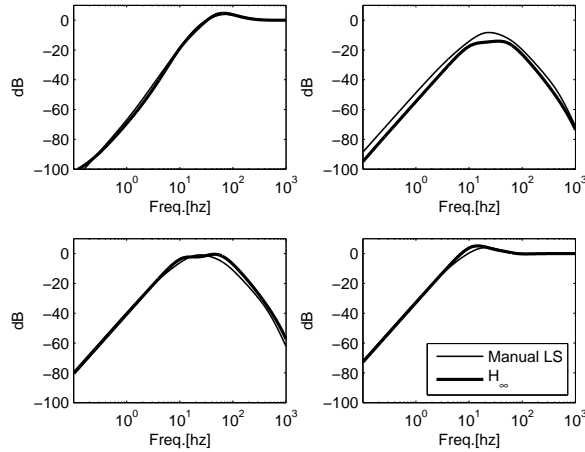


Figure 4.32: Bode plot of elements of sensitivity function for \mathcal{H}_∞ and manual loopshaping design for noise direction induced by $\beta = \frac{\pi}{3}$.

A more general design approach was presented using \mathcal{H}_∞ -synthesis. The approximate relations can be used to choose realistic weighting filters that enforce non-uniform closed loop functions. The \mathcal{H}_∞ design method is able to handle larger systems than 2×2 , small misalignment angles and small gain differences of the subsystems. Above all, the \mathcal{H}_∞ design method enforces robustness margins in the intermediate frequencies and guarantees that the system is closed loop stable.

It is shown that the output directions of the sensitivity function are determined by the space of the dominant noise signals. In a control problem where noise is not performance limiting, the output directions of the sensitivity function may be shaped to confine the response to dominant disturbances to a subspace that is of less interest for performance. Again, misalignment between the input and output space of the sensitivity function can give rise to robustness problems, especially with the manual loopshaping method.

In the example, the directions of the open loop were completely determined by the controller. For more general plant structures, those directions will be influenced by the directions of the plant as well. Furthermore, in general, the open loop function is not commutative, so that robustness margins can be different at different loopbreaking points. In all these cases, the proposed manual loopshaping method may fail. We hope that the insights obtained with this rather simple case inspires \mathcal{H}_∞ -design for more complicated applications.

The manual loopshaping method presented here results in constant input and output directions of the controller for all frequencies. This is especially limiting

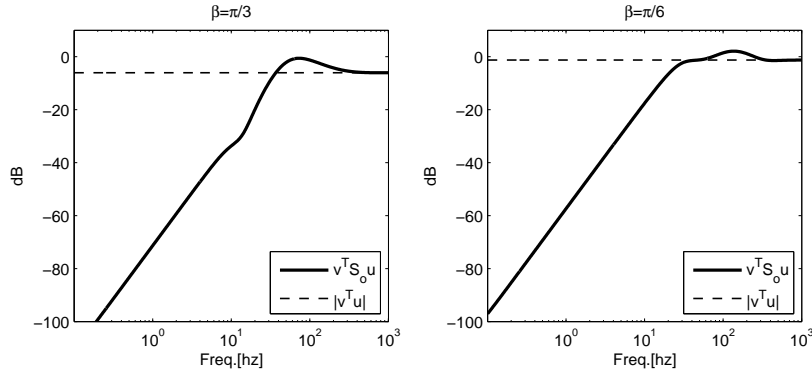


Figure 4.33: Bode diagram of $v_2^T S_o u_1$ and $|v_2^T u_1|$ of \mathcal{H}_∞ design for $\beta = \frac{\pi}{3}$ and $\beta = \frac{\pi}{6}$.

at the intermediate frequency regions. It is interesting to investigate manual loopshaping methods that allow the input and output directions of the controller to vary per frequency. In most cases, this will imply that a centralized controller is to be designed. Hence, it is expected that complexity will increase significantly, even for relative simple 2×2 systems. Direct optimization may be applied to find controller parameters, [63], but it is expected that application of norm based techniques such as \mathcal{H}_∞ -design may be more transparent in use.

Still, as already considered in Section 2.2, fundamental performance limitations do apply. In Figure 4.33, the scalar sensitivity function is depicted to show the frequency wise tradeoff in the directions of noise and disturbances, v_2, u_1 respectively. Apart from the offset due to $|v_2^T u_1|$, the same waterbed effect as in SISO systems applies. However, as we use centralized control, we are able to manage disturbance and noise rejection performance tradeoffs at different frequencies and in different directions more directly, avoiding unnecessary conservatism.

4.3.5 Conclusions

It is shown that relations from [42], that are used to describe ill-conditioned plant dynamics, can be used to derive guidelines for rejection of disturbances and noise that have different gain in different directions (non-uniform gain). As the closed loop functions are non-uniform, centralized controllers are to be designed. A manual loopshaping method is proposed that can be applied when disturbances and noise are sufficiently misaligned and separated per frequency. Also, asymptotic relations between closed loop and open loop transfer functions are used to design non-diagonal weighting filters for \mathcal{H}_∞ design. An example is provided where it is shown that \mathcal{H}_∞ design is able to handle more general situations than the manual design procedure. Where the manual loopshaping design procedure is satisfactory,

the \mathcal{H}_∞ design is shown to result in the same closed loop functions.

4.4 MIMO control design of a metrological AFM

In this section, an alternative control design for a MIMO metrological atomic force microscope (AFM) is proposed using the concepts developed in this thesis. It is demonstrated how the plant model structure assumed in Section 4.2, may be applied to another type of systems than the rigid body system of Section 4.2.2. Also, the implication of such a structural assumption is illustrated by comparing the design with that of the decentralized control design method of Section 2.3. This metrological AFM is extensively discussed in [87, 88]. Metrological AFM's are used to characterize *transfer standards*. These transfer standards can then be used to calibrate commercial AFM's. In most earlier work reported in literature, similar systems are controlled following SISO design approaches, [2, 117], even though concerns have been raised about neglecting the MIMO aspects of such systems, [88, 105]. In [87] plant interaction was analyzed and a decentralized feedback control design was proposed. It was also concluded that interaction limited the ability to reduce tracking errors by means of high bandwidth feedback control. In this section, it is illustrated how more detailed design methods can lead to simple yet high fidelity feedback controllers. It is illustrated how plant interaction limits the achievable bandwidth of decentralized control design. Three different design approaches are discussed.

The first design approach uses a plant model with the structural restrictions following from the assumptions of Section 4.2. It is illustrated that the control design can be very transparent at the costs of introducing conservatism. The second design approach makes explicit use of the MIMO freedom by using the directionality of the disturbances in the manual loop shaping design of a centralized feedback controller. Herein, it is illustrated how the manual centralized control design method of Section 4.2 can be used for this application. The third design approach uses the concepts from Section 2.3 for independent decentralized control design. With this, the structural assumptions of the first and second design are not required. It is shown that this may result in a higher bandwidth controller. In each design, all multivariable aspects of the metrological AFM are taken into account. For all design strategies presented here, only non-parametric models of the plant are required. The designs are discussed in Section 4.4.5.

4.4.1 The metrological AFM

The metrological AFM, as depicted in Fig. 4.34a, is used to characterize the surface of a sample (the transfer standard) by measuring the displacements of the stage in z-direction while moving the sample in the xy plane, Fig. 4.34b. The stage, that carries the sample, has to perform a scanning trajectory in the

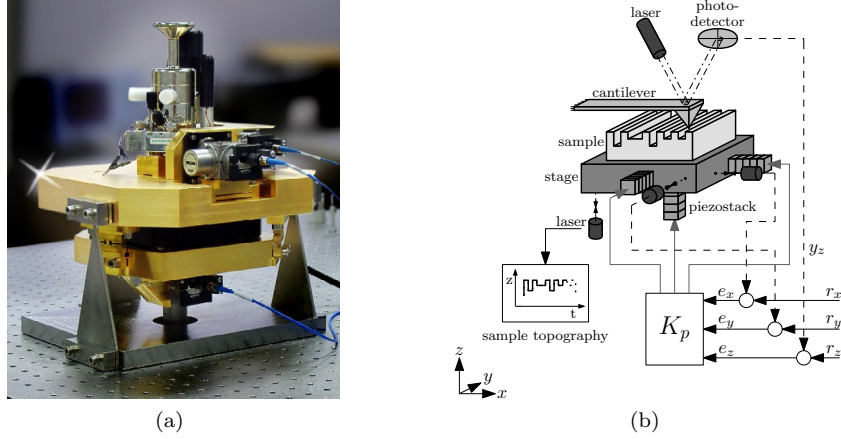


Figure 4.34: The metrological AFM. *a)* Photograph of the metrological AFM. *b)* Schematic model of the metrological AFM, K_p is the controller in physical coordinates, [87].

xy -plane with high fidelity. The distance between the transfer standard and the cantilever beam in z -direction is regulated to be constant. For control in this direction, the deflection of the cantilever beam is measured with a photo-detector. The displacement of the stage in xy -direction is measured with an interferometer. A separate laser, not used for control design, measures the displacement of the stage in z -direction. This measurement is used to characterize the sample, see Fig. 4.34b. The stage is driven by piezo-stack actuators in three cartesian degrees of freedom, x, y, z . The MIMO plant with physical inputs $u = [u_x, u_y, u_z]^T$ and physical outputs $y = [y_x, y_y, y_z]^T$, is defined as,

$$y = G_p u. \quad (4.57)$$

The frequency response functions of all elements of G_p are depicted in Fig. 4.35. Due to the limited stiffness of the connections of the piezo actuators, a resonance mode appears in the x -axis at 121Hz. The same phenomenon occurs in the y -axis at 122Hz. These mode shapes appear to behave in each axis independently. The resonance at 44Hz in the y -axis is due to flexibility of the stage in y -direction. Resonances above 200Hz are due to position dependent actuator dynamics, [87]. As a result of sophisticated mechanical construction, the cross-talk due to plant interaction is small. Below 100Hz, the non-diagonal terms of the plant are approximately 40dB smaller than the diagonal terms, hence the contribution of the non-diagonal terms is approximately 1%.

Unlike common commercial AFM's, the positioning accuracy is much more important than the scanning speed of this metrological AFM. As discussed in [87], compensation of hysteresis and position feedforward control in x, y -axes suffices to achieve acceptable tracking accuracy. A major concern however, is the in-

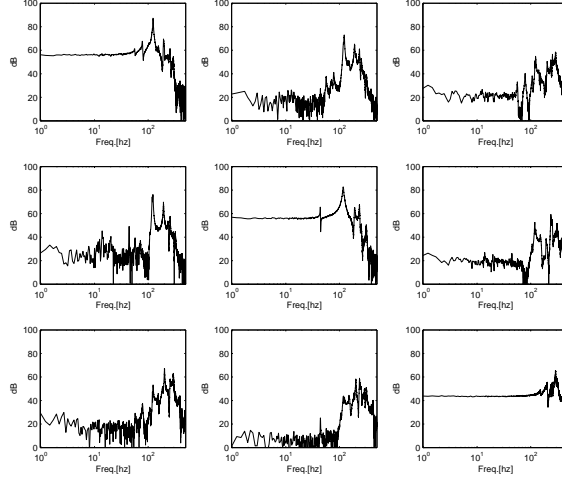


Figure 4.35: Bode magnitude diagram of the metrological AFM in physical coordinates, G_p .

fluence of low frequency disturbances, high frequency sensor noise and model uncertainty. Also, in contrast to [87], a controller is designed that is capable of tracking constant velocity (scanning) trajectories. Furthermore, it is investigated how cross-talk between different controlled axes can be reduced even further.

Feedback control design can be more transparent if the plant model is simplified. A first simplification is made by scaling the diagonal terms of the plant G_p to 0dB at the intended cross-over frequencies by means of a diagonal pre-multiplication matrix T_{us} . This matrix can be interpreted as a proportional action of the controller. Furthermore, it is immediately noticed that the flexible mode at 44Hz in the y -axis may cause performance limitations. A skew notch, $N_y(s)$, is tuned to compensate for the associated local phase loss. The plant to be controlled is then defined as,

$$G(s) = G_p(s)T_{us}N(s), \quad (4.58)$$

with

$$N(s) = \text{diag}\{1, N_y(s), 1\}, \quad T_{us} = (\text{diag}\{|g_{p,jj}(j\omega_{bw})|\})^{-1}. \quad (4.59)$$

We only study the disturbance rejection case when the stage is regulated at a fixed position. From a standstill experiment, the output disturbance $d_o(t)$ can be reconstructed. The spectra of each output disturbance is shown in Fig. 4.36. With the principal component analysis discussed in Chapter 3, we find the matrix W , so that,

$$d_o(t) = W^{-1}z(t) \quad (4.60)$$

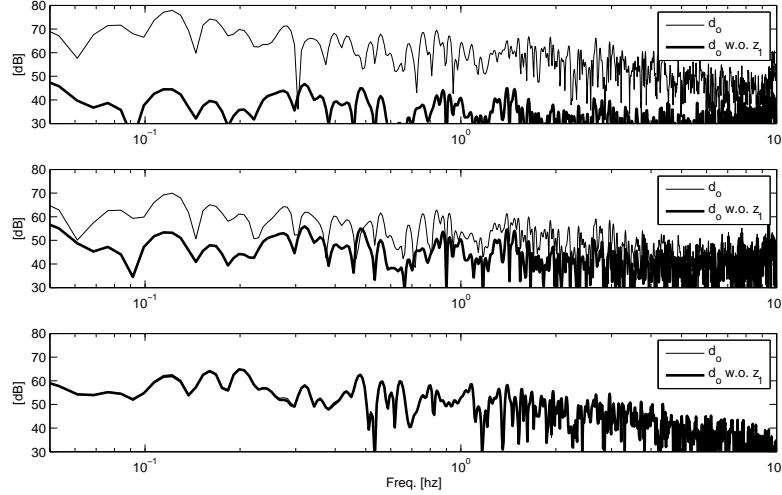


Figure 4.36: Spectra of the output disturbances d_o in each axis of the AFM (thin). Spectra of the output disturbances if the first principal component of d_o is perfectly rejected.

where $z(t)$ are the three principal components of $d_o(t)$. The directions of disturbances due to each principal component are the directions of the columns of,

$$W^{-1} = \begin{bmatrix} -2.75 & 0.55 & 0.01 \\ -0.95 & -1.60 & 0.02 \\ 0.03 & 0.04 & 0.87 \end{bmatrix}. \quad (4.61)$$

The disturbances due to the first principal component have direction $\bar{d}_{z_1} = [-0.95, -0.33, 0.01]^T$, which is the first column of W^{-1} scaled to unity, see Def. 2.1.3. The spectra of the output disturbances due to only the second and third principal component are shown in Fig. 4.36. It is visible that the disturbances in the x and y axis act mostly in the direction \bar{d}_{z_1} . This strong directional dependence of the disturbance may be used in control design.

The objective is to reject output disturbances. This is achieved when,

$$S_o = S_d(I + E_T T_d)^{-1} \quad (4.62)$$

is small. Herein, $S_o = (I + GK)^{-1}$, $S_d = (I + G_d K)^{-1}$ and $T_d = S_d - I$, where G_d contains only the diagonal terms of G and interaction is modeled as multiplicative output uncertainty,

$$E_T = (G - G_d)G_d^{-1}. \quad (4.63)$$

see also Section 2.3.1. A second objective is to reduce cross-talk closed loop. Therefore, we define $y_d = T_d r$, (4.62), and use the property $T_o - T_d = S_d - S_o$, so that,

$$\begin{aligned} y - y_d &= (T_o - T_d)r \\ &= S_o E_T T_d r, \end{aligned} \quad (4.64)$$

see [153]. The cross-talk as a result of plant interaction is reduced by feedback control when (4.64) is small. This happens at frequencies where S_o is small. Cross-talk increases at frequencies where S_o is large. A third requirement is imposed by the uncertain plant dynamics above 200Hz. As the frequencies of the resonance modes vary, it is not possible to use plant inversion at those frequencies. Hence, roll-off of the open loop function is required at high frequencies. Three approaches to design a feedback controller are considered in the next sections.

4.4.2 Uniform controller design

In this design approach, it is illustrated how a simplified plant model can be used for control design. We refer to this design as the uniform control design. The simplified plant model is chosen to satisfy the assumptions of Section 4.2, namely the plant model, $G_d(s)$, should have the form $G_d(s) = g(s)I$. For the metrological AFM, scaled with T_{us} and pre-compensated with notch N , (4.58), one may choose $g(s) = 1$. Hence, the simplified plant model equals,

$$G(s) = G_p(s)T_{us}N(s) \quad (4.65)$$

$$= G_d + E(s), \quad G_d = I. \quad (4.66)$$

Herein, $E(s)$ contains both diagonal and non-diagonal terms, Fig. 4.37. A decentralized controller is designed for each axis. In order to track constant velocity reference profiles, a double integrator in the open loop is required according to the internal model principle, [84, p.24]. We design for each axis a proportional gain, double integrator and a lead-lag with a second order low-pass filter,

$$k_i(s) = \frac{k_p}{s^2} \cdot \frac{s + 2\pi f_z}{s + 2\pi f_p} \cdot \frac{(2\pi f_{lp})^2}{s^2 + 2\zeta_{lp}2\pi f_{lp}s + (2\pi f_{lp})^2}, \quad i = \{x, y, z\}. \quad (4.67)$$

Herein, the parameters are manually tuned so that the cross-over frequency of the open loop is 10Hz in each axis. A sufficient condition for closed loop stability follows from Thm. 2.3.1, using $E = (G(s) - I)$, $S_d = (I + K)^{-1}$ and $T_d = I - S_d$. The system is closed loop stable if for each frequency the following holds,

$$\bar{\sigma}(T_d) \leq \mu_{T_d}^{-1}(E) \quad (4.68)$$

where $\bar{\sigma}(T_d) = \max_i |T_{d,ii}|$. In Fig. 4.38, it is shown graphically that this condition is achieved. This is also confirmed by Fig. 4.39. Herein, it is shown that the characteristic loci of $L_{unif} = GK$ do not encircle the point $(-1, 0)$, hence the system is closed loop stable. The output sensitivity function S_o and the sensitivity

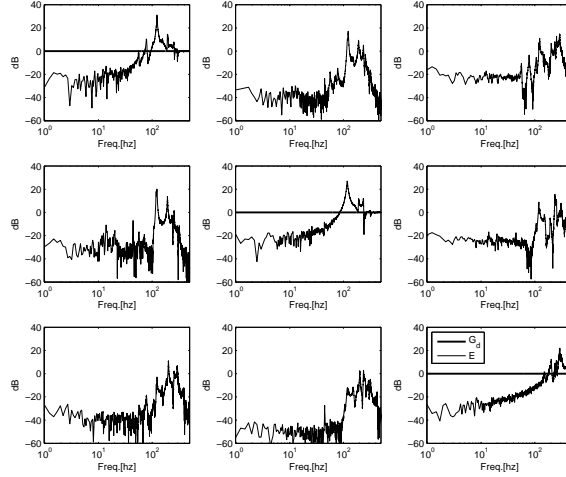


Figure 4.37: The simplified model of the AFM $G_d = I$ and the model uncertainty E .

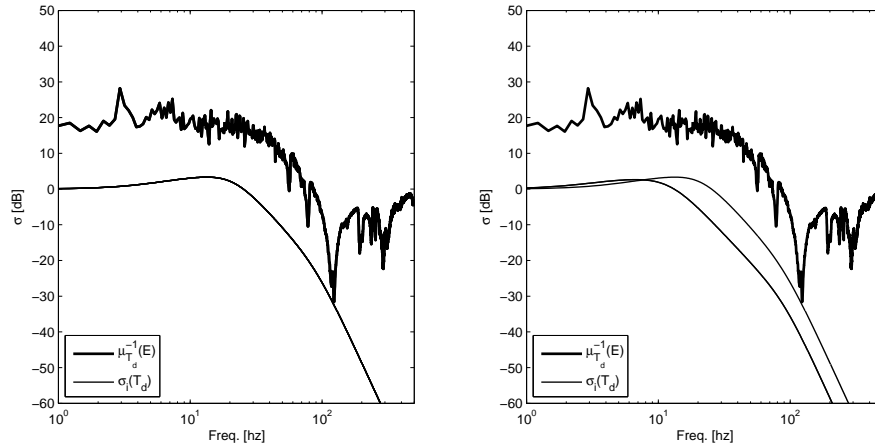


Figure 4.38: Sufficient condition for stability the uniform (left) and the disturbance decoupling (right) controller.

function with the simplified model S_d are shown in Fig. 4.40. It is visible that output disturbances at low frequencies can successfully be rejected. At frequencies above 10Hz, the sensitivity function is large and the disturbance rejection performance is worse or equal to that of the system operating without feedback

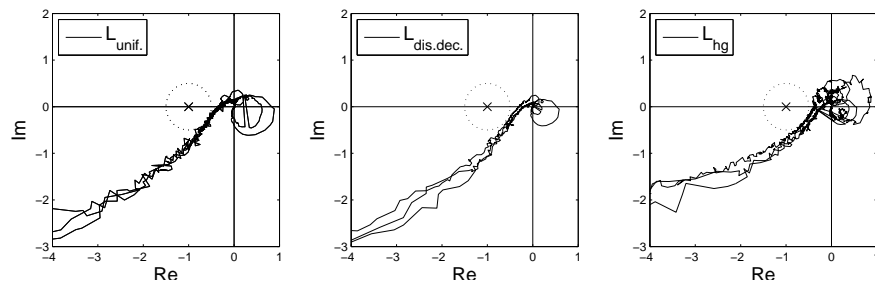


Figure 4.39: Nyquist diagram of the characteristic loci of L for the uniform feedback design (left), disturbance decoupling design (middle) and the high bandwidth decentralized design (right).

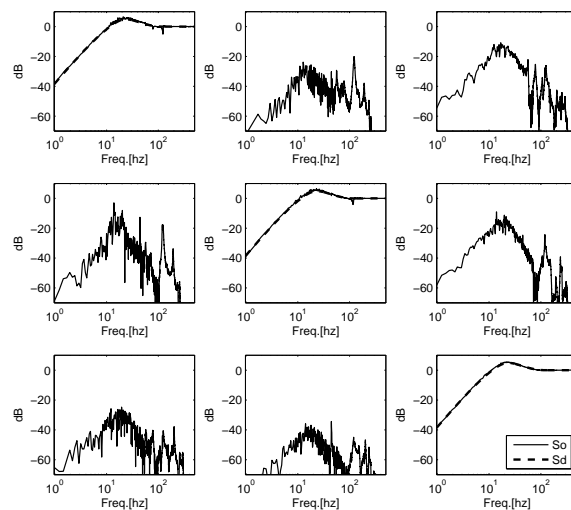


Figure 4.40: Bode magnitude of the output sensitivity function with the decentralized uniform gain design (using the simplified model), S_o and S_d .

control.

4.4.3 Disturbance decoupling design

With the disturbance decoupling design, disturbances are rejected in a specific direction, where in orthogonal directions the gain of the sensitivity function is allowed to increase. This may lead to a lower bandwidth design in directions that

are less relevant for disturbance rejection. Hence, the costs of feedback control can be reduced to some extent. The disturbance decoupling design uses the same simplified plant as the uniform control design, (4.65). The disturbances at the output of the plant, in direction, \bar{d}_{z_1} , are to be rejected. We define the matrix U with $U^T U = I$, where the first column of U has the direction \bar{d}_{z_1} . The other two columns of U are chosen orthogonal to \bar{d}_{z_1} . The controller is defined as,

$$K(s) = U K_d(s) U^T. \quad (4.69)$$

where K_d is diagonal. The first diagonal element of K_d is the controller in the disturbance direction \bar{d} . In this direction, a controller is designed with a structure similar to (4.67) so that the open loop cross-over frequency is 15Hz. In the orthogonal directions, bandwidth may be reduced and therefore controllers are designed so that the open loop has a cross-over frequency of 8Hz. The sufficient condition for closed loop stability, (4.68), is shown graphically in Fig. 4.38. The loop related to the direction \bar{d} limits the achievable disturbance rejection. In directions orthogonal to \bar{d} , the complementary sensitivity functions are smaller at high frequencies. In those directions, a higher level of sensor noise or plant uncertainty can be tolerated. From Fig. 4.38 and the characteristic loci of $L_{dist.dec} = GK$ in Fig. 4.39 it is visible that the system is closed loop stable. As a result of the lower bandwidths in orthogonal disturbance directions, high frequency dynamics are less amplified. Therefore, the characteristic loci at high frequencies are smaller than with the design of Section 4.4.2.

As the open loop function in physical coordinates has large non-diagonal terms at low frequencies, the output sensitivity function has large non-diagonal terms, Fig. 4.41. Therefore, closed loop cross-talk between the xyz -axis is larger than with the design of Section 4.4.2. At low frequencies, the non-diagonal terms of the sensitivity function based on the model (4.65), namely S_d , are close to the non-diagonal terms of S_o . Hence, for this application, one can successfully shape the low frequency disturbance rejection properties of S_o on the basis of the simplified plant model.

4.4.4 High bandwidth decentralized independent control

In this part, a decentralized controller is designed using the concepts of Section 2.3.1. We refer to this design as the high bandwidth decentralized design. The plant model used for this design is based on the diagonal terms of $G(s)$, namely $G_d(s)$. The plant interaction is modeled as multiplicative output perturbations $E_T(s)$, so that,

$$\begin{aligned} G(s) &= G_p(s) T_{us} N(s) \\ &= G_{nd}(s) + G_d(s) \\ &= (I + E_T(s)) G_d(s). \end{aligned} \quad (4.70)$$

Herein, $E_T(s)$ has only non-diagonal terms, see Fig. 4.42. Note that E_T does not

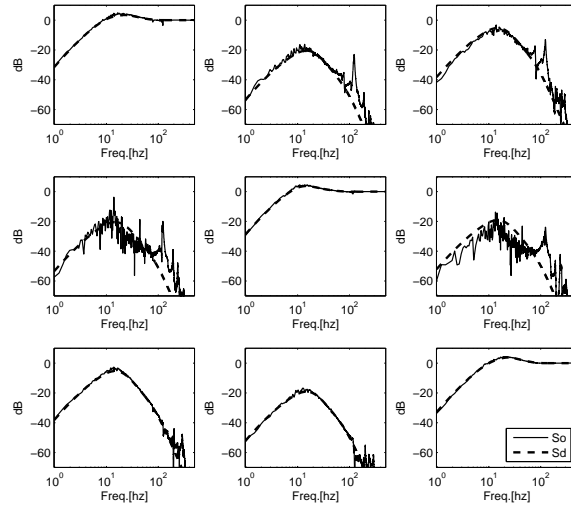


Figure 4.41: Bode magnitude of the output sensitivity function with disturbance decoupling design approach (using the simplified model), S_o and S_d .

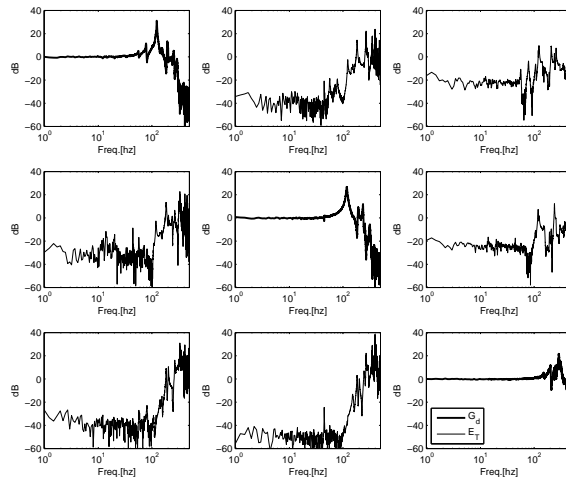


Figure 4.42: Bode magnitude diagram of the diagonal terms of G , G_d , and the interaction as multiplicative output perturbation E_T .

equal E from (4.65). With $E_T = (G - G_d)G_d^{-1}$ the sufficient condition for closed

loop stability can be derived using Thm. 2.3.1. The closed loop system is stable if for all frequencies holds that,

$$\sigma(T_d) \leq \mu_{T_d}^{-1}(E_T) \quad (4.71)$$

In this design, dynamics on the diagonal terms of the plant are taken into account that was considered as uncertainty in Section 4.4.2, Section 4.4.3. Therefore, compared to the designs proposed earlier, the bandwidth in x and y axes can be increased to 20Hz. In z direction, it is expected that the bandwidth can be increased even further. The sufficient condition for stability, (4.71), is a single bound on the control design of all axes. When the bandwidth in each axes is different, this can be rather conservative. A design with a cross-over frequency of the z -axis at 45Hz is stable according to the characteristic loci of $L_{hg} = GK$, see Fig. 4.39. However, the sufficient condition for closed loop stability is not achieved, Fig. 4.43. A way to reduce this conservatism is to design a diagonal weighting filter W that has no effect on the spectral radius condition,

$$\rho(E_T(j\omega)W(j\omega)W^{-1}(j\omega)T_d(j\omega)) < 1, \quad \forall \omega, \quad (4.72)$$

but provides more freedom in the sufficient condition for closed loop stability, [92]. The closed loop is stable if for each frequency holds that,

$$\bar{\sigma}(W^{-1}T_d) \leq \mu_{T_d}^{-1}(E_TW). \quad (4.73)$$

The weighting filter is only used for analysis. If W is chosen diagonal, one can emphasize the contribution of each loop to the maximum singular value of T_d . The complementary sensitivity function in the z -direction rolls off at higher frequencies (approximately 50Hz) than the complementary sensitivity functions of the xy -axis. Therefore, the contribution of the x,y axis designs to $\sigma_i(T_d)$ may be increased at high frequencies. At the same time, the weighting filter W may result in a smaller value of $\mu_{T_d}(E_TW)$. Therefore, for this application, we choose,

$$W(s) = \text{diag}\{w(s), w(s), 1\}, \quad w(s) = \frac{\omega_w^2}{s^2 + 2\zeta_w\omega_w s + \omega_w^2} \quad (4.74)$$

with $\omega_w = 2\pi 50$, $\zeta_w = 0.8$. As shown in the right-hand side of Fig. 4.43, the bound due to $\mu_{T_d}(E_TW)$ is reduced at higher frequencies so that the weighted sufficient condition for closed loop stability is satisfied.

The output sensitivity function is shown in Fig. 4.44. It is visible that at low frequencies, the non-diagonal terms are considerably smaller than with the low bandwidth uniform design, Fig. 4.40. At frequencies above 100Hz, non-diagonal terms are much larger compared to the design in Fig. 4.40. Therefore, closed loop cross-talk between the axes is reduced at low frequencies, but increased at higher frequencies. A more detailed comparison with the other designs is made in the next section.

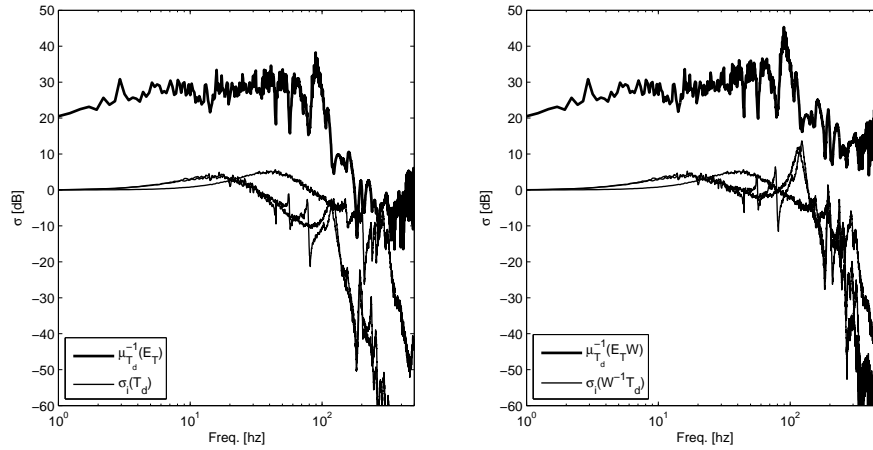


Figure 4.43: Sufficient condition for stability with the high bandwidth decentralized controller. Left: sufficient condition is not achieved. Right: sufficient condition, with scaling matrix W , is achieved.

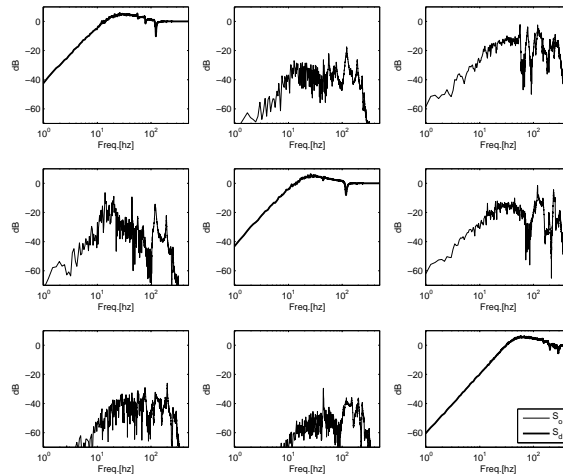


Figure 4.44: Bode magnitude of the output sensitivity function using the decentralized high bandwidth design, S_o and S_d . The diagonal terms of S_o are almost identical to S_d .

4.4.5 Discussion

With the decentralized control design, the non-diagonal terms of the plant were treated as uncertainty. It was shown that the bandwidth in x,y directions can be

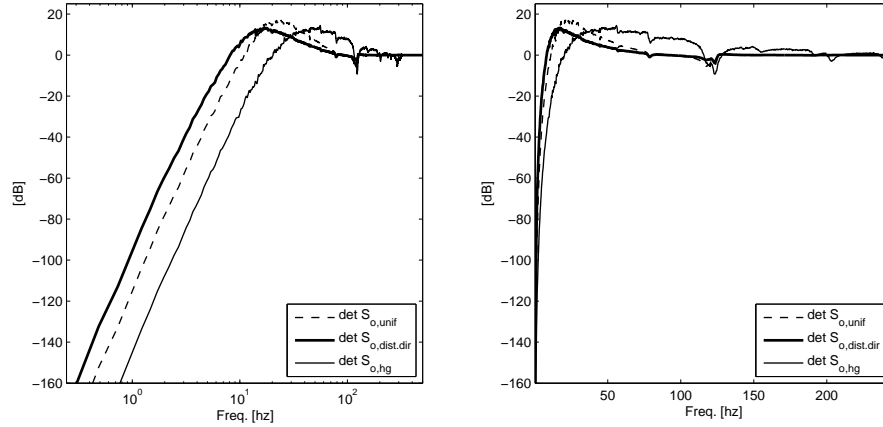


Figure 4.45: Determinant per frequency of the output sensitivity functions with three design approaches. Left: logarithmic frequency scale, Right: linear frequency scale.

increased slightly compared to an approach that uses (4.65) as the plant model. In the z -direction, bandwidth of the decentralized control design is much higher (50Hz). Stability could be proven by introducing a weighting factor in the sufficient condition for closed loop stability. The same weighted sufficient condition can be applied for the uniform design, Section 4.4.2. The cross-over frequency of the z -axis can then be increased from 10Hz to 40Hz. In spite of this, the assumption of a plant structure $G(s) = g(s)I$, still leads to conservatism which results in a lower maximum achievable bandwidth.

As an indication of the disturbance rejection quality, one can study the determinant of the output sensitivity function per frequency, Fig. 4.45. The disturbance decoupling design results in less net disturbance rejection at low frequencies than the uniform design. As a consequence of the waterbed effect, the net amplification of disturbances at high frequencies is smaller. The decentralized control design seems to have the best disturbance rejection at low frequencies, at the cost of amplifying disturbances and sensor noise at high frequencies. The determinant of the sensitivity function is plotted against a linear frequency scale in the right side of Fig. 4.45. Herein, it is clearly visible that disturbances at frequencies above the bandwidth are significantly amplified.

To study the rejection of disturbances with the direction \bar{d} at the output of the plant to the z -axis, we can plot $S_{vu} = v^T S_o \bar{d}$, for $v = [0, 0, 1]^T$, shown at the left side of Fig. 4.46. The disturbance decoupling design has the same disturbance rejection performance as the uniform design. The high bandwidth decentralized control design has a better low frequency disturbance rejection performance, at

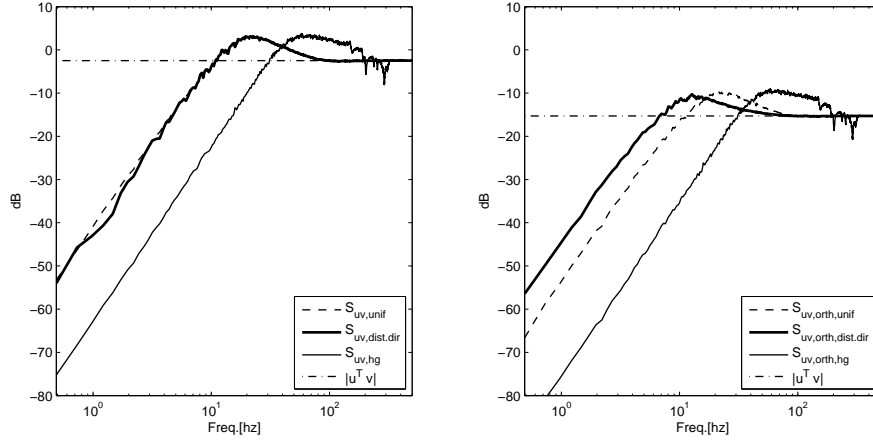


Figure 4.46: The output sensitivity S_{uv} , Left: from the disturbance in direction \bar{d} to the z axis. Right: from disturbances in a direction orthogonal to \bar{d} to the z axis.

the cost of amplifying significantly more disturbance at frequencies above the bandwidth. Disturbance rejection for disturbances with a direction orthogonal to \bar{d} is worse with the disturbance decoupling design compared to the uniform design, right side of Fig. 4.46. This is explained as the gain of the controller associated with those directions, is smaller. From both figures, it is visible that the high bandwidth decentralized control design has the best low frequency disturbance rejection for any disturbance direction.

The complementary sensitivity function for all three designs is shown in Fig. 4.47. At frequencies below 20Hz, the closed loop interaction is smallest with the high bandwidth decentralized control design. Above, 100Hz however, the non-diagonal terms are significantly larger than with the other designs. The design with disturbance decoupling, introduces non-diagonal terms in the output sensitivity function. As holds that, $T_o = I - S_o$, the magnitude of the non-diagonal terms of the output sensitivity function are equal to the magnitude of the non-diagonal terms of the complementary sensitivity function. Therefore cross-talk from the reference trajectory to the output of the plant increases. If the reference trajectory is in a direction orthogonal to \bar{d} , the tracking performance of the disturbance decoupling design may be worse than the uniform or high bandwidth decentralized design, see again Fig. 4.46. This is because the disturbance decoupling design only rejects disturbances in a particular chosen direction, while in orthogonal directions bandwidth was reduced to minimize cross-talk at high frequencies.

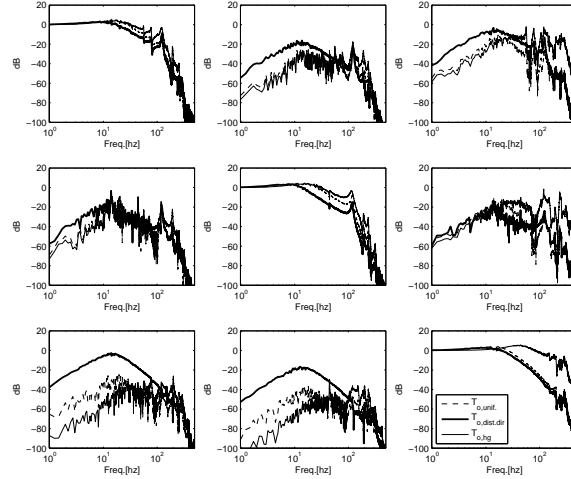


Figure 4.47: Bode magnitude of the complementary sensitivity function for the low bandwidth uniform design $T_{o,unif.}$, the disturbance decoupling design $T_{o,dist.dec}$ and the high bandwidth decentralized control design $T_{o,hg}$.

4.4.6 Conclusions

The three design approaches used in this section show that the feedback controller design for the metrological AFM can be performed using the design techniques discussed in this thesis. The model structure assumptions from Section 4.2, are shown to introduce conservatism. Nevertheless, a simplified model for control design delivers a transparent, physically interpretable control design approach. All design methods discussed in this application use non-parametric plant models. The simplified plant model approach can be used straightforwardly to simplify norm based control design. If low bandwidth controllers are required, the plant can be described as a constant frequency independent matrix.

In each design approach, the achievable bandwidth is limited. Therefore, increasing disturbance rejection at low frequencies implies increasing closed loop cross-talk and increasing the amplification of disturbances and sensor noise at higher frequencies. The disturbance decoupling design approach facilitates good disturbance rejection in relevant directions and less gain in orthogonal directions. Therefore, the costs of feedback control can be reduced with this design approach.

4.5 Concluding remarks

In this chapter, it was investigated and illustrated how directions of disturbances and sensor noise can be accommodated in feedback control design. In Section 4.1, results of the blind identification procedure of Chapter 3 are used to design non-diagonal weighting filters for \mathcal{H}_∞ loopshaping design. It was shown how multivariable extensions of the Bode integral relations imply tradeoffs in disturbance rejection with different weighting filters for \mathcal{H}_∞ loopshaping design. It was shown that accommodating sources of disturbances, and directions of disturbances, may lead to less severe frequency wise sensitivity function tradeoffs.

In Section 4.2, a method is developed to design centralized controllers with manual loopshaping techniques. With this, it is shown how, for a specific class of plants, the sensitivity function can be designed to reject disturbances in each orthogonal direction independently. The results of manual loopshaping are almost similar to those obtained with \mathcal{H}_∞ loopshaping. The design method was successfully applied to a model of a waferstage. A multiloop SISO design approach, that does not take into account directions of disturbances explicitly, was shown to be infeasible for this application.

All earlier sections focussed on the accommodating directions of disturbances. In Section 4.3, manual and \mathcal{H}_∞ loopshaping design guidelines are derived to accommodate directions of disturbances and sensor noise. It is shown that manual loopshaping can be applied if directions of sensor noise and directions of disturbances are sufficiently misaligned. The \mathcal{H}_∞ loopshaping method can also be applied for cases where directions of sensor noise and disturbances are not misaligned.

Several feedback design approaches are applied to a metrological atomic force microscope in Section 4.4. Herein, it is demonstrated that accommodating disturbances may lead to lower bandwidth feedback control designs. It is shown that the structural assumptions on the plant dynamics, that are required for manual centralized control design, are restrictive compared to the independent decentralized control design approach discussed in Chapter 2.

Therefore, we conclude that manual loopshaping methods are extended to accommodate directions of disturbances and sensor noise for a specific class of plants and disturbances. Also, at least for these cases, (non-diagonal) weighting filter design for \mathcal{H}_∞ loopshaping is elucidated.

Chapter 5

Conclusions and Recommendations

5.1 Conclusions

In this thesis, the rejection of disturbances in multivariable motion systems is investigated. Herein, the multivariable aspects of disturbances are characterized and accommodated in feedback control. Using the properties of motion systems and disturbances with frequency independent directions, a design method for manual and \mathcal{H}_∞ loopshaping is developed. This leads to the following concluding remarks.

It is shown how dominant dynamics of motion systems can be described as modal, dyadic or Pseudo SVD systems. Dynamics, e.g., due to plant interaction, that are not described with this, can be treated as uncertainty in the generalized plant framework. It is shown how the implications of this uncertainty can be translated to bounds on allowable (simplified) closed loop functions. With this, manual and \mathcal{H}_∞ loopshaping design for SISO and MIMO motion systems can be simplified significantly. This is illustrated with application to an active vibration isolation system, Section 2.5, model of a waferstage, Section 4.2, and a metrological atomic force microscope, Section 4.4.

A method is developed to acquire a physically motivated model for fixed direction disturbances in multivariable systems. Herein, the directions of disturbances and the root causes (sources) of disturbance are characterized. By application to an active vibration isolation system, it is shown how the location of sources can be recovered. It is shown how directions of disturbances can be physically interpreted and used to simplify multivariable control design.

Inherent limitations imply tradeoffs in achievable performance for MIMO systems. For frequency independent input and output directions of the sensitivity function, these limitations are analogous to those in SISO systems. To reduce the costs of disturbance rejection feedback control, sensitivity functions are only to be minimized in directions and at frequencies that are relevant for disturbance rejection. To account for the directional aspects of disturbances, centralized controllers may therefore be applied, even in cases where the plant dynamics are decoupled.

A design method to accommodate directions of disturbances and sensor noise in feedback control is developed. It is shown how models of fixed direction disturbances naturally result in non-diagonal weighting filters for \mathcal{H}_∞ loopshaping. Also, a manual loopshaping method for centralized controllers is developed for a specific class of plants. With this, the sensitivity functions can be designed to account for directional characteristics of disturbances. Furthermore, it was studied how directions of disturbances and directions of sensor noise can be accommodated in feedback control. A manual loopshaping method is developed that can be used when directions of disturbance and sensor noise are sufficiently misaligned. For more general alignment cases, it is shown how \mathcal{H}_∞ loopshaping can be applied. A metrological atomic force microscope is used to illustrate different feedback control design approaches.

5.2 Recommendations

In this thesis, it is shown how manual and \mathcal{H}_∞ loopshaping can be used to accommodate directions of disturbances for a specific class of control problems. It is expected that the application area can be extended by further research on the following issues.

The model assumptions required for the blind identification limit application of this method to a wider class of problems. To extend the application field, methods must be investigated that enable identification of more sources than observed disturbances, see [33]. Furthermore, dynamic (frequency dependent direction) disturbance models can be identified with the concepts discussed in [27, 139]. These advanced disturbance identification techniques motivate the application of more advanced (not necessarily LTI) controllers as reported in [1, 57, 78, 138]. For these, not LTI, controllers, the inherent limitations discussed in this thesis do not apply, [119].

Manual loopshaping techniques may be extended by combining the insights of this thesis with concepts of Quantitative Feedback Control Theory (QFT) as developed in, [58, 150]. Methods to design centralized controllers with QFT are discussed in [50, 51]. Future research may focus on the accommodation of direc-

tionality of disturbances within the QFT framework. Also, the sufficient conditions for closed loop stability and performance developed in this thesis can be formulated in a loopshaping QFT framework.

It is shown in Chapter 3 that the contribution of each identified source to the total servo error can be studied independently. This can be considered as a natural extension of dynamic error budgeting techniques as discussed in [68]. Aside from this analysis, one may consider control synthesis techniques that allow transparent tradeoffs in rejecting disturbances due to different sources. In work not reported here, we investigated multichannel multicriteria \mathcal{H}_2 synthesis techniques. In [34], multichannel multicriteria \mathcal{H}_2 synthesis was studied using the concepts of [71]. Also, it was investigated how multichannel \mathcal{H}_2 problems can be formulated as LMI's using the techniques of [6]. Both approaches provided reasonable results on simple systems, but showed to be very sensitive to numerical errors when used for realistic motion systems. More promising results were achieved using the multiobjective design approach proposed in [67]. This approach is restricted to specially structured generalized plants. In all studied techniques, the order of the controller transfer function increases significantly. To obtain controllers that can be implemented on a practical setup, controller order reduction techniques are to be used. This often gives rise to numerical issues when applied to realistic motion systems. However, it is expected that with alternative problem formulations and ongoing developments in numerical techniques, some of these issues can be resolved in the near future.

For a specific class of problems, the choice of weighting filters for \mathcal{H}_∞ loopshaping is elucidated. In order to enable \mathcal{H}_∞ design for industry, accurate parametric models of the plant are required. Therefore, it is recommended to develop practically feasible techniques for plant identification and model (and controller) order reduction techniques, see e.g. [96]. Also, disturbance models may be acquired as a by-product of plant identification techniques, [95, 127]. Hence, it is interesting to study relationships between the blind identification method proposed in this work and identification techniques developed in [127, 131].

Appendix A

Figures AVIS control design

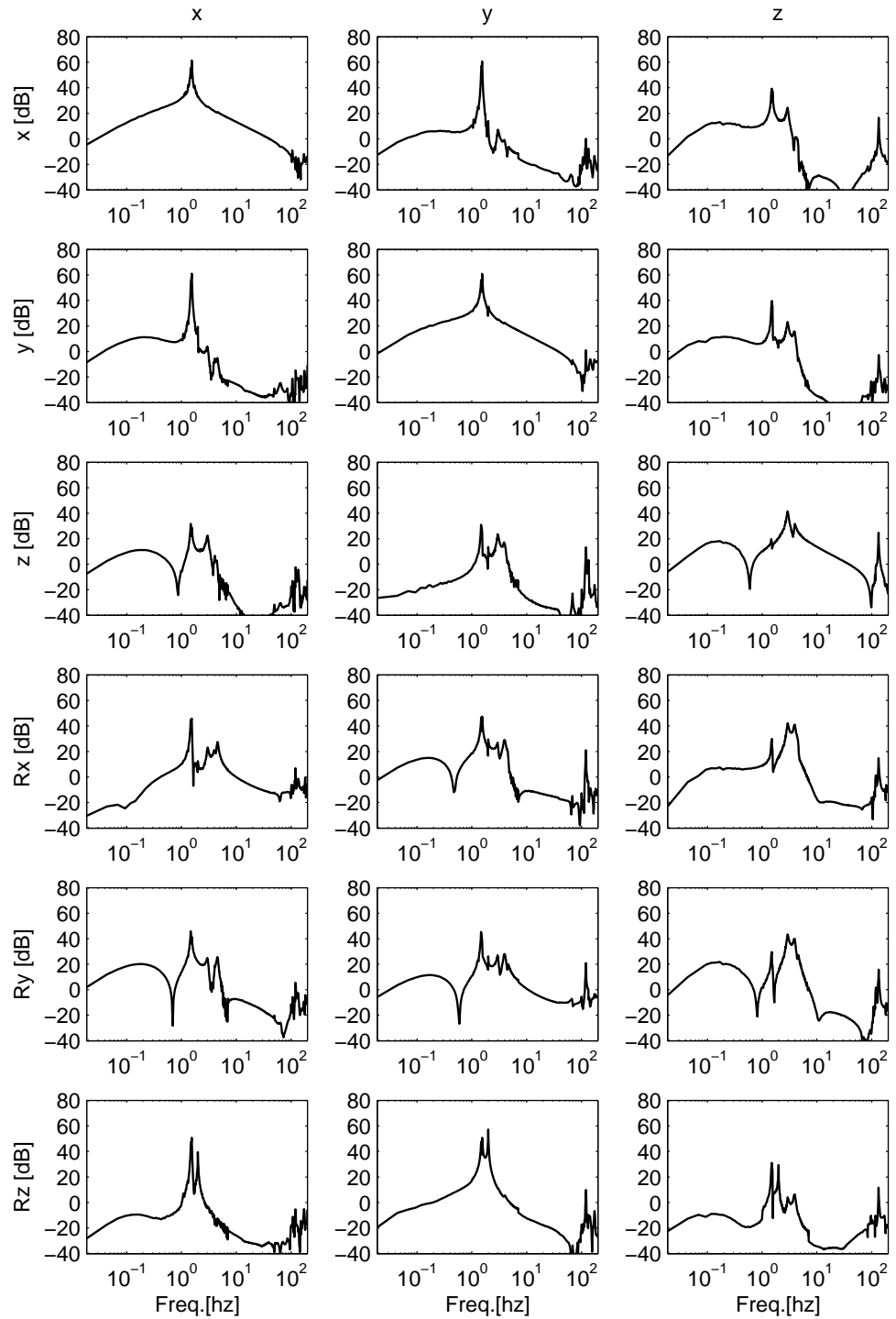
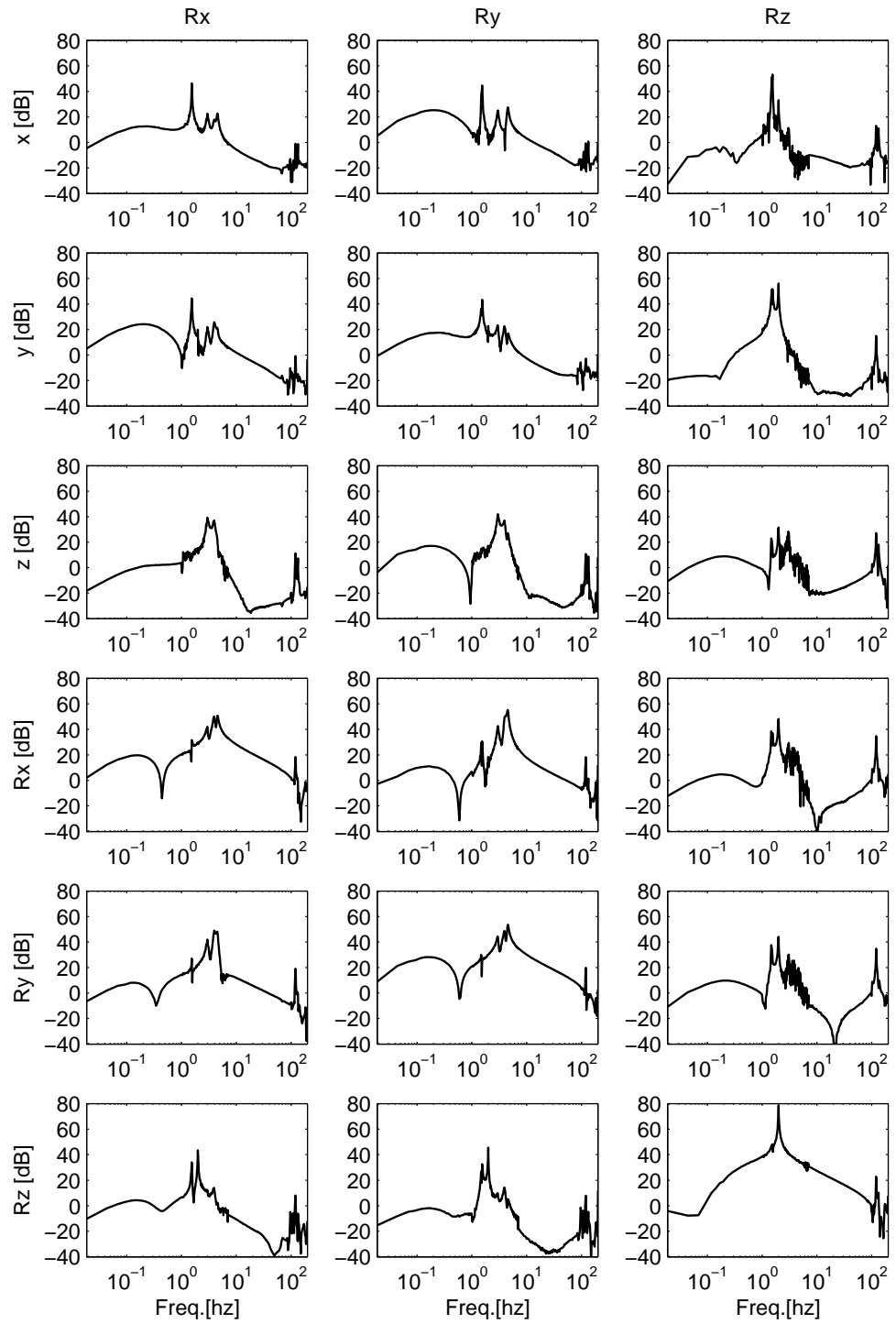


Figure A.1: Bode magnitude of plant (AVIS).



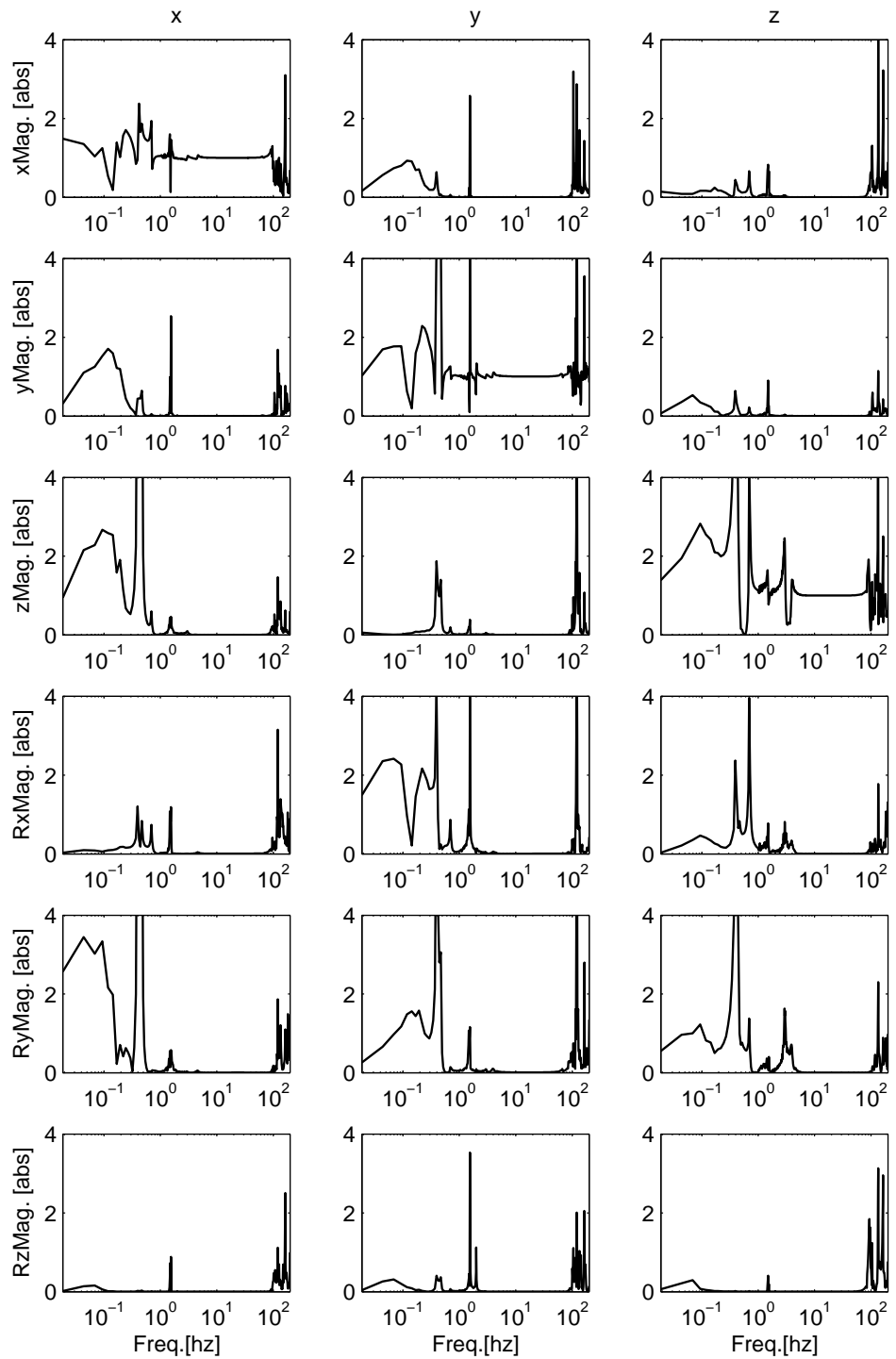
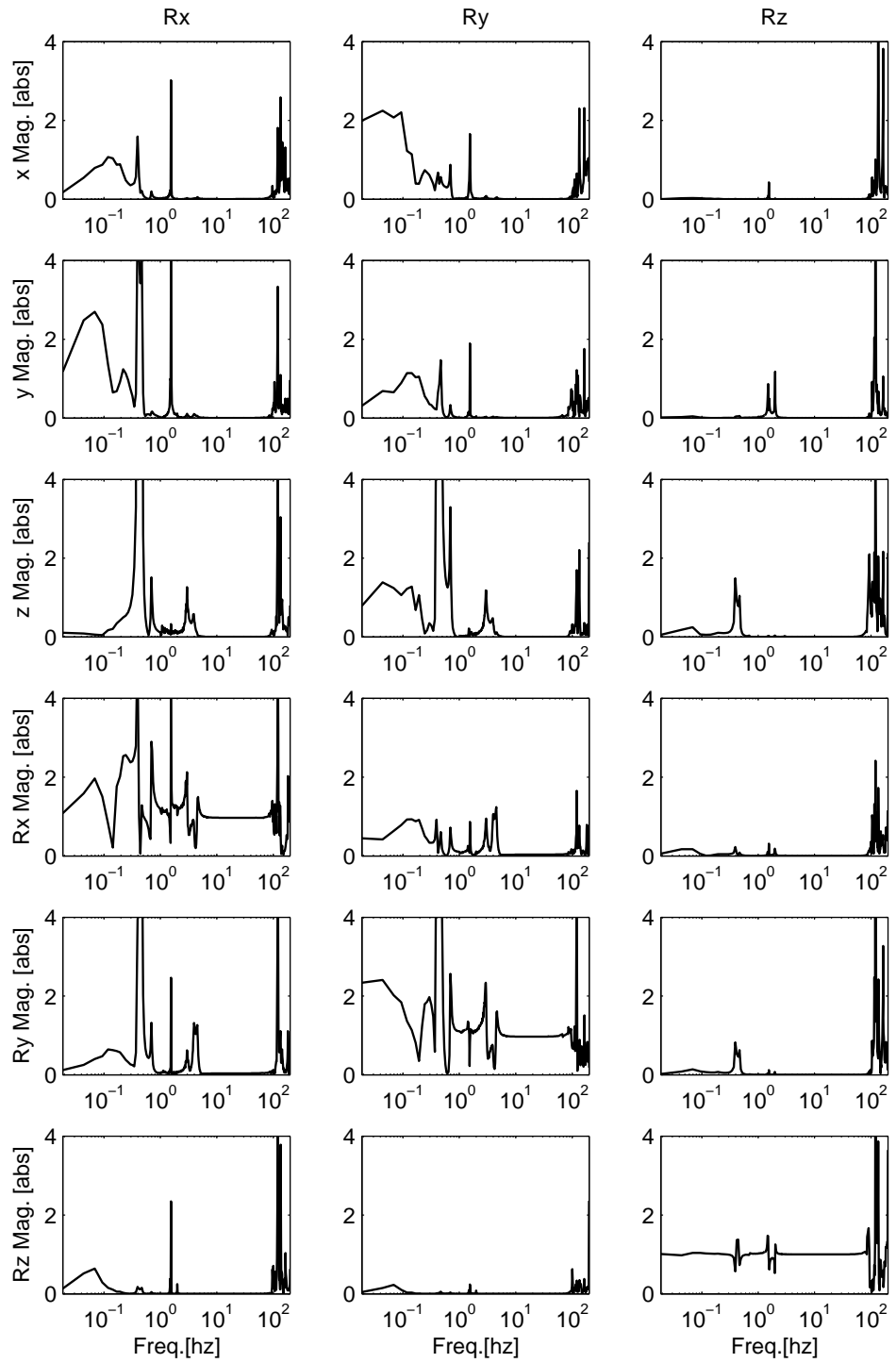


Figure A.2: Relative gain array of the AVIS.



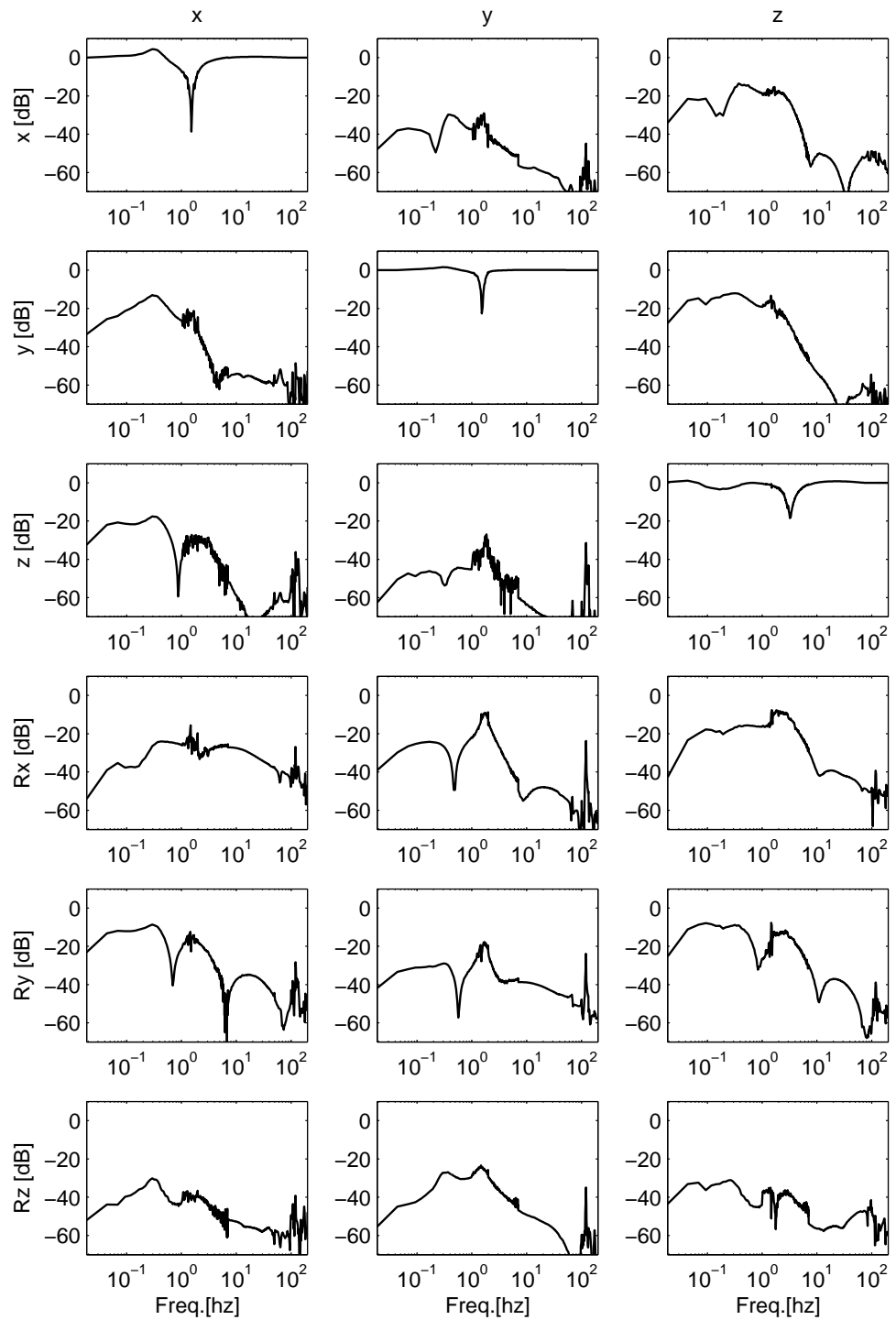
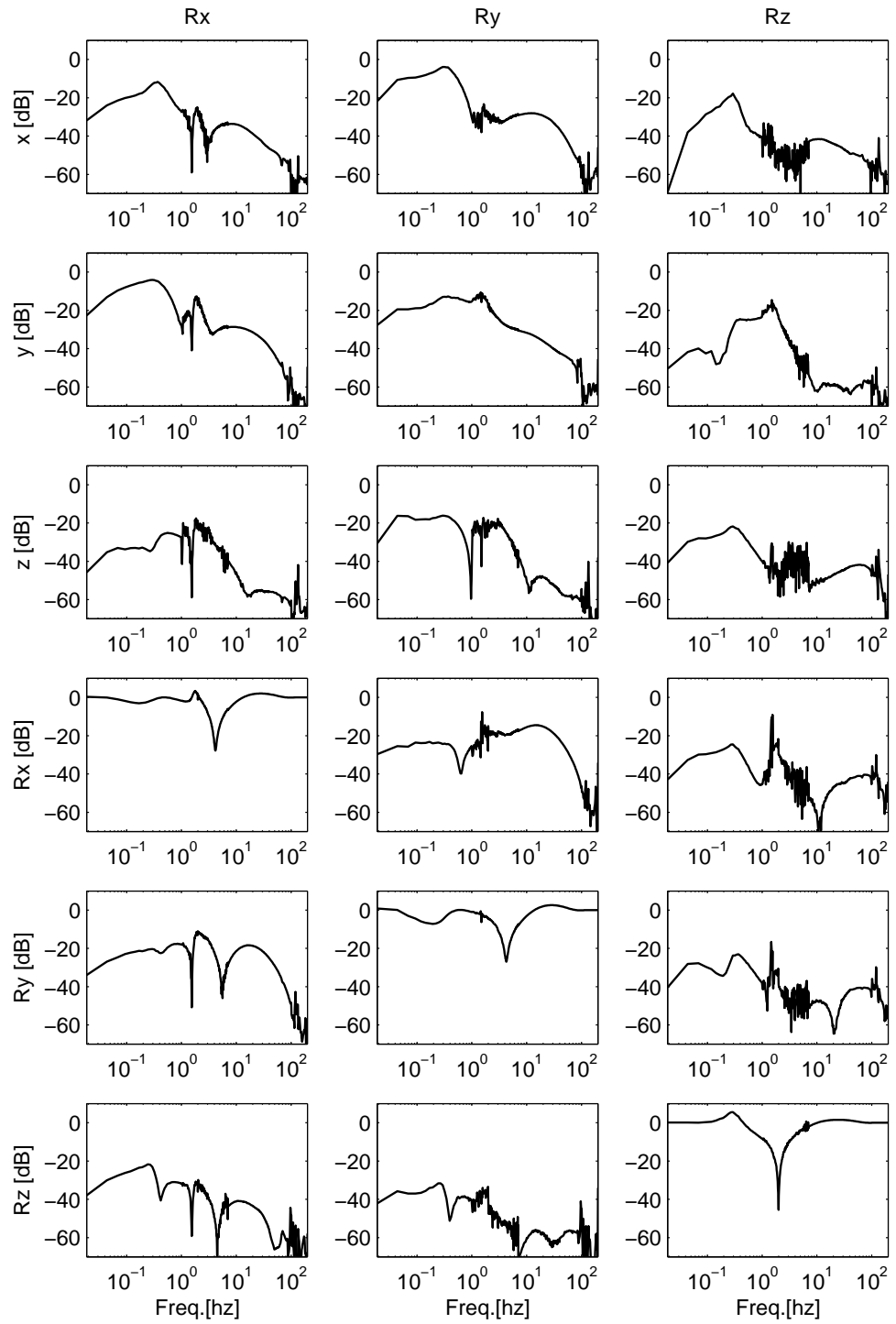


Figure A.3: Bode magnitude of the output sensitivity function using decentralized feedback control (AVIS)



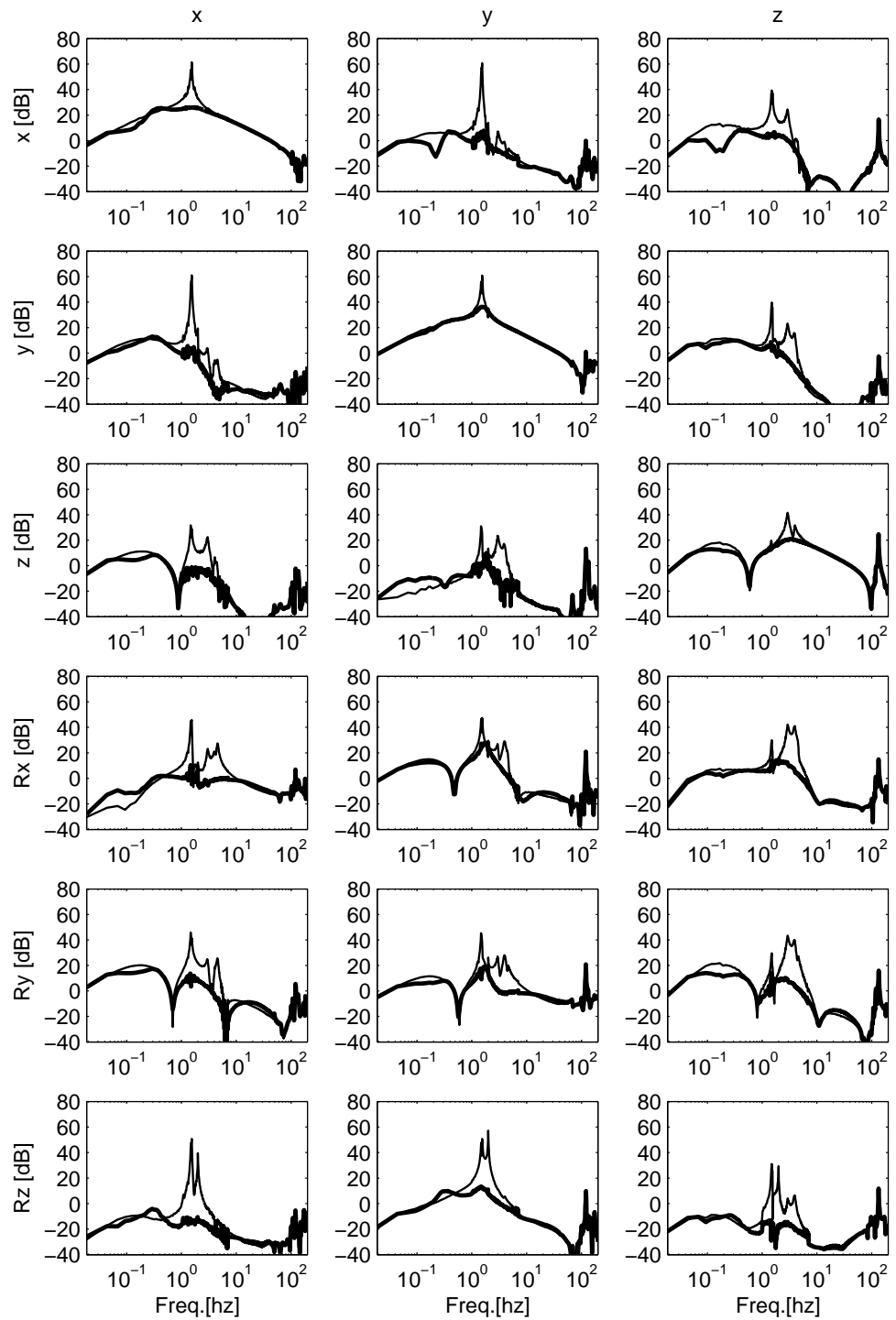
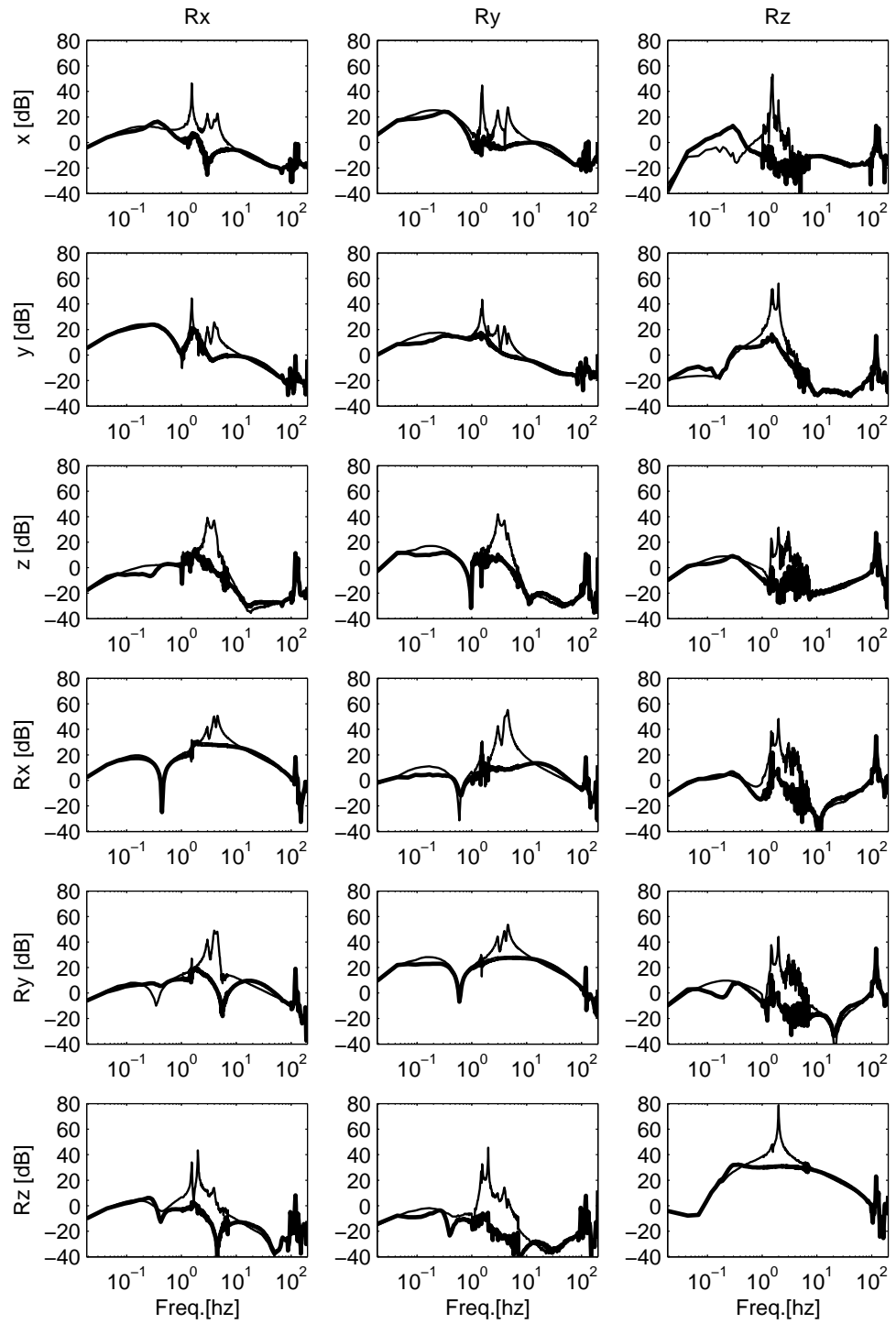


Figure A.4: Bode magnitude of the plant and the process sensitivity function



Appendix B

Principal angles

Here we show that the principal angles between subspace \mathbf{U}_1 and \mathbf{V}_1 can be calculated from the alignment between \mathbf{U}_1 and \mathbf{V}_2 provided that $\mathbf{V}_1 \perp \mathbf{V}_2$. The reasoning is based on Theorem 2.3 of [130] and the appendix of [46]. Let the columns of \tilde{U} span \mathbf{U} with $U \in \mathbf{U}$. Let the columns of \tilde{V} span \mathbf{V} with $V \in \mathbf{V}$. Then, there exist unitary matrices $P_1 \in \mathbb{C}^{k \times k}$, $P_2 \in \mathbb{C}^{(n-k) \times (n-k)}$, $Q_1 \in \mathbb{C}^{k \times k}$, $Q_2 \in \mathbb{C}^{(n-k) \times (n-k)}$, so that $P = \text{diag}\{P_1, P_2\}$, $Q = \text{diag}\{Q_1, Q_2\}$ and,

$$V^H U = P \tilde{V}^H \tilde{U} Q^H \quad (\text{B.1})$$

where for $2k \leq n$,

$$\tilde{V}^H \tilde{U} = \left[\begin{array}{c|cc} \bar{C} & \bar{S} & 0 \\ -\bar{S} & \bar{C} & 0 \\ \hline 0 & 0 & I_{n-2k} \end{array} \right] \quad (\text{B.2})$$

with $\bar{C} = \text{diag}\{\cos \theta_i\}$, $\bar{S} = \text{diag}\{\sin \theta_i\}$. The proof of this can be found in Section 3 of [9]. If $2k > n$, the identity block appears in the upper left-hand corner. Using (B.2), we can write,

$$\begin{aligned} V^H U &= \left[\begin{array}{c|c} V_1^H U_1 & V_1^H U_2 \\ \hline V_2^H U_1 & V_2^H U_2 \end{array} \right] \\ &= \left[\begin{array}{c|c} P_1 \bar{C} Q_1^H & P_1 \left[\begin{array}{c|c} \bar{S} & 0 \\ \hline \bar{C} & 0 \end{array} \right] Q_2^H \\ \hline P_2 \left[\begin{array}{c|c} \bar{S} & 0 \\ \hline 0 & I \end{array} \right] Q_1^H & P_2 \left[\begin{array}{c|c} \bar{C} & 0 \\ \hline 0 & I \end{array} \right] Q_2^H \end{array} \right] \quad (\text{B.3}) \end{aligned}$$

This illustrates that the first k singular values of $V_1^H U_2$ are the sinusoids of the principal angles between subspace \mathbf{U}_1 and \mathbf{V}_1 . Therefore we can calculate the principal angles θ_i as, $\theta_i = \arcsin \sigma_i(V_1^H U_2)$ or $\theta_i = \arccos \sigma_i(V_1^H U_1)$ for $i = 1, \dots, k$.

Bibliography

- [1] W. Aangenent. *An exploration of nonlinear control for linear motion systems*. PhD thesis, Technische Universiteit Eindhoven, 2008.
- [2] D. Abramovitch, S. Andersson, L. Pao, and G. Schitter. A tutorial on the mechanisms, dynamics, and control of atomic force microscopes. In *Proceedings of the American Control Conference*, pages 3488–3502, 2007.
- [3] D. Abramovitch, T. Hurst, and D. Henze. The PES pareto method: Uncovering the strata of position error signals in disk drives. In *Proceedings of the American Control Conference*, volume 5, pages 2888–2895, 1997.
- [4] J. Anthonis and H. Ramon. Linear mechanical systems and dyadic transfer function matrices. *Automatica*, 39:1353–1363, 2003.
- [5] J. Antoni. Blind separation of vibration components: Principles and demonstrations. *Mechanical Systems and Signal Processing*, 19:1166–1180, 2005.
- [6] P. Apkarian, H. Tuan, and J. Bernussou. Analysis, eigenstructure assignment and \mathcal{H}_2 multi-channel synthesis with enhanced LMI characterizations. In *Proceedings of the Conference on Decision and Control*, 2000.
- [7] A. Belouchrani, K. Abed-Meraim, J. Cardoso, and E. Moulines. A blind source separation technique using second-order statistics. *IEEE Transactions on Signal Processing*, 45(2):123–145, 1997.
- [8] A. Belouchrani and A. Cichocki. Robust whitening procedure in blind source separation context. *IEE Electronics Letters*, 36:2050–2051, 2000.
- [9] A. Bjorck and G. Golub. Numerical methods for computing angles between linear subspaces. *Mathematics of Computation*, 27(123):579–594, 1973.
- [10] H. Bode. *Network Analysis and Feedback amplifier design, twelfth printing*. D. van Nostrand company inc., 1945.
- [11] M. Boerlage. Open-loop techniques for the reduction of servo errors during jerk phase, applied to the atlas waferstage short stroke. Technical report,

- Fontys University of Applied Sciences, Mechanical Engineering, Mechatronics, 2000.
- [12] M. Boerlage. An exploratory study on multivariable control for motion systems, masters thesis. Master's thesis, Eindhoven University of Technology, 2004.
- [13] M. Boerlage. MIMO jerk derivative feedforward for motion systems. In *Proceedings of the American Control Conference*, pages 3892–3897, 2006.
- [14] M. Boerlage, R. Middleton, B. de Jager, and M. Steinbuch. Rejection of fixed direction disturbances in multivariable electromechanical motion systems. In *Proceedings of the IFAC World conference*, pages 176–181, 2008.
- [15] M. Boerlage, M. Steinbuch, and G. Angelis. Frequency response based multivariable control design for motion systems. In *Proceedings of the Conference on Control Applications*, 2005.
- [16] M. Boerlage, M. Steinbuch, P. Lambrechts, and M. van de Wal. Model-based feedforward for motion systems. In *Proceedings of the Conference on Control Applications*, volume 2, pages 1158–1164, 2003.
- [17] M. Boerlage, M. Steinbuch, and R. Tousain. Setpoint relevant feedforward design for motion systems. In *Proceedings of the ASPE Spring Topical Meeting, Control of Precision Systems*, volume 32, pages 104–1010, 2004.
- [18] M. Boerlage, R. Tousain, and M. Steinbuch. Jerk derivative feedforward control for motion systems. In *Proceedings of the Conference on Control Applications*, pages 4843–4848, 2004.
- [19] S. Boyd and C. Desoer. Subharmonic functions and performance bounds on linear time-invariant feedback systems. *IMA Journal of Mathematics, Control and Information*, pages 153–170, 1985.
- [20] E. Bristol. On a new measure of interactions for multivariable process control. *IEEE Transactions on Automatic Control*, 11:133–134, 1966.
- [21] D. Bristow, M. Tharayil, and A. Alleyne. A survey of iterative learning control. *IEEE Control Systems Magazine*, 26(3):96–114, 2006.
- [22] G. Bryant and L. Yeung. *Multivariable control system design techniques, dominance and direct methods*. John Wiley & Sons, 1996.
- [23] J. Burl. *Linear Optimal Control*. Addison Wesley, 1999.
- [24] J. Cardoso. Blind signal separation: statistical principles. *Proceedings of the IEEE*, 9(10):2009–2026, 1998.
- [25] J. Cardoso and A. Soulmiac. Jacobi-angles for simultaneous diagonalization. *SIAM Journal on Matrix Analysis and Applications*, 17(1):161–164, 1996.

- [26] J. Chen. Sensitivity integral relations and design–tradeoffs in linear multivariable feedback systems. *IEEE Transactions on Automatic Control*, 40(10):1700–1716, 2002.
- [27] J. Chen, G. Chen, Z. Ren, and L. Qiu. Extended argument principle and integral design constraints, part i: a unified formula for classical results. In *Proceedings of the Conference on Decision and Control*, pages 4984–4989, 2000.
- [28] M. Chiu and Y. Arkun. A methodology for sequential design of robust decentralized control systems. *Automatica*, 28(5):997–1001, 1992.
- [29] S. Chughtai and N. Munro. Diagonal dominance using LMIs. *IEE Control Theory and Applications*, 151(2):225–233, 2004.
- [30] P. Comon. Independent component analysis, a new concept? *Signal Processing*, 36(3):287–314, 1994.
- [31] R. Craig and A. Kurdila. *Fundamentals of structural dynamics, Second edition*. John Wiley & Sons, 2006. ISBN 0571430447.
- [32] J. de Best. Controlling the twin drive by decoupling. Technical Report DCT 2004.93, Technische Universiteit Eindhoven, 2004.
- [33] L. De Lathauwer and J. Castaing. Blind identification of underdetermined mixtures by simultaneous matrix diagonalization. *IEEE Transactions on signal processing*, 56(3):1096–1105, 2008.
- [34] T. Donkers. Making spatial trade-offs using multiobjective \mathcal{H}_2 synthesis. Bachelor’s thesis DCT 2006.109, Technische Universiteit Eindhoven, 2006.
- [35] J. Doyle. Analysis of feedback systems with structured uncertainties. *IEE Proceedings, Part D, Control Theory and Applications*, 129(6):242–250, 1982.
- [36] J. Doyle. Advances in multivariable control, lecture notes ONR, honeywell workshop. Technical report, Honeywell, 1984.
- [37] J. Doyle, K. Glover, P. Khargonekar, and B. Francis. State–space solutions to standard \mathcal{H}_2 and \mathcal{H}_∞ control problems. *IEEE Transactions on Automatic Control*, 34(8):831–847, 1989.
- [38] J. Doyle and G. Stein. Multivariable feedback design: concepts for classical modern synthesis. *IEEE Transactions on Automatic Control*, 26(1):4–16, 1981.
- [39] R. Ehrlich, J. Adler, and H. Hindi. Rejecting oscillatory, non-synchronous mechanical disturbances in hard disk drives. *IEEE Transactions on Magnetics*, 37(2):646–650, 2001.
- [40] Integrated Dynamics Engineering. Website may 2008. URL <http://www.ideworld.net/>.

-
- [41] B Francis and W. Wonham. The internal model principle for linear multivariable regulators. *Applied Mathematics and Optimization*, 2(2), 1975.
 - [42] J. Freudenberg. Plant directionality, coupling and multivariable loop-shaping. *International Journal of Control*, 51(2):365–390, 1990.
 - [43] J. Freudenberg and Karnik. A. Reverse engineering a multivariable controller: A case study. In *Proceedings of the American Control Conference*, pages 733–738, 2005.
 - [44] J. Freudenberg, C. Hollot, R. Middleton, and V. Tsochinda. Fundamental design limitations of the general control configuration. *IEEE Transactions on automatic control*, 48(8):1355–1370, 2003.
 - [45] J. Freudenberg and D. Looze. Right half plane poles and zeros and design tradeoffs in feedback systems. *IEEE Transactions on Automatic Control*, 30(6):555–565, 1985.
 - [46] J. Freudenberg and D. Looze. The relation between open-loop and closed-loop properties of multivariable feedback systems. *IEEE Transactions on Automatic Control*, 31(4):333–340, 1986.
 - [47] J. Freudenberg and D. Looze. *Frequency Domain Properties of Scalar and Multivariable Feedback Systems, Lecture Notes in Control and Information Sciences*. Springer-Verlag, 1988.
 - [48] J. Freudenberg and R. Middleton. Design rules for multivariable feedback systems. In *Proceedings of the Conference on Decision and Control*, pages 1980–1985, 1996.
 - [49] J. Freudenberg and R. Middleton. Properties of single input, two output feedback systems. *International Journal of Control*, 72(16):1446–1465, 1999.
 - [50] M. Garcia-Sanz and I. Egaña. Quantitative non-diagonal controller design for multivariable systems with uncertainty. *International Journal of Robust Nonlinear Control*, 12:321–333, 2002.
 - [51] M. Garcia-Sanz and I. Egaña. Nondiagonal qft controller design for a three-input three-output industrial furnace. *Journal of Dynamic Systems, Measurement, and Control*, 128, 2006.
 - [52] W. Gawronski. *Advanced Structural Dynamics and Active Control of Structures*. Springer-Verlag, 2004.
 - [53] G. Golub and C. Loan. *Matrix Computations*. Johns Hopkins, 1996.
 - [54] G. Gómez and G. Goodwin. Integral constraints on sensitivity vectors for multivariable linear systems. *Automatica*, 32:499–518, 1996.
 - [55] G. Goodwin, S. Graebe, and M. Salgado. *Control system design*. Prentice Hall, 2001.

-
- [56] P. Grosdidier and M. Morari. Interaction measures for systems under decentralized control. *Automatica*, 22:309–319, 1986.
- [57] M. Heertjes, F. Cremers, R. Rieck, and M. Steinbuch. Nonlinear dynamic servo control for optical storage drives with improved shock performance. *Control Engineering Practice*, 13(10), 2005.
- [58] I. Horowitz. Survey of quantitative feedback theory (QFT). *International Journal of Control*, 53:255–291, 1991.
- [59] M. Hovd, R. Braatz, and S. Skogestad. SVD controllers for \mathcal{H}_2 -, \mathcal{H}_∞ - and μ -optimal control. *Automatica*, 33(3):433–439, 1997.
- [60] M. Hovd and S. Skogestad. Sequential design of decentralized controllers. *Automatica*, 30(10):1601–1607, 1994.
- [61] D. Hrovat. Survey of advanced suspension developments and related optimal control applications. *Automatica*, 33:1781–1817, 1997.
- [62] X. Huang, R. Horowitz, and Y. Li. A comparative study of MEMS microactuators for use in a dual-stage servo with an instrumented suspension. *IEEE Transactions on Mechatronics*, 11(5):524–532, 2006.
- [63] Y. Hung and A. MacFarlane. *Multivariable Feedback: A Quasi-classical Approach, Lecture Notes in Control and Information Sciences*. Springer-Verlag, 1982.
- [64] R. Huston. *Multibody Dynamics*. Butterworth-Heinemann, London, 1990.
- [65] A. Hyvarinen, J. Karhunen, and E. Oja. *Independent components analysis*. John Wiley & Sons, 2001.
- [66] D. Inman. *Vibration with control*. John Wiley & Sons, 2006.
- [67] Stoustrup J. and Niemann H. Multiobjective control for multivariable systems with mixed-sensitivity specifications. *International Journal of Control*, 66:225–243, 1997.
- [68] L. Jabben. *Mechatronic design of a magnetically suspended rotating platform*. PhD thesis, Technische Universiteit Delft, 2006.
- [69] C. Johnson. Accommodation of disturbances in optimal control problems. *International Journal of Control*, 15(2):209–231, 1972.
- [70] C. Johnson. *Theory of Disturbance-Accommodating Controllers, Control and Dynamic Systems – Advances in Theory and Applications*, volume 12. Academic Press, 1976.
- [71] P. Khargonekar and M. Rotea. Multi objective optimal control of linear systems: The quadratic norm case. *IEEE Transactions on Automatic Control*, 36(1):14–24, 1991.

- [72] B. Kim Keun and Chung Kyun W. Advanced disturbance observer design for mechanical positioning systems. *IEEE Transactions on industrial electronics*, 50(6):1207–1216, 2003.
- [73] S. Koekebakker. Decoupling by means of $\mathcal{H}_{\infty, f}$ control, application to a wafer stage. Master's thesis, Delft University of Technology, 1993.
- [74] B. Kouvaritakis, J. Rossiter, and J. Wang. Generalized nyquist bands for structured and highly structured uncertainty. *International Journal of Control*, 53(6):1295–1309, 1991.
- [75] P. Lambrechts, M. Boerlage, and M. Steinbuch. Trajectory planning and feedforward design for high performance motion systems. In *Proceedings of the Conference on Control Applications*, pages 4637–4642, 2004.
- [76] P. Lambrechts, M. Boerlage, and M. Steinbuch. Trajectory planning and feedforward design for electromechanical motion systems. *Control Engineering Practice*, 13(2):145–157, 2005.
- [77] H. Latchman, O. Crisalle, and V. Basker. The Nyquist robust stability margin, a new metric for the stability of uncertain systems. *International Journal of Nonlinear and Robust Control*, 7:211–226, 1997.
- [78] K. Lau. *Time domain Feedback Performance limitations - Extensions to Nonlinear, Switched and Sampled systems*. PhD thesis, The University of Newcastle, Australia, 2002.
- [79] J. Lee, Y. Chait, and M. Steinbuch. On QFT tuning of multivariable μ controllers. *Automatica*, 36:1701–1708, 2000.
- [80] R. Li and X. Wang. Dimension reduction of process dynamic trends using independent component analysis. *Computers and Chemical Engineering*, 26(3):467–473, 2002.
- [81] L. Ljung. *System identification, theory for the user, Second edition*. Prentice-Hall, 2006.
- [82] A. MacFarlane. A survey of some recent results in linear multivariable feedback theory. *Automatica*, 8(4):455–492, 1972.
- [83] A. MacFarlane. *Frequency-response methods in control systems*. IEEE Press. New York., 1979.
- [84] J. Maciejowski. *Multivariable feedback design*. Addison-Wesley, 1989.
- [85] D. Mayne. The design of linear multivariable systems. *Automatica*, 9:201–207, 1973.
- [86] D. Mayne. Sequential design of linear multivariable systems. *Proceedings of the IEE*, 126:568–572, 1979.

-
- [87] R. Merry, M. Uyanik, R. van den Molengraft, R. Koops, M. van Veghel, and M. Steinbuch. Identification, control and hysteresis compensation of a 3 DOF metrological afm. *Asian Journal of Control*, 2008. Submitted.
- [88] R. Merry, M. Uyanik, R. van den Molengraft, R. Koops, M. van Veghel, and M. Steinbuch. Modeling, identification and control of a metrological atomic force microscope with a 3dof stage. In *Proceedings of the American Control Conference*, volume 6, 2008.
- [89] R. Middleton. Trade-offs in linear control system design. *Automatica*, 27: 281–292, 1991.
- [90] R. Middleton and G. Goodwin. *Digital control and estimation. A unified approach*. Prentice-Hall, Inc., 1990.
- [91] S. Moheimani, D. Halim, and A. Fleming. *Spatial Control of Vibration: Theory and Experiments*. World Scientific, 2003.
- [92] M. Morari and E. Zafiriou. *Robust process control*. Prentice-Hall, 1989.
- [93] P. Odgaard and M. Wickerhauser. Karhunen–Loève (PCA) based detection of multiple oscillations in multiple measurement signals from large-scale process plants. In *Proceedings of the American Control Conference*, pages 5893–5898, 2007.
- [94] M. Olanrewaju and M. Al-Arfaj. Impact of disturbance magnitudes and directions on the dynamic behavior of a generic reactive distillation. *Chemical Engineering and Processing*, 45:140–149, 2006.
- [95] T. Oomen and O. Bosgra. Estimating disturbances and model uncertainty in model validation for robust control, Submitted for (conference) publication. In *Conference on Decision and Control, Accepted*, 2008.
- [96] T. Oomen and O. Bosgra. Robust-control-relevant coprime factor identification: A numerically reliable frequency domain approach. In *Proceedings of the American Control Conference*, pages 625–631, 2008.
- [97] T. Oomen, M. van de Wal, and O. Bosgra. Design framework for high-performance optimal sampled-data control with application to a wafer stage. *International Journal of Control*, 80(6):919–934, 2007.
- [98] D. Owens. Dyadic approximation method for multivariable control systems analysis with a nuclear reactor application. *IEE Proceedings Control & Science*, 120:801–809, 1973.
- [99] D. Owens. Structural modification of dyadic transfer-function matrices using feedback. *Electronics Letters*, 9(16):379–380, 1973.
- [100] D. Owens. Dyadic expansion for the analysis of linear multivariable systems. *IEE Proceedings Control & Science*, 121:713–716, 1974.

-
- [101] D. Owens. Dyadic approximation about a general frequency point. *Electronics Letters*, 11(15):331–332, 1975.
- [102] D. Owens. *Feedback and multivariable systems*. Peter Peregrinus Ltd., 1978.
- [103] D. Owens. A historical view of multivariable frequency domain control. In *Proceedings of the IFAC World congress*, 2002.
- [104] G. Pang and A. MacFarlane. *An Expert Systems Approach to Computer-Aided Design of Multivariable Systems, Lecture Notes in Control and Information Sciences*. Springer-Verlag, 1987.
- [105] L. Pao, J. Butterworth, and D. Abramovitch. Combined feedforward/feedback control of automic force microscopes. In *Proceedings of the American Control Conference*, 2007.
- [106] L. Parra and P. Sajda. Blind source separation via generalized eigenvalue decomposition. *Journal of Machine Learning Research*, 4:1261–1269, 2003.
- [107] D. Pham and J. Cardoso. Blind separation of instantaneous mixtures of non stationary sources. *IEEE Transactions on Signal Processing*, 49(9):1937–1848, 2001.
- [108] R. Pintelon, P. Guillaume, Y. Rolain, J. Schoukens, and H. Van hamme. Parametric identification of transfer functions in the frequency domain, a survey. In *Proceedings of the Conference on Decision and Control*, pages 557–566, 1993.
- [109] I. Postlethwaite and Y. Foo. Robustness with simultaneous pole and zero movement across the $j\omega$ -axis. *Automatica*, 21:433–443, 1985.
- [110] I. Postlethwaite and A. MacFarlane. *A Complex Variable Approach to the Analysis of Linear Multivariable Feedback Systems*, volume 12 of *Lecture Notes in Control and Information Sciences*. Springer-Verlag, 1979.
- [111] N. Rademakers. Modelling, identification and multivariable control of an active vibration isolation system. Master’s thesis, Technische Universiteit Eindhoven, 2005. DCT 2005.63.
- [112] J. Rijnsdorp. Interaction in two-variable control systems for distillation columns i: theory. *Automatica*, 3:15–28, 1965.
- [113] H. Rosenbrock. *Computer-aided control system design*. Academic Press, 1974.
- [114] R. Sánchez-Peña and M. Sznaier. *Robust systems, theory and applications*. John Wiley & Sons, 1998.
- [115] M. Schneiders. *Overactuated motion control; a modal approach*. PhD thesis, Technische Universiteit Eindhoven, 2008.

-
- [116] E. Schrijver and J. van Dijk. Disturbance observers for rigid mechanical systems: Equivalence, stability, and design. *Journal of Dynamic Systems, Measurement, and Control*, 124:539–548, 2002.
- [117] A. Sebastian and S. Salapaka. Design methodologies for robust nano-positioning. *IEEE Transactions on Control Systems Technology*, 13:868–876, 2005.
- [118] N. Sebe. A unified approach to decentralized controller design. In *Proceedings of the Conference on Decision and Control*, pages 1086–1091, 2003.
- [119] M. Seron, J. Braslavsky, and G. Goodwin. *Fundamental Limitations in Filtering and Control*. Springer-Verlag, 1997.
- [120] C. Servière and P. Fabry. Principal component analysis and blind source separation of modulated sources for electro-mechanical systems diagnostic. *Mechanical Systems and Signal Processing*, 19:1293–1311, 2005.
- [121] S. Shahruz. Design of disturbance observers for multi-input multi-output systems. *ASME Journal of Vibration and Acoustics*, 130:1–7, 2009.
- [122] S. Skogestad and M. Morari. Effect of disturbance directions on closed-loop performance. *Ind. Eng. Chem. Res.*, 26(1):2029–2035, 1987.
- [123] S. Skogestad and M. Morari. Some new properties of the structured singular value. *IEEE Transactions on Automatic Control*, 33(12):1151–1154, 1988.
- [124] S. Skogestad and M. Morari. Robust performance of decentralized control systems by independent designs. *Automatica*, 25(1):119–125, 1989.
- [125] S. Skogestad and I. Postlethwaite. *Multivariable feedback control, analysis and design*. Wiley, 2005.
- [126] G. Sleijpen and H. Van der Vorst. A Jacobi-Davidson iteration method for linear eigenvalue problems. *SIAM Journal on Matrix Analysis and Applications*, 17(2):401–425, 1996.
- [127] T. Söderström and P. Stoica. *System Identification*. Prentice-Hall, 1989.
- [128] G. Stein and M. Athans. The LQG/LTR procedure for multivariable feedback control design. *IEEE Transactions on Automatic Control*, 32:105–114, 1987.
- [129] M. Steinbuch and M. Norg. Advanced motion control: an industrial perspective. *European J. of Control*, 4(1):278–293, 1998.
- [130] G. Stewart. Error and perturbation bounds for subspaces associated with certain eigenvalue problems. *SIAM Review*, 15(4):727–764, 1973.
- [131] P. Stoica and R. Moses. *Spectral Analysis of Signals*. Prentice-Hall, 2005.

-
- [132] V. Sule and V. Athani. Directional sensitivity tradeoffs in multivariable feedback systems. *Automatica*, 27(5):869–872, 1991.
- [133] T. ten Dam. Disturbance characterization for MIMO control. Master’s thesis, Technische Universiteit Eindhoven, 2008. DCT 08.001.
- [134] N. Thornhill. Finding the source of nonlinearity in a process with plant-wide oscillation. *IEEE Transactions on Control Systems Technology*, 13:434–443, 2005.
- [135] N. Thornhill and A. Horch. Advances and new directions in plant-wide disturbance detection and diagnosis. *Control Engineering Practice, In Press*.
- [136] L. Tong, R. Liu, V. Soon, and Y. Huang. Indeterminacy and identifiability of blind identification. In *IEEE Transactions on Circuits and Systems*, volume 38, pages 499–509, 1991.
- [137] L. Tong, V. Soon, R. Liu, and Y. Huang. AMUSE a new blind identification algorithm. In *Proceedings of the ISCAS*, 1990.
- [138] R. Tousain, J. Boissy, M. Norg, M. Steinbuch, and O. Bosgra. Suppressing non-periodically repeating disturbances in mechanical servo systems. In *Proceedings of the Conference on Decision and Control*, volume 3, pages 2541–2542, 1998.
- [139] J. Tugnait. Identification and Deconvolution of Multichannel Linear Non-Gaussian Processes Using Higher Order Statistics and Inverse Filter Criteria. *IEEE Transaction on Signal Processing*, 45(3):658–672, 1997.
- [140] D. Vaes, K. Smolders, J. Swevers, and P. Sas. Multivariable control for reference tracking on half car test rig. In *Proceedings of the Conference on Decision and Control and the European Control Conference*, pages 6498–6503, 2005.
- [141] D. Vaes, W. Souverijns, J. De Cuyper, J. Swevers, and P. Sas. Optimal decoupling for improved multivariable controller design, applied on an automotive vibration test rig. In *Proceedings of the American Control Conference*, volume 1, pages 785–790, 2003.
- [142] M. van de Wal and A. de Jager. A review of methods for input/output selection. *Automatica*, 37(4):487–510, 2001.
- [143] M. van de Wal, G. van Baars, F. Sperling, and O. Bosgra. Multivariable \mathcal{H}_∞, μ feedback control design for high-precision wafer stage motion. *Control Engineering Practice*, 10(7):739–755, 2002.
- [144] J. van de Wijdeven and O. Bosgra. Stabilizability, performance, and the choice of actuation and observation time windows in iterative learning control. In *Proceedings of the Conference on Decision and Control*, pages 5042–5047, 1997.

-
- [145] R. van den Bleek, M. Boerlage, and A. Jager. MIMO \mathcal{H}_∞ control design for the avis, internal report. Technical Report DCT 2007.005, Technische Universiteit Eindhoven, 2007.
- [146] J. VanAntwerp, A. Featherstone, and R. Braatz. Robust cross-directional control of large scale sheet and film processes. *Journal of Process Control*, 11:149–177, 2001.
- [147] M. Wax and J. Sheinvald. A least-squares approach to joint diagonalization. In *IEEE Signal Processing Letters*, volume 4, pages 52–53, 1997.
- [148] P. Wortelboer. *Frequency-Weighted Balanced Reduction of Closed-Loop Mechanical Servo Systems: Theory and Tools*. PhD thesis, Delft University of Technology, The Netherlands, 1994.
- [149] P. Wortelboer, M. Steinbuch, and O. Bosgra. Iterative model and controller reduction using closed-loop balancing, with application to a compact disc mechanism. *International Journal of Robust and Nonlinear Control*, 9(3): 123142, 1999.
- [150] O. Yaniv. *Quantitative Feedback Design of Linear and Nonlinear Control Systems*, volume 509. The Springer International Series in Engineering and Computer Science, 1999.
- [151] A. Yeredor. Blind separation of Gaussian sources via second-order statistics with asymptotically optimal weighting. *IEEE Signal Processing Letters*, 7(7):197–200, 2000.
- [152] A. Ypma, A. Leshem, and R. Duin. Blind separation of rotating machine sources: bilinear forms and convolutive mixtures. *Neurocomputing*, 49(1): 349–368, 2002.
- [153] G. Zames. Feedback and optimal sensitivity: model reference transformations, multiplicative seminorms and approximate inverses. *IEEE Transactions on Automatic Control*, 26:301–320, 1981.
- [154] K. Zhou, J. Doyle, and K. Glover. *Robust and optimal control*. Prentice Hall, 1996.
- [155] M. Zibulevsky and B. Pearlmutter. Second order blind source separation by recursive splitting of signal subspaces. In *Proceedings ICA 2000*, pages 489–491, 2000.

Summary

Due to ever increasing demands in industry, the number of applications of multiple input multiple output (MIMO) control systems has increased drastically in the last decades. Although considerable progress has been made in the development of theoretical tools, feedback control design for MIMO systems still poses complexity issues for both academia and the practising engineer. In an effort to reduce design complexity, many aspects of MIMO systems are disregarded in most practical applications, at the cost of potential achievable performance.

One of the important tasks of feedback control is the ability to reject disturbances. In MIMO systems, gain, phase, and directions play an important role in the systems ability to reject disturbances. The directional, multivariable, aspects of disturbances necessitate approaching the MIMO control problem in its full complexity. The goal of this work is to make directional aspects an integral part of MIMO control design. Herein, the focus is on applications of motion control systems. The contribution of this work is two-fold.

The first contribution of this work is the development of techniques to characterize multivariable disturbances. A non-parametric component analysis method is developed to identify both the directional aspects of disturbances and the root cause (source) of disturbances in multivariable closed loop controlled systems. Indices are developed to quantify directionality of disturbances and, possibly, simplify multivariable control design. These techniques are applied to an active vibration isolation platform. It is shown how the location of sources can be recovered using only closed loop measurements. Furthermore, it is demonstrated how multivariable control design can be simplified. With this, it is demonstrated how multivariable aspects of disturbances can be interpreted physically and exploited in control design.

The second contribution of the work involves the development of control design methods that take advantage from the multivariable aspects of disturbances. The focus is on systems where the plant dynamics are decoupled while disturbances may act on may decoupled parts of the plant at the same time. Methods are developed to design non-diagonal weighting filters for \mathcal{H}_∞ control synthesis. Fur-

thermore, manual frequency domain loopshaping techniques are developed for the design of centralized MIMO controllers that accommodate directions of disturbances and sensor noise. It is illustrated with several examples that, using these developed techniques, directions of disturbances and noise can be successfully integrated in control design for multivariable motion systems.

Samenvatting

Vanwege de strengere prestatie-eisen gesteld binnen de industrie, is het aantal toepassingen van regelaars met meerdere in- en uitgangen (MIMO) in de laatste decennia drastisch toegenomen. Vele ontwikkelingen in systeemtheorie ten spijt, blijft het ontwerpen van MIMO regelaars een uitdaging voor zowel de academicus als de ingenieur. In een poging de complexiteit van het ontwerpproces te verminderen, worden veel aspecten van het MIMO systemen verwaarloosd. Dit gaat vaak ten koste van de mogelijk haalbare prestatie.

Een belangrijke taak van regelaars door middel van terugkoppeling is het vermogen om exogene verstoringen te onderdrukken. In MIMO systemen zijn de versterking, fase en richting belangrijke systeem eigenschappen die de mate van verstoringsonderdrukking bepalen. De richtingsafhankelijkheid van MIMO systemen vereist dat het ontwerpprobleem van MIMO regelaars in zijn volle complexiteit wordt beschouwd. Het doel van dit werk is om het aspect van richtingsafhankelijkheid op te nemen in het ontwerpproces van MIMO regelaars voor bewegingssystemen. De bijdrage van dit werk is tweeledig.

De eerste bijdrage van dit werk is een methode om multivariabele verstoringen te karakteriseren. Een niet-parametrische componenten analyse is ontwikkeld om zowel de richting als de bronnen van verstoringen in een gesloten lus regelsysteem te identificeren. Indices zijn ontwikkeld om de richtingsafhankelijkheid van verstoringen te kwantificeren en het ontwerp van MIMO regelaars mogelijkkerwijs te vereenvoudigen. Deze technieken zijn toegepast op een actief trillingsisolatiesysteem. Hiermee kunnen de locaties van de verstoringsbronnen worden bepaald. Tevens is aangetoond dat het ontwerp van de MIMO regelaar voor deze opstelling, dankzij de verkregen inzichten in de multivariabele verstoringssituatie, sterk kan worden vereenvoudigd.

De tweede bijdrage van dit werk bestaat uit een aantal regelaar ontwerpmethoden om multivariabele aspecten van verstoringen en meetruis te benutten. De nadruk ligt hierbij op situaties waarbij de systeemdynamica wel, maar de verstoringsdynamica niet ontkoppeld is. Methoden zijn ontwikkeld om niet-diagonale weegfilters voor \mathcal{H}_∞ regelaar synthese te ontwerpen. Bovendien worden handmatige,

frequentie gebaseerde technieken ontwikkeld om richtingsafhankelijke, gecentraliseerde regelaars te ontwerpen. Deze technieken worden geïllustreerd met enkele voorbeelden van bewegingssystemen. Dit laat zien dat, voor een bepaalde klasse van systemen, richtingen van verstoringen en meetruijs op een succesvolle wijze in het ontwerp van MIMO regelaars kunnen worden opgenomen.

Dankwoord

Hoewel er maar één naam op deze kaft prijkt, is dit werk tot stand gekomen dankzij de inzet van vele mensen. Allereerst wil ik mijn promotor Maarten Steinbuch bedanken voor de inspiratie, visie, het enthousiasme en de zeer kundige wijze waarmee hij mij en mijn project richting heeft gegeven. De mogelijkheid om kennis over te dragen met colleges, PATO cursus, werkbezoek in Ierland en diverse conferenties hebben veel meerwaarde gegeven aan mijn werk en bijgedragen aan mijn persoonlijke ontwikkeling. Ook wil ik mijn co-promotor Bram de Jager bedanken voor de wekelijkse begeleiding. De nuchtere en kritische terugkoppeling zijn van grote invloed geweest in het richten van mijn energie en het behalen van dit eindresultaat.

I would like to thank professor Rick Middleton for the fruitful months at the Hamilton Institute. Thank you very much for the hospitality and the exciting and inspiring brainstorm sessions.

Veel elementen in dit werk zijn te danken aan interactie met studenten. Jeroen, Marc, Roel, Tijs en Thijs bedankt! Voor de toepassing op de metrologische AFM (Chapter 4) ben ik Roel Merry dankbaar. Ook wil ik Rob Tousain, Marc van de Wal en Georgo Angelis bedanken voor de discussies tijdens en na de Q-meetings bij Philips Applied Technologies. Ook de vele vruchtbare, maar net zo goed de niet vruchtbare, discussies op kamer WH -1.138 waren van grote waarde. Bedankt “roomies” Maurice, Michiel, Kira, Dennis en in het bijzonder Jeroen; dankzij jou heb ik de details van ons vak als delicatessen leren waarderen. Moge het kamerkarma weer met jullie zijn. Ik bedankt alle mede-AIO-ers voor de nuttige discussies en de gezellige reizen na afloop van diverse conferenties. Daarnaast dank ik het secretariaat; Lia, Caroline en Petra, voor de levenswijsheid en de vermakelijke gesprekken bij de koffie.

Als laatste bedank ik mijn familie, Papa, Mama, Frédérique en Raymond voor de ondersteuning, het inlevingsvermogen en de stimulans om mijn dromen in korte tijd te verwezenlijken.

Matthijs Boerlage

Eindhoven, juli 2008

Curriculum Vitae

- April 14, 1978 Born in Nijmegen, The Netherlands.
- 1991-1995 High School (HAVO), Katholiek Gelders Lyceum, Arnhem.
- 1995-1996 Microsystems Technology, University of Applied Sciences Utrecht.
- 1996-2000 Bachelor study in Mechatronics and Mechanical Engineering. Fontys University of Applied Sciences Eindhoven. Internships at Océ Technologies B.V, Venlo and Northumbria University upon Tyne, Newcastle, United Kingdom. B.Sc. thesis project at ASML Veldhoven; jerk derivative (snap) feedforward.
- 2000-2004 Master study in Mechanical Engineering. Eindhoven University of Technology. Control Systems Technology. M.Sc. thesis project (Cum Laude) at Philips Applied Technologies, Eindhoven; exploratory study on multivariable control for motion systems. Awarded with the KIVI (Royal Institution of Engineers, The Netherlands) graduate award for the best M.Sc. thesis in Mechanical Engineering 2003-2004.
- 2004-2008 Ph.D. Candidate. Control Systems Technology group. Faculty of Mechanical Engineering, Eindhoven University of Technology. Promotor: Maarten Steinbuch, Co-promotor: Bram de Jager. Lecturer of M.Sc. course Advanced motion control and Advanced motion control course PATO (Post-academic Technical Education). Visiting scientist at The Hamilton Institute, National University of Ireland, Maynooth. Best session presentation award at the American Control Conference 2004, Boston USA.
- 2008- Control Systems Research Engineer. Hybrid & Renewable Energy Systems Lab General Electric Global Research Europe, Munich, Germany.